THE ROLE OF RADICALS SUPPLIED DIRECTLY AND INDIRECTLY ON IGNITION

A Dissertation
Presented to
The Academic Faculty

by

Jaecheol Kim

In Partial Fulfillment
of the Requirements for the Degree
Doctor of Philosophy in the
School of Aerospace Engineering

Georgia Institute of Technology
December 2014

THE ROLE OF RADICALS SUPPLIED DIRECTLY AND INDIRECTLY ON IGNITION

Approved by:

Professor Jeff Jagoda, Advisor
School of Aerospace Engineering
Georgia Institute of Technology

Professor Jerry Seitzman
School of Aerospace Engineering
Georgia Institute of Technology

Hightower Professor Suresh Menon
School of Aerospace Engineering
Georgia Institute of Technology

Dr. David Scarborough
School of Aerospace Engineering
Georgia Institute of Technology

Dr. Woong-sik Choi
Gasoline Engine Performance Test Team
Hyundai Motor Company

Date Approved: August 19 2014

ACKNOWLEDGEMENTS

I would like to express my sincere appreciation and thanks to my advisor Professor Dr. Jeff Jagoda. I would like to thank you for guidance, patience and for encouraging my research. I would also like to thank Dr. Suresh Menon, Dr. David Scarborough and Dr. Woong-sik Choi for being part of my thesis reading committee and for providing valuable comments and suggestions to improve the quality of my thesis. In addition, I would like to make special thanks to Dr. Jerry Seitzman for serving on my thesis committee and his valuable advice and guidance on my research.

I would like to thank current and old colleagues in Combustion Lab, Yongjea, Juhyung, Dong-hyuk, Alex and Brandon for their encouragement, valuable discussions and friendship. I also thank my friends in AE departments for their supporting and encouraging me.

My special thanks to my parents for their endless love and support.

TABLE OF CONTENTS

LIST OF TABLES

Page

LIST OF FIGURES

Page

SUMMARY

The ignition process is a critical consideration for combustion devices. External energy transfer to the combustor is required for ignition in common combustion systems. There are many ways to deposit energy into the flow but a standard method is a spark discharge because it is simple, compact, and reliable. Sparks can be categorized as either inductive or capacitive sparks that use a coil or an electrical resonance circuit with capacitor, respectively, to amplify the voltage. The creation of a successful ignition event depends on the spark energy deposited into the flow, the initial composition, pressure, temperature, turbulence level of flow etc. The deposited energy by the spark into the flow is critical for estimation of initial energy available for ignition of the mixture. Therefore, the electrical characteristics of the sparks were investigated under various flow conditions. Then measurements of deposited energy into the flow were conducted using a very accurate experimental procedure that was developed in this research. The results showed considerable electric energy losses to the electrodes for the relatively long, inductive sparks. However, the short, capacitive spark deposits electric energy into the flow with minimal loss (above 90% deposition efficiency). In addition, the characteristics of inductive spark are affected by flow velocity and by the existence of a flame. However, variations in the flow conditions do not affect the characteristics of the capacitive spark such as voltage-current time trace and energy deposition efficiency.

Two ignition systems using above mentioned two spark types were developed. First, the capacitive spark energy was directly deposited into the premixed flow. Most researchers have not concentrated on the early initiation process but on the flame growth. Therefore, the generated kernel formed by the energy deposition was observed and

characterized using optical methods, immediately following the spark. In addition, the mixing effect for this ignition kernel with surrounding gas was simulated using a numerical method. Based on the time trace of the OH* chemiluminescence, the reaction starts with the discharge and it is continuous until combustion begins. This means that in the presence of a high density spark in premixed flow, there exists no traditional delay as defined by other researchers for auto ignition.

A simple Radical Jet Generator (RJG) was developed that is able to ignite and stabilize a flame in a high-speed flow. The inductive spark initiates the combustion in the RJG chamber. The RJG then injects the partially-burned products carrying large amounts of heat and radicals into a rapidly moving flammable main stream. Then it ignites and stabilizes a flame. The RJG requires low levels of electrical power as long as the flow velocity is relatively low since most of the radicals are produced by the incomplete combustion in its chamber. The importance of radicals was analyzed by RJG experiments and numerical methods. The reaction zone for RJG using a rich mixture was located both inside and outside of the RJG chamber. Therefore, the RJG using a rich mixture performed better in the ignition and stabilization of combustion in the main flow. According to an analysis using the CHEMKIM simulation software combined with the San Diego chemical mechanism, the RJG jet resulting from a rich mixture contains more radicals and intermediates than that produced by a lean mixture for the same sensible enthalpy. In addition, the burned gas contains less radicals and intermediates than the partially burned gas.

If the RJG is operating with a high speed main flow, the flow rate through the RJG chamber must be increased to allow the radical jet to penetrate well into the rapid flow

due to their higher injection velocity. Unfortunately, this leads to unsteady combustion in the RJG, which results in the pulsation of the radical jet. This reduces the number of radicals injected into the main flow. To investigate this operating condition, special attention was focused on four possible factors: unburned reactant pockets caused by motion of the spark channel, spark frequency, flame propagation speed and ignition delay. It was shown that the unsteadiness is affected by the flame speed and ignition delay because the frequency of pulsation in the chamber is highly dependent on the equivalence ratio. In addition, the interaction between the RJG operation and the combustion dynamics in the main combustor was documented. The acoustic pressure oscillations in the main combustor were suppressed when the RJG jet was turned on because the reaction region is relocated by the operation of the RJG.

CHAPTER 1: INTRODUCTION

1.1 Background

Ignition can be defined as "the process whereby a material capable of reacting exothermically is brought to a state of rapid combustion" [1]. Alternatively, ignition can be described in terms of a rapid change in temperature. Furthermore, ignition can be categorized as either auto ignition or forced ignition. Auto ignition does not require an external source and can, in principle, occur at any initial temperature. However, if the initial temperature is too low, the reaction rate is very slow. In fact, the Arrhenius reaction rate expression shows that reaction rate increases exponentially with temperature. Therefore, a practical reaction rate requires an elevated ignition temperature for most fuel-air mixtures. In contrast, forced ignition needs an external energy source. Forced ignition is achieved if enough net energy is transferred from the ignition source to a flammable mixture to sufficiently excite, ionize and dissociate the molecules. The deposited energy determines the initial condition of the kernel, which is created and then changes as it is convected downstream. As the kernel moves, it grows due to mixing and thermal expansion. The growth rate is related to the turbulence level around the kernel [2] and the temperature inside the kernel [3]. Furthermore, the kernel can encounter variations in mixture fraction as it travels through a region where air and fuel mix. A critical factor for successful ignition is the energy density inside the kernel, when it initiates the reaction in a flammable mixture.

The probability that the kernel will ignite is high if an ignition source of sufficient energy is placed near a mixture within the flammability limit. However, in practical systems, such as non-premixed combustors, the igniter is generally located near a wall

where the flow is almost pure air [4]. The probability of ignition is affected by the conditions through which the kernel must travel before it reaches the nearly flammable mixture. These conditions include fuel-air mixture fraction, temperature, pressure, turbulence level and ignition energy.

There are many ways to deposit the ignition energy into the flow. The most conventional method is spark ignition. Spark ignition is used in almost all automobile and aircraft engines because it is simple, compact and reliable for extended periods of use. Therefore, this work focuses on spark ignition.

The next important process in combustion is flame stabilization. Flames propagate by diffusing heat and radicals produced in the reaction zone into the reactants. In order to stabilize the flame, its propagation speed should equal the flow speed. There are various techniques to stabilize a flame in high-speed flows. In gas turbine main combustors, stability is generally achieved through the use of swirlers, which create a recirculation zone. In afterburners, a bluff body is usually inserted into the flow, and combustion is stabilized in the turbulent, relatively low-velocity wake behind it. However, the presence of the bluff body results in a pressure loss in the flow. Furthermore, the metal flame holder is heated by the exhaust flow even when the afterburner is off, and, therefore, radiates in the infrared spectrum, which can be detected by enemy aircraft and/or missiles. This is particularly bothersome since the afterburner is typically on for less than a minute, if at all. However, the above disadvantages persist throughout the mission.

An alternative method of igniting and holding a flame in a rapidly moving flow is via the use of a steady plasma [5, 6]. This concept has been researched since the experimental work by Harrison et al. [7]. For example, a plasma torch has been studied as

an ignition source for high-speed vehicles such as scramjet engines. It dissociates a non-combustible gas and injects the produced radicals and heat into the main stream where combustion is to be stabilized. Here, the discharge modifies the flame speed [8, 9] by adding radicals to the flow without generating any significant pressure losses [10-15]. This method provides flame holding that is generally more efficient than that provided when a plasma adds heat directly to the flow [16, 17]. However, generating an plasma of inert gas does consume considerable electrical power and does require heavy, specialized power electronics, which makes it less than ideal for use in aircraft engines.

1.2 Literature review

1.2.1 Electrical aspects of spark ignition

Sparks are a commonly used method to initiate the combustion of a flammable mixture. A spark can be generated by an electrical power supply or by a laser device. The laser device can induce the breakdown of gas by transferring energy from the photons emitted by the laser to the gas molecules [18-21]. This laser can ignite the combustible mixture via several types of energy transfer [22]. The first method is laser thermal ignition. The thermal energy from the laser directly excites the translational, rotational and vibrational energy of the molecules. After the energy of the photon is transferred to the molecules, the bonds between atoms break and the atoms react with other atoms. The second ignition method occurs via a laser-induced photochemical process. The photons emitted from the laser impact the molecules, which in turn produce a highly-reactive radical. The radical then creates the self-sustaining flame. The third method of ignition is laser-induced resonant breakdown ignition. This ignition process involves non-resonant

multi-photon photo-dissociation. The photo-dissociation process results in resonant photoionization.

Finally, laser-induced spark ignition is the fourth laser-induced ignition method. This laser-induced spark discharge process is very similar to the conventional spark after the photon impacts the molecules. However, the volume of the initial ignition kernel is much smaller than that of a conventional spark. Because the laser can concentrate energy from the power supply on a very small volume of gas, the temperature and energy densities are higher than in the case of a conventional spark. The ability to create this high density radical is an advantage of laser-induced spark ignition. Furthermore, the laser can be tuned to excite a particular molecular energy level which concentrates the energy where it is most productive. Electrodes are also not necessary for the laser device to function. Therefore, there are no heat losses through the electrodes and the flow region in the combustion chamber is not disturbed by the electrodes. Due to these features, this system has the advantage of providing a more reliable engine. Laser-induced spark research can also help us better understand the spark phenomenon and its application for ignition.

The duration of sparks used in advanced gas turbine engines is much shorter than that of traditional sparks, which last for about a millisecond. These high-energy and short-duration spark characteristics can be analyzed using laser-induced spark ignition, which provides similar spark characteristics without interference from the electrodes. However, the laser-induced spark requires optical access as well as a complicate and therefore, heavier systems than does the electric spark system. Laser based system are, therefore, less practical for most jet engine application and an electrical spark device is more commonly used.

According to E.M. Bazelyan [23] when the spark is initiated, electrons in the air are accelerated by the applied electrical field which causes them to collide with neutral atoms and molecules. At this time, the spark discharge is in non-equilibrium and is weakly ionized (corona stage). In other words, the electron temperature is very different from the translational temperature. In addition, the degree of ionization is much lower than that expected for thermodynamic equilibrium corresponding to the actual temperature of electrons. During this first stage (composed mostly of a non-equilibrium, weakly ionized plasma), streamers generated at the anode propagate to the cathode (Figure 1 from [24]) [24-27]. Once the streamers reach the cathode, a conductive channel is formed with current delivered from the power supply. If the current supplied is sufficient, the first stage develops into a spark breakdown discharge. If not, it forms a corona discharge.

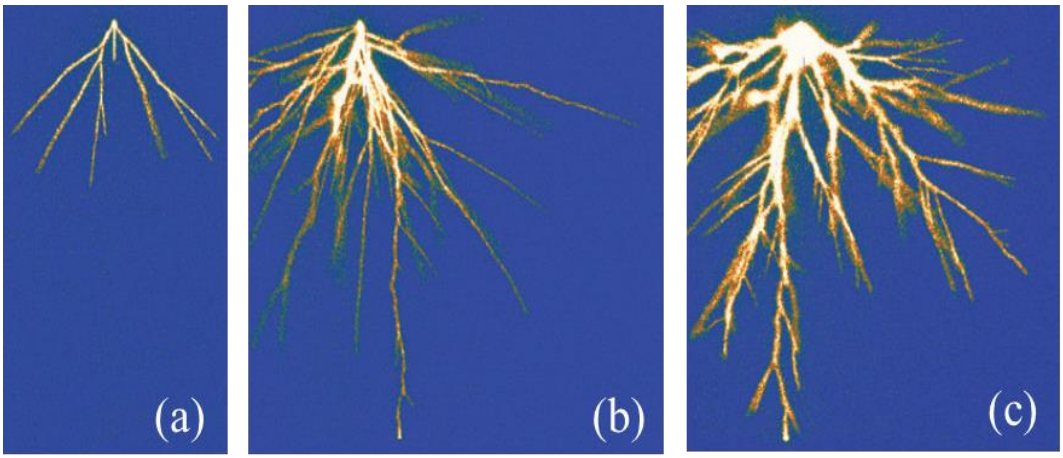

Figure 1. CCD photos of the point-wire discharge in air using 5μs optical gate. Applied voltages: (a) at 7.5 kV, (b) and (c) at 12.5 kV. For (a) and (b) the semiconductor switch is used, for (c) the spark gap [24].

The initial generation of electrons, mentioned above, is affected by the material of the electrodes. Atoms in the metal are separated by very short distances and the electron

movement is affected by the grouping of the metal atoms. Therefore, the barrier energy required to generate free electrons depends on the atom density in the metal of the electrode. Electrons with sufficient energy penetrate through the barrier by heating. However, the barrier level can be reduced by applying an electric field [28]. According to Ballal[29], the boiling temperature of the electrode material affects the minimum ignition energy (MIE), i.e., the MIE increases with increasing boiling temperature. If a dielectric barrier covers the electrodes, the current from the power supply is limited and the streamer discharge cannot transit to a spark discharge. In that case, this dielectric discharge usually forms a corona discharge, which is a non-equilibrium or non-thermal discharge. Its energy is deposited into the vibrational and electronic degrees of freedom of the gas [30, 31].

Later, the discharge process reaches equilibrium as the electrons collide with the heavy particles (arc stage, strongly ionized plasma) [23, 32]. Low-energy electrons can excite the vibrational energy of molecules; this is more common than rotational excitation. The energy is then transferred to the translational mode. In the air-only case, the relaxation time is proportional to the gas temperature and inversely proportional to the H_2O concentration. The electrons are energized when they collide with other particles that acquired energy during the non-equilibrium state, rather than drawing their energy from the electric field. The energy distribution of atoms or molecules follows a Maxwellian distribution.

The power supply cannot discharge a huge number of electrons in the early stage of the spark discharge because the conductivity is not high enough at the weakly-ionized non-equilibrium stage. Once the electrons ionize the atoms or molecules sufficiently, the

electron temperature becomes similar to the translational temperature of the heavies as more electrons are supplied by the power supply. The electron temperature is approximately the same as in the weakly ionized plasma because ionization is still needed to maintain a constant state. However, the gas is heated to the electron temperature because of the high degree of ionization. It leads to high conductivity, which results in great energy release. The strength of the electric field sustaining the equilibrium plasma is about a tenth of that of the non-equilibrium plasma. This is because the electrons are energized by the field while collisions between ions results in further ionization.

According to the above procedure for generating a spark, the spark consists of three fundamental, consecutive discharge modes: breakdown, arc and glow [32, 33]. These three modes have different abilities to ignite combustible mixtures. The breakdown mode shows the best ignition performance [34-36]. This mode is in a highly non-equilibrium state. Most of the energy is transferred through non-thermal forms during this mode, which has a very short duration (~10nsec). In other words, most of the energy supplied is transferred without losses. The direct impacts of electrons on the gas molecules can dissociate and ionize the molecules to turn the gas into a plasma. During the arc mode, when sufficient current is delivered by the power supply, most of the energy is transferred thermally, with much longer duration than the breakdown mode. Therefore, a significant amount of energy is used not for dissociating the gas but for heating it up. In addition, there are significant energy losses, through mass diffusion and conduction through the metal electrodes. The glow mode is similar to the arc mode, except with a higher voltage (300-500V) and much lower current (<200mA). We can, therefore, expect that the breakdown mode is more efficient for the production of radicals, and that the

energy associated with radicals is more effective for ignition resulting in shorter ignition delays and wider flammability limits than when the energy is thermally transferred to the gas [34]. There is no significant difference in these electrical discharge characteristics between air and a fuel/air combustible mixture in the spark gap. The breakdown threshold energy, however, decreases with increase in pressure because the higher collision frequency, which enhances the destruction of molecular bonds. This pressure dependence has been shown to vary as $P^{-\alpha}$, where the value of α is affected by the initial composition of the gas.

Ballal [29] suggested that, ignition performance would increase if one could reduce spark duration since this would minimize heat losses. This results in an optimum spark duration for ignition which depends on flow velocity (Figure 2 from [29]). Kono [37] investigated the optimum duration for various spark modes, while Ballal [29] showed that the amount of heat losses depends on discharge type and includes conduction, thermal radiation, turbulent diffusion and forced convection. In addition, the spark emits UV radiation, which is not a significant part of the total energy loss from the spark. Furthermore, according to [38], they focused the UV from the plasma kernel on a point to ignite the flammable mixture. However, UV radiation at energy levels of interest in combustion engines contributes little to flame ignition.

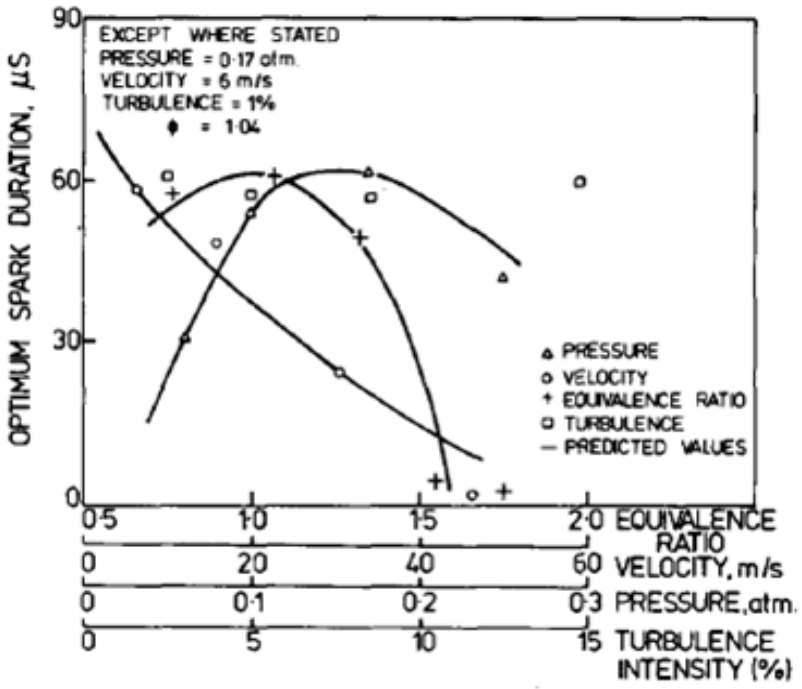

Figure 2. The influence of flow parameters and equivalence ratio on optimum spark duration [29].

1.2.2 Measurement considerations

High-accuracy voltage and current measurements are very important in characterizing the electrical aspects of the spark because the voltage-current (VI) time scale of the spark is very short and has a very wide range (from ns to ms) and very high magnitude (several kV for a few millimeter gap). In addition, the spark is a very strong source of EM noise. Furthermore, the resistance, inductance and capacitance of wire connections can affect the VI characteristics of the spark [39]. Therefore, the VI measurement should be conducted with well-defined devices, as described in [40]. For the capacitive and the inductive sparks, the capacitor and inductor store the charge before it discharges through the inter-electrode gas. Some researchers [41] have estimated spark

energy by calculating the energy stored in the capacitor or inductor. They assumed that all the stored energy inside these devices was deposited into the gas.

1.2.3 Spark kernel evolution

Once the electrical energy has been transferred into the reactants, the spark ignition process is initiated when a kernel is generated, and completed when a flame propagate through the reactants [4, 42, 43]. Due to the fast deposition of spark energy, the initial pressure in the discharge region is very high (~ 200 bar [34]). This high pressure results in the formation of a shock, which interacts with the spark kernel [44]. In addition, for the opposed rod type electrode configuration, the flow stream forms vortices near the electrode. In addition, the kernel expansion is restricted by the electrodes according to [42]. Due to this complicated flow pattern near the electrodes, the kernel shape and evolution is not simple. It was observed using various numerical and experimental approaches [3, 34, 43, 45-49] in an effort to understand the flow pattern.

According to the traditional ignition model [1, 19], the kernel develops into a flame if the heat generation inside the kernel is higher than the heat losses from the kernel. In addition, in a non-premixed environment, the kernel can be initiated in a non-ignitable region and then has to travel through the flow to a location where ignition can occur. During this time the kernel expands while reactions occur in it [1]. Arpaci et al. [3, 34, 46, 47] investigated the kernel expansion and Sher [48] and Beduneau [49] showed that kernel growth is a function of spark duration and breakdown energy. According to Arpaci's detailed result [3], a spark kernel, which contains enough energy to cause ignition grows with time, corresponding to a 1/5 power law. After a critical time the kernel either decays, or grows further following a 2 power law if conditions are

appropriate for ignition. This critical time depends on the mixture properties, and corresponds to the chemical reaction time necessary to take over the expansion mechanism of the kernel. In addition, the kernel transitions from a toroidal shape to a spherical shape [50].

1.2.4 Radical effect on spark initiated combustion

The surplus energy in the kernel produces additional radicals and ions inside the kernel. These reactive species, derived from the plasma of the spark, decrease ignition delay times and increase burning velocity, which are strongly related to the flame stabilization and propagation process [6, 9, 31, 35, 41, 51-59]. W. Kim et al. [14, 60-62] suggest that repetitively-pulsed, non-equilibrium plasma discharges can stabilize a flame by supplying radicals that can survive for relatively long periods (~1-10msec). In addition, Takita et al. [9, 55, 63] numerically showed that ignition delay is shortened by adding radicals. Mintoussov et al. [59, 64] suggest that discharge-induced electrical excitation, followed by vibrational excitation, affects flame propagation velocity. The amount of radicals and activated species was calculated using a plasma solver [61, 65-70]. A Boltzmann equation solver (BOLSIG etc. [70]) was used by many researchers to acquire electron transport coefficients and rate coefficients. Plasma composition was then calculated based on selected elemental reactions, which were, in turn, based on the transport coefficient and rates.

Dixon-Lewis [51, 53] varied the ratio of chemical energy (H atom) to heat energy for ignition in both cylindrical and spherical flame using a numerical technique. He shows that the H atom is a more efficient ignition agent than is heat. Furthermore, Wiriyawit [52] suggests that the ignition energy supplied as an OH radical is more effective than

either heat or energy in form of H atoms. Sloane [54] showed also that ignition energy provided in the form of dissociation accelerates the ignition and combustion processes (Figure 3 from [54]), but that there is no obvious improvement on the MIE. Those results were obtained using both numerical and theoretical approaches. Zhang [71-73] determined the radical effect on ignition as opposed to that of heat using theoretical technique. However, it is very hard to find experimental data to validate their conclusion.

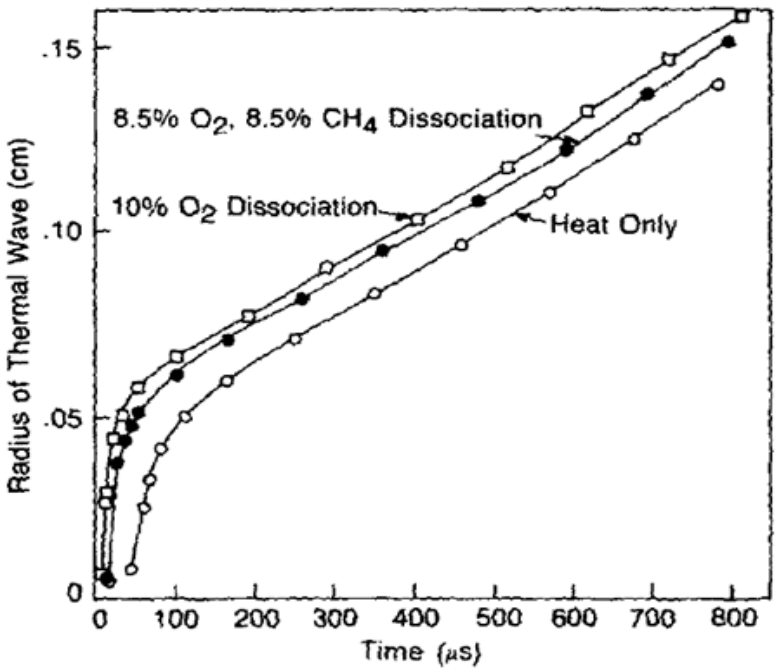

Figure 3. Radial position of the exothermic wave (identified as the location of maximum heat release rate due to chemical reactions) as a function of time for three different ignition energy distributions and the same total ignition energy of 0.259 mJ [54].

Generally, a spark discharge generates heat and radicals directly in the combustor. However, there is an indirect method to supply the heat and radicals using a pre-chamber to improve combustion. This will prevent blow out in, for example, supersonic combustion [7, 13-15, 62, 73-78]. Prior researchers have used a plasma chamber where

an operating gas is decomposed using electric energy. Alternatively a normally non-flammable mixture is allowed to react. The radicals and heat generated are injected into the main combustor through a nozzle. The sizing of this nozzle is a critical parameter for the performance of the pilot [65].

Atomic N is a long-lasting species and atomic H diffuses rapidly, which makes these species suitable for such devices. Weinberg [7, 78, 79] developed such an air based plasma jet to promote combustion. However, it needed a significant amount of power (~1000W).

A comparison between radical and heat effects on ignition and combustion is necessary for the understanding of spark ignition. However, most researchers are unable to separate these effects. The exception is Takita [14]. He studied the effects of radicals and heat on supersonic combustion. Takita used O_2, N_2 and Ar as feed gasses. His results show that the O_2 and N_2 plasma jets performed better than that fed with Ar, because the Ar jet contained fewer radicals and, therefore more heat than the others.

Ignition delay and flame speed are very important combustion characteristics. These parameters are closely related to combustor performance. In the literature, there are many studies of ignition delay [6, 27, 31, 35, 55, 56, 80, 81]. It is commonly defined as the time elapsed from the onset of the energy transfer from an external source to rapid combustion. Usually, a pressure or temperature sensor is used to detect the delay in a closed reactor [35]. This sensor measures the pressure or temperature for the whole volume of the vessel. In other words, the time trace of the sensor signal represents the pressure or temperature increase in the whole chamber region due to the propagation of flame, as well as any rapid local combustion at a specific region. However, temperature

or pressure measurements are not a proper technique for determination of ignition delays in a flowing gas. Therefore, some researchers [6, 55, 56] have used chemiluminescence to detect the delay under these circumstances. However, they have not clearly defined the ignition delay in their experiment. They have used global signals of chemiluminescence emitted from the entire flow reactor. This measurement does not represent the local combustion process we are interested in, but rather records the process for the whole facility. We require a detection method that can directly monitor the local ignition time in a single predetermined zone.

Gussak [82] determined that products from the pre-chamber can decrease the ignition delay and combustion duration by a factor of 5-7 and 3-4, respectively. A 10% improvement in combustion efficiency is achieved and the overall combustion becomes exceptionally stable and reproducible. Another study [83] confirmed that active oxygen is an important factor in enhancing methane conversion and energy efficiency in a discharge reactor. Ethane is the primary product that forms at short residence times and low energies.

A recirculation zone to decrease flow speed (e.g., by a bluff body etc.[84-87]) is necessary to stabilize the flame. In addition, the flame speed must be increased. The flame speed is affected by reaction rate, diffusivity of gas and turbulence level [88-94]. In spark-induced ignition, the radical can change the reaction rate [41, 58, 59, 64, 95, 96] as well as the ignition delay by changing the chemical kinetics process. Takita [9] showed that radical (O,H, N) addition increases the flame speed. There is a possibility to enhance the flame speed using plasma-induced turbulence [97] or by applying an electric field around the flame [98].

1.3 Overview of present work

In this thesis, we used two systems to supply energy with high energy density into the flow. First, energy from a spark is directly deposited into the flow. Most researcher have not concentrated on the detail of the initiation process but, rather, on the flame growth. Therefore, we focused on the electrical energy transfer during the first stage of the ignition process. Then, the kernel generated due to the energy deposition was recorded and characterized using, for example, optical methods. In addition, the effect of mixing with the surrounding on the ignition kernel was analyzed using a numerical model.

Another energy deposition method is the Radical Jet Generator (RJG). As mentioned, the radicals as well as heat have important effects on the ignition process. The importance of radicals was analyzed in the RJG experiments. A normal ignition system cannot control the relative amount of the radicals and heat it provides for a given energy. However, using the RJG, we can control this ratio which allows us to investigate the importance of the radical on the ignition process, as well as flame stabilization in the main combustor.

Additional phenomena, such as combustion dynamics, are worth observing, due to irregular ignition in the RJG chamber and main combustor. Furthermore, the interaction between the jet injected by RJG and the ignition/combustion in the main combustor were investigated.

CHAPTER 2: EXPERIMENTAL SETUP AND MEASUREMENTS WITH ERROR ANALYSIS

Several different setups were used for spark and radical jet ignition experiments. This chapter introduces two spark generation systems that were designed for ignition of a fuel-air mixture and a Radical Jet Generator for ignition and stabilizing a flame. The combustion characteristics were observed using optical and electrical measurements. Even though all devices were carefully calibrated in this experiment, all measurements inevitably include an element of uncertainty, related to the precision of the instruments or the measurement technique. These uncertainties propagate as errors to the final answer through the calculation procedures. In this research, for example, uncertainty in the calculated equivalence ratio depends on uncertainties in measured values like the volume flow rates of fuel and air. Therefore, the accuracy of measurements of each variable has been carefully analyzed.

2.1 Spark generation

Two spark-generation systems were considered for generating discharges with different characteristics: a long-duration spark generated using an inductive circuit, and a short duration spark produced by a capacitive circuit. The former was installed in the RJG while the latter was used in the energy deposition and kernel evolution experiment.

2.1.1 Inductive (long-duration) spark

An inductive ignition system was used to produce a relatively long-duration spark to deliver energy into the flow. The duration of the spark was approximately 100 μs with a maximum repetition rate of 12 kHz. A schematic of the spark generation system is shown

in Figure 4. A sinusoidal input voltage from a function generator was initially amplified to about 100 volts using a power amplifier (Crown, Macro tech 1200). A transformer further increased the amplifier's output signal, which resulted in an electric breakdown of the gas between the electrodes.

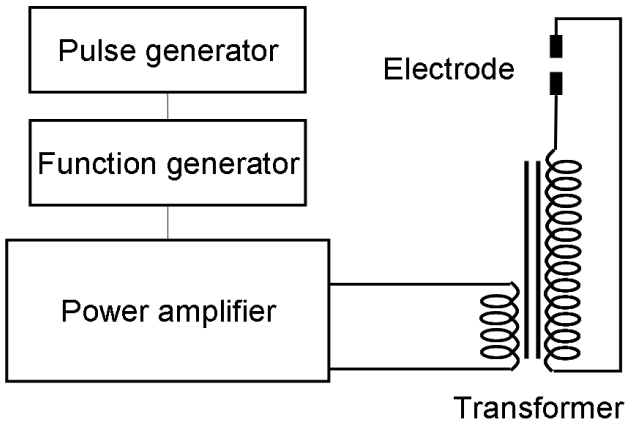

Figure 4. Long duration spark generation system.

2.1.2 Capacitive (short-duration) spark

A copper vapor laser power supply was modified to deliver a high-energy, short-duration spark. (See the circuit diagram in Figure 5 for a detailed schematic.) While the thyratron was off, the 16nF capacitor was charged. It then discharged through the electrode pair. The 1nF capacitor was charged during the initial breakdown, and then discharged in order to augment the main flow of electricity through the spark. The inductance helped the thyratron shut off after discharging the 16nF and 1nF capacitors. Once the thyratron was off, the 16nF capacitor started to charge again, and the cycle repeated. The inductance and capacitance of the wire that connected the components determined the duration and current level of the spark. The spark duration can be calculated using an LC circuit analysis [99]. The predicted spark duration was about 1.1

μs, which agreed well with the measured value. However, the breakdown voltage did not depend on this circuit. Instead it was determined by the properties of the electrodes and of the gas between them. The spark discharge frequency could be changed by adjusting the trigger pulse of the thyratron in the circuit.

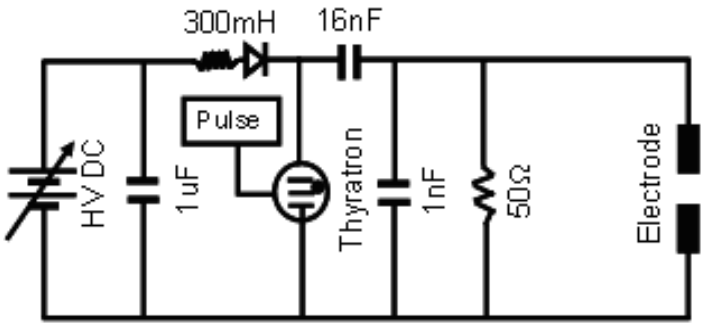

Figure 5. Capacitive spark power supply circuit.

The power supply was connected to a pair of co-linear copper electrodes with a 3.2mm diameter and a 6.3mm gap. The cathode was insulated from the test facility using 12.7mm diameter Teflon tubing. The anode was grounded to the optical table as was the ground of the power supply.

2.2 Electrical measurement

Traditionally, the current is measured using a shunt resistor with a known value of resistance because it is theoretically well defined and has, in principal, no limitations on response time and measurement range. This method can be applied to direct and alternating currents. The electrons impact the gas molecules and cause the gas to lose its dielectric characteristics, which lowers the electrical resistance of gas. Due to this time dependence of the resistance of the gas in the gap, the shunt resistor should be selected

with care. In general, the resistor has much lower resistance than the gas at room temperature and is connected in series with the spark. The high voltage from the power supply is applied to the electrode gap before or during the breakdown, but high voltage is applied at the shunt resistor only after the breakdown. This divided voltage or power at the shunt is a loss that is not delivered to the spark. There is another consideration for selecting the shunt. The resistor inevitably has an inductive characteristic because of the time-varying current. The error due to inductance becomes severe for fast varying current like a pulse as shown in Eq.2.1.

$$V = iR + L\frac{di}{dt} \tag{2.1}$$

The current in the inductive spark circuit was measured using the shunt method because of the relatively low level and low time variations of the current. However, the capacitive system generates a very high current and a short duration discharge that both cause potentially significant errors. Therefore, the current probe applied in the capacitive system is a kind of transformer, the Pearson 6600, which has a fast response time (5nsec). It was used to measure the high peak current encountered in short-duration sparks. It transforms the magnetic field around anode wires into a voltage signal. This non-contact measurement system detects the electromagnetic field generated by the current in the wire. Due to its characteristics, this probe is hardly affected by the external noise that can be produced by the high voltage spark.

For accurate voltage and current measurements of the spark, the voltage and current probes should be located as close to the spark as possible as. However, it is not possible to connect the probes to the spark directly. A high voltage probe, the Tektronix P6015A, measures the potential over the igniter assembly including the electrodes, wire, and

connector. This means the potential drop due to the impedance in electrical connections is included in the voltage measurement. The voltage drop was inevitable, even though we used pure copper electrodes and a minimized contact resistance connector. The spark voltage was, therefore, determined by subtraction of the voltage drop due to impedance of the electrodes calculated from inductance and resistance. To estimate the voltage drop over the electrodes, the measured current for the discharge was used, and the inductance and resistance can be found from the copper property data. It is assumed that the capacitance of the electrode itself has no effect on the voltage measurement after breakdown. The capacitance only has an effect on the rate of voltage increase when the potential is initially applied at the electrodes, because the power supply charges or energizes the electrodes (capacitance of electrodes) before the breakdown. In addition, the capacitance of electrodes is very small, and the voltage increase before breakdown does not contribute to the energy supplied to the gas. This results in the effect of the resistance (16.8 μΩ) on the energy calculation being very small. As shown in Figure 6, there is no variation in the final delivered energy to the spark when the impedance is considered. The initial energy flows through the electrodes and then comes back to the power supply, due to the inductance that stores the electric energy. The negative voltage observed at the end of discharge can explain the back-flow of energy. If the resistance is significant, the measured final energy will be overestimated, because the resistance inside the electrodes thermally dissipates energy that, in the analysis, is assumed to be delivered to the spark. Therefore, the material of the electrodes is very important when conducting the estimation of electric energy deposition.

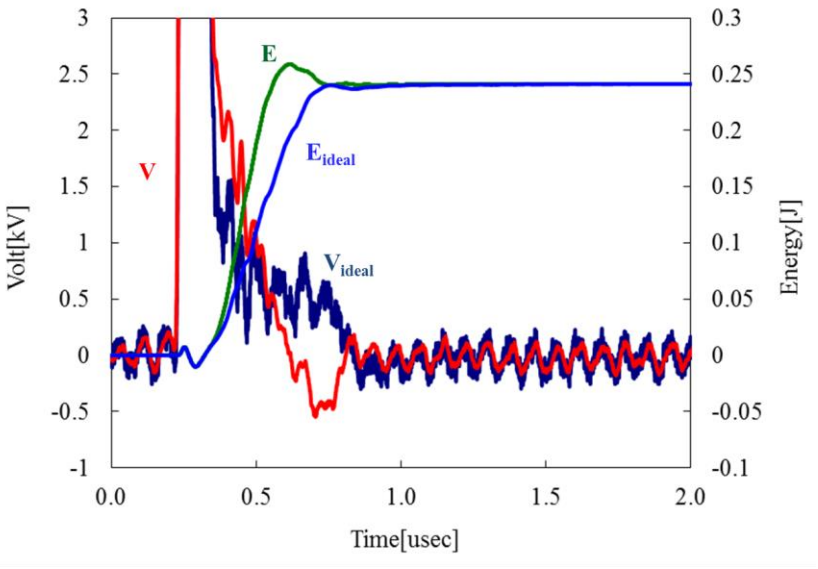

Figure 6. Influence of the electrode impedance on the voltage measurement and energy calculation of spark (the 'ideal' means that the value without the influence of the electrode impedance).

2.3 Premixed flow facility for spark kernel ignition

A test facility was developed to estimate the energy from a spark deposited into a gas flow and to observe the evolution of a spark kernel generated by a capacitive circuit. The facility consisted of a channel 19.1mm wide and 31.8mm high (Figure 7). Air or a fuel-air mixture were supplied through a section filled with steel beads (7.8mm diameter), and terminated using a perforated plate, which assured a uniform flow. This flow passed through a turbulence screen (48.2% blockage ratio, round wire, d=0.6mm) that was installed to control the turbulence level around the electrodes. The test section held a pair of tipped, co-linear copper electrodes, 3.2mm in diameter. It was fitted with a pair of quartz windows for optical access. The plasma kernel, once initiated by the spark discharge, was carried by the flow through a 127mm-long insulated channel of constant cross section. The flow rate could be adjusted to range from 8m/s to 40m/s mean flow velocity at the electrode gap. To quantify the level of turbulence, a hot-wire probe was

placed 1mm upstream of the electrodes. The turbulent intensity at the center of the spark gap was about 5% for both low and high-speed flows with the screen. An example of the velocity spectrum is shown in Figure 8.

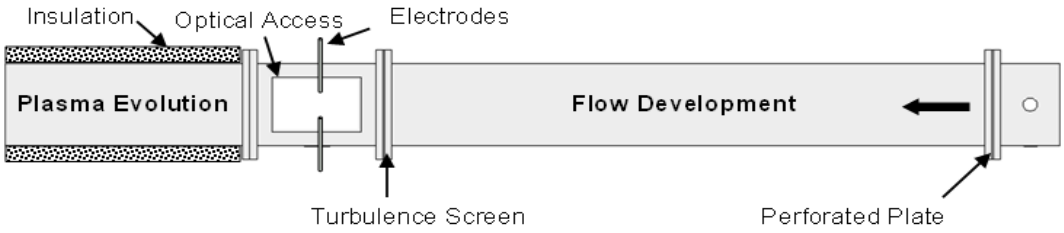

Figure 7. Flow facility for the short-duration spark ignition problem.

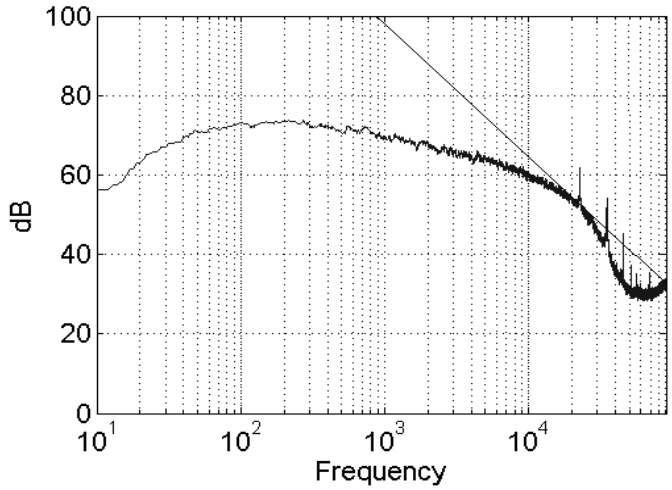

Figure 8. Velocity spectra for 33 m/s flow velocity with screen at the electrode (the peaks above 11 kHz are noise that can also be found under other flow conditions).

For premixed fuel-air experiments, the equivalence ratio was calculated from volumetric rotameter measurements for air and fuel. The rotameters were calibrated using a drum flow meter. As shown in Figure 9, the difference between the drum meter and the factory supplied rotameter general calibration is only 5.5% for air. After this calibration, the flow rate obtained using velocity integration was compared with the rotameter

reading for each velocity measurement to ensure accuracy. This calibration was repeated for the fuel flow meter with a 6% max difference with the drum meter.

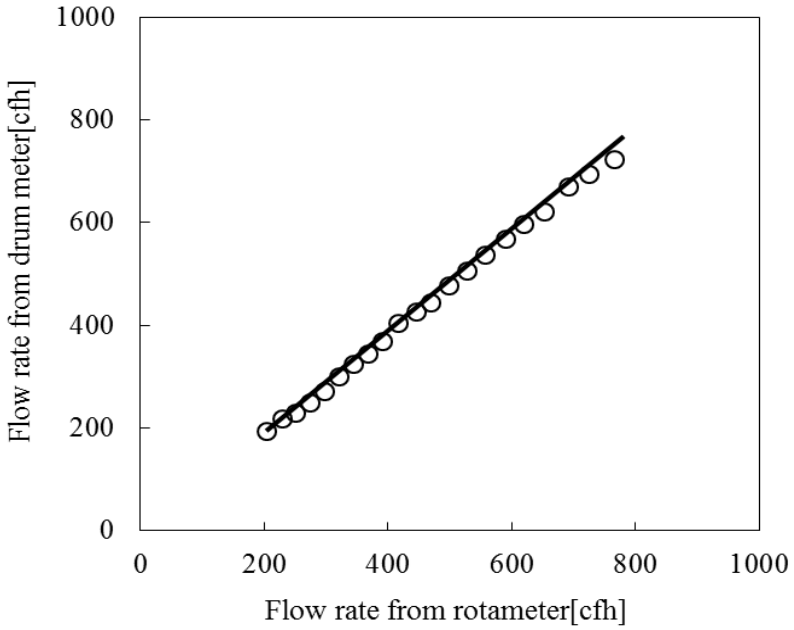

Figure 9. Comparison between flow rate from rotameter and drum meter, average error: 5.5% (the flow rate from the rotameter is based on the factory calibration).

2.4 Radical Jet Generator with inductive spark system

The effect of electricity on the combustion process is well established [100]. As early as 1970 arcs were used to stabilize flames [7]. Recently, researchers [17] have developed a RF plasma that can stabilize combustion in relatively high speed flows using the effect of radicals. This is inherently preferable because the effect of radicals on the stabilization of combustion is more efficient than that of heat and less electrical energy is, therefore, required. However, the techniques developed in those studies require complex and heavy electronic equipment, which is likely to be an obstacle in practical, aircraft related

applications. Therefore, a more traditional electrical system combined with a small dump combustor configuration was used in this study.

A relatively simple Radical Jet Generator (RJG, Figure 10) was developed that was able to ignite and stabilize a flame in a high-speed flow. A methane-air mixture entered the cavity of the RJG and was ignited with a high-frequency, long-duration and low-energy density spark. This spark was discussed earlier in this chapter. The hot, partially-burned products were injected into a main stream.

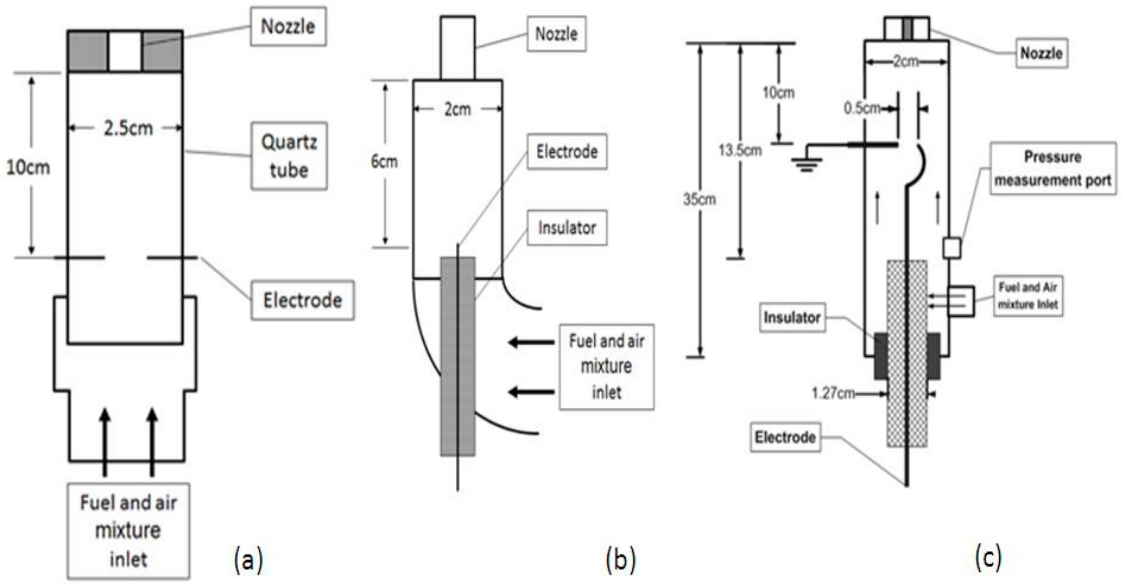

Figure 10. Schematics of the Radical Jet Generators.

Three types of RJGs were developed. The quartz tube RJG in **Error! Reference source not found.**(a) was used to take high speed images of combustion inside its chamber. The RJG in **Error! Reference source not found.**b has a step to attach the flame inside the chamber. Finally, the RJG in Figure 10(c) is fabricated out of steel and designed to endure the pressure build-up it experiences due to pulsations when operated at high flow rates. Quartz windows in the sidewalls provide optical access to this RJG. A

static pressure port allows the fluctuating pressure to be measured. The details of the RJG and its attachments to the main combustors are shown in Figure 11.

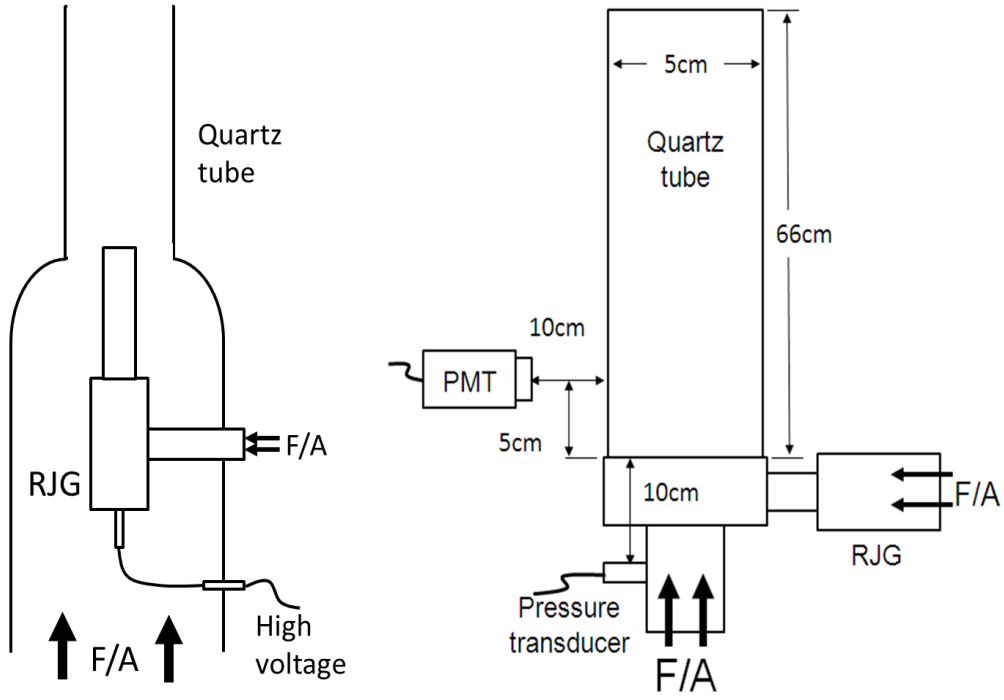

Figure 11. Attachments of RJG.

The RJG's performance depended in part on the depth to which the radical pool could penetrate into the main flow, which exceeds 100m/sec in a typical gas turbine application. This means that the jet issuing from the RJG into the cross flow needs to be fast. To increase the flow velocity, the exit nozzle of the RJG needed to be small. This small orifice, along with the combustion process inside the chamber, built up the pressure inside the RJG. To prevent the pressure propagation to upstream flow supply, a sonic orifice was installed upstream of the RJG's combustion chamber. The overall experimental configuration consisting of the RJG, the ignition system, and the

diagnostics is shown schematically in Figure 12. This configuration was built to investigate the combustion inside RJG.

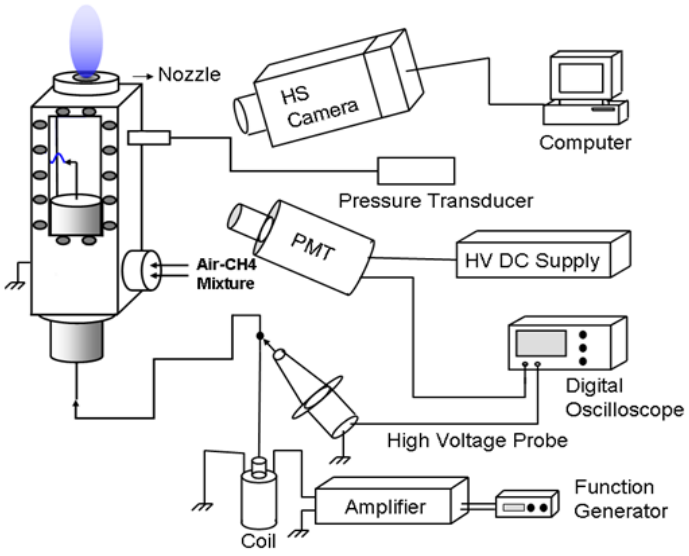

Figure 12. Measurements for RJG.

The heat release and pressure fluctuations in the RJG in **Error! Reference source not found.**(c) were recorded using a photomultiplier tube (PMT) and a pressure transducer, respectively. The PMT measured the spontaneous emission of OH from the reacting flow, which was assumed to be a measure of the chemical reaction rate, and, therefore, of the instantaneous heat release rate. The pressure transducer was mounted, in a semi-infinite tube configuration, 1.5m from the RJG in order to prevent it from overheating. This introduced a slight time delay that was corrected for during data processing, assuming actual room temperature in the tube.

The effect of the reactant flow on the high frequency spark and the resulting combustion process in RJG in **Error! Reference source not found.**(a) were observed

through the quartz window using a high speed Kodak Intensified Imager & EM Processor.

2.5 Methodology for measurement of deposited energy; calorimeter approach

2.5.1 Preliminary test for energy deposition from inductive spark

A RJG fabricated out of metal to sustain excess pressure fitted with insulated quartz tube as shown in Figure 13 was used to measure the energy deposited in the gas. It has a converging nozzle fitted to its exit and operates with a single electrode that discharges the electric current to the body. A thermocouple measured the temperature of the air heated by the spark at three points of the channel exit and an enthalpy balance was used to determine the energy deposited. Additionally, a calibrated resistor in line with the amplifier and ignition coil measured the current entering the amplifier. As mentioned earlier, measuring the current using a shunt resistor is not accurate, and there is high level of heat transfer through the electrodes when the duration of the spark is long. In addition, the electrical energy is measured far from the electrodes. Therefore, the energy deposition results for inductive sparks are not very accurate.

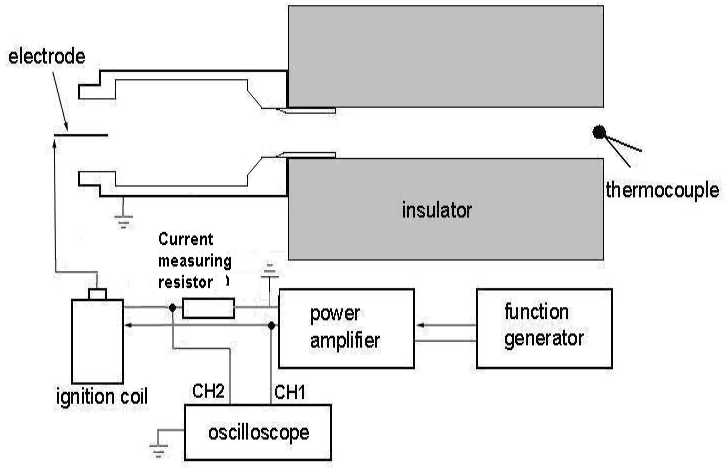

Figure 13. Setup for inductive spark power evaluation.

2.5.2 Energy deposition from capacitive spark

The amount of deposited energy in the gas flow must be accurately known in order to determine the initial conditions of the spark. In the experiment using capacitive spark, the deposited energy was estimated by firing a set of sparks and allowing the resultant kernels to move downstream in a channel until ions and radicals have relaxed into thermal energy and sharp gradients of temperature have smoothed out. The temperature and flow velocity distributions at the exit of the channel were then measured to determine the energy flux.

Velocity measurements

For low air velocity, the Pitot tube is a very accurate device for hot or cold gas flow velocity measurement as long as the temperature of the flow is also recorded. It consists of static and stagnation pressure ports, and a differential pressure gauge. The major source of error in measuring velocity is the pressure gauge that was used. Two different pressure gauges were used for low and high flow velocity measurement. The nominal error in the gauge is 1% of full scale and it resulted in a velocity error as shown in Figure 14. If it is used for the proper flow rate or velocity range, the error is low enough for measurement with a Pitot tube. The integrated flow rate obtained with the Pitot tube was within 5% of the value obtained using a carefully-calibrated rotameter.

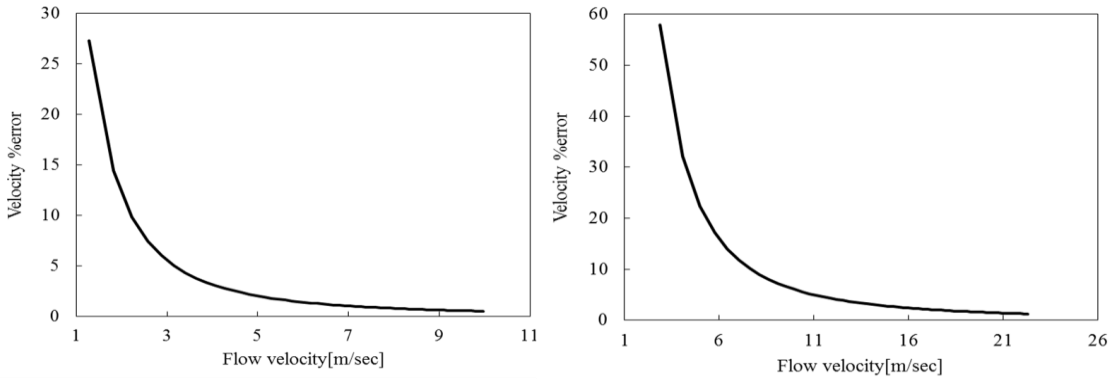

Figure 14. Velocity measurement errors of Pitot tube measurements for low (left, low pressure range gauge) and high (right, high pressure range gauge) flow velocity in the facility channel.

A grid for integrating the temperatures and velocities across the calorimeter tube exit was carefully chosen. It was observed that the velocity and temperature spatial gradients were high near the channel wall. Therefore, the velocity distribution in cold flow near the wall was measured by hot-wire technique with very fine spatial resolution and the results used to decide on the proper grid size. The final measurements were carried out using the Pitot tube, which has a lower spatial resolution than the hot-wire method. The profile (Figure 15) shows that the velocity increases exponentially near the wall due to the boundary layer and then increases linearly from around 3mm. Therefore, in this investigation, a finer grid was selected as the wall was approached.

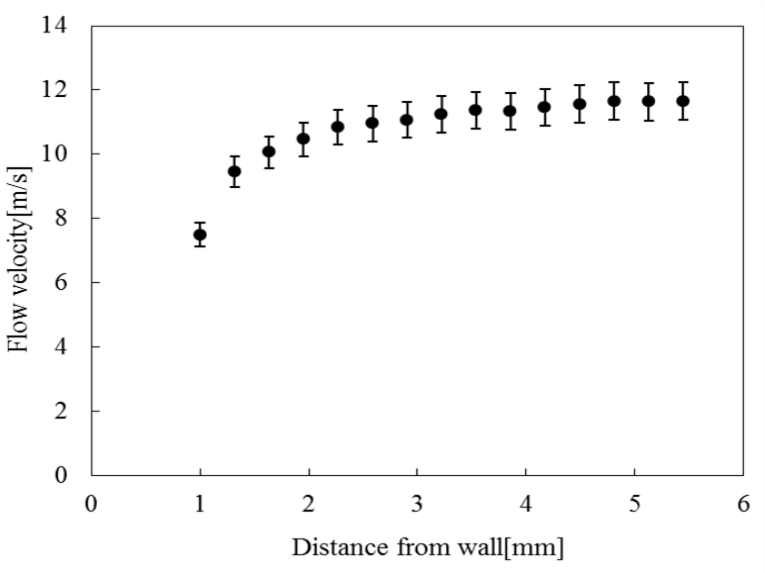

Figure 15. Velocity profile near the wall.

Temperature measurements

The temperature distribution was measured at the exit of the channel to accurately estimate the energy flux of the flow. For a discharge of 0.25J electrical energy across the electrodes at 300Hz and a 10m/sec flow and assuming a deposition efficiency of 100%, the estimated average temperature increase between entrance and exit plane is approximately 30C. This means that a thermistor must be used to provide the high-accuracy temperature measurement needed. The 44032 OMEGA thermistor has an accuracy of 0.1C in the -30C to 50C range. The thermistor's resistance varies with temperature. To measure and log the voltage in the DAQ, a certain level of current is applied to the thermistor. It is possible to increase the thermistor body temperature by self-heating which can result in a temperature measurement error. As shown in Figure 16, the estimated temperature error in range of the estimated operating temperature is sufficiently low.

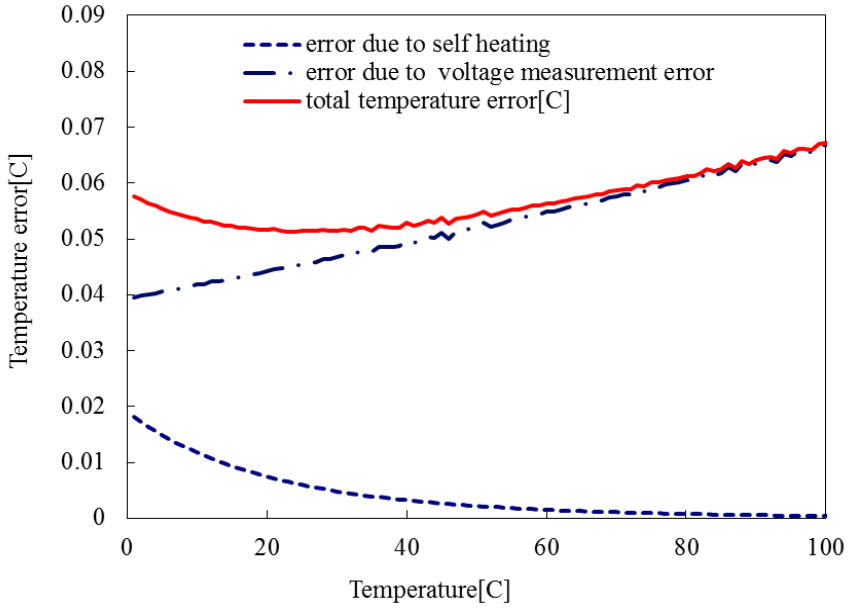

Figure 16. Thermistor temperature error due to self-heating.

However, this thermistor has a slow response and, therefore, cannot detect rapid temperature changes. The spark pulse duration is about 1μsec and repetition rate is up to 300Hz. This causes rapid changes in flow temperature which the thermistor cannot follow. Therefore, the thermistor measures only time averaged values, and an analysis had to be conducted to confirm that the actual average temperature is close to that measured.

In a simple analysis of the temporal response of the thermistor, the conductive heat transfer through lead wires was neglected because the lead wire had a diameter of only 0.2mm (Figure 17).

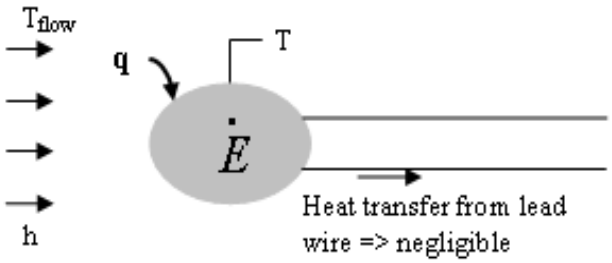

Figure 17. Heat transfer model for thermistor, T_{flow}: flow temperature, T: thermistor temperature, h: convective heat transfer coefficient.

In addition, the temperature distribution inside the solid thermistor bead was neglected. The calculated Biot number was 0.004, which means that conductive heat resistance in the solid was much smaller than convection over the bead. Therefore, the temperature could be assumed to be uniform throughout the solid bead. The energy transferred to the bead of the thermistor results in a temperature increase in the thermistor, according to Eq. 2.2.

$$-hA(T - T_{flow}) = \rho Vc\frac{dT}{dt} \tag{2.2}$$

where h, A, c, V, T and T_{flow} are the heat transfer coefficient, surface area, specific heat, volume, thermistor temperature and flow temperature.

As mentioned earlier, 0.25J sparks were pulsed at a rate of 300Hz. The spark raises the temperature of the flow significantly which produces steep temperature gradients. However, these gradients smooth out significantly by the time the kernel has convected 5" downstream to the measurement location. For this analysis the temperature distribution was, therefore, assumed to be sinusoidal at the measurement location, where the local temperature (T_{flow}) is given by

$$T_{flow} = T_a + \frac{\Delta T}{2}(1 - \cos wt) \tag{2.3}$$

where T_a is ambient temperature and ΔT is the amplitude of the temperature fluctuation. If

$$\theta \equiv T - T_{flow} \tag{2.4}$$

Eq.2.2 can be rewritten using Eq.2.3 and Eq.2.4 as

$$\frac{d\theta}{dt} + \frac{A}{\rho Vc} h\theta = -\frac{w\Delta T}{2} \sin wt \tag{2.5}$$

Let $m \equiv \frac{\rho Vc}{A}$ then Eq.2.5 becomes

$$\frac{d\theta}{dt} + \frac{h}{m}\theta = -\frac{w\Delta T}{2} \sin wt \tag{2.6}$$

A simple ODE, whose solution with proper initial conditions is

$$T = T_{flow} - \frac{w\Delta T}{2} e^{-\int \frac{h}{m} dt} \int e^{\int \frac{h}{m} dt} \sin wt dt \tag{2.7}$$

If the convective heat transfer coefficient, h, were to be constant, the average temperature of the thermistor, $\overline{T}$, and of the flow, $\overline{T_{flow}}$, would be equal. Unfortunately, the convective heat transfer coefficient is a function of Reynolds number and temperature. Therefore, Eq.2.7 had to be solved using a numerical method after the convective heat transfer coefficient has been calculated as a function of the Nusselt number.

It might be more realistic to represent the flow temperature as a series of pulses, rather than a sinusoid. For the pulse temperature model, Eq.2.3 was then replaced by a pulsing temperature profile before it was solved numerically. Figure 18 shows how the

temperature measured by the thermistor adjusts after having been inserted into a flow with pulsating temperature as predicted by the model.

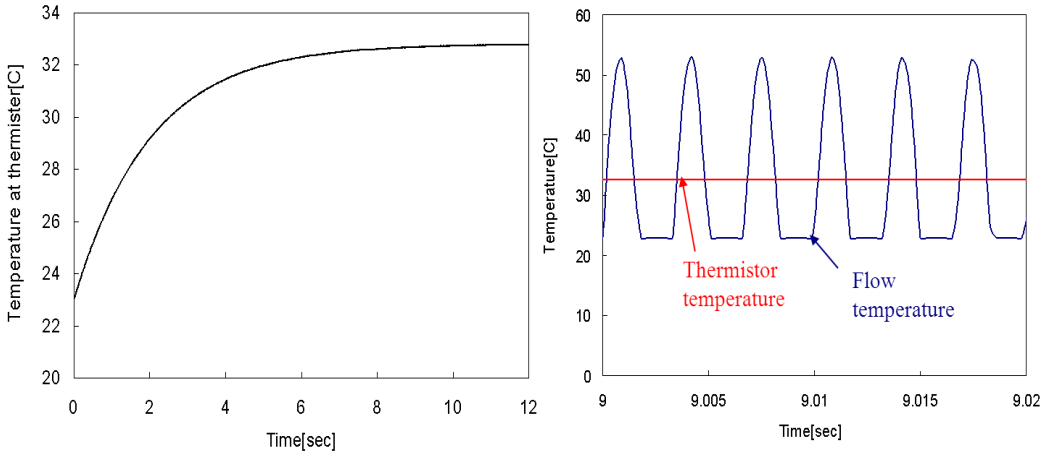

Figure 18. Calculated thermistor temperature based on the model on LHS, the simulated flow temperature and calculated thermistor temperature during steady state of thermistor temperature on RHS (flow temperature fluctuation: 30C @300Hz).

The thermistor temperature approaches the steady state after about 15 seconds, and the difference between the average temperature of the flow and that of the thermistor was calculated to be only 0.3C under typical operating conditions (10m/s flow velocity, 300Hz spark pulsation and 30C temperature fluctuations).

During actual energy deposition measurements, the temperature was only recorded after 60sec in case the neglected heat losses by conduction through the lead wire delayed the temperature from reaching a steady state. To reduce heat losses to the flow channel it was insulated with fiberglass.

The thermistor is a passive sensor and the variation of its resistance was monitored by measuring the voltage change across it in a circuit with a constant current power

supply. It was difficult to measure the signal from the sensor because EMP noise generated by the spark interfered with the data acquisition since the sensor acted as an antenna. Using an IEEE 802.11g Wi-Fi connection significantly reduced the high voltage noise from the spark. In addition, the known spark frequency was filtered out so that the EMP noise could be removed.

The upstream and downstream temperatures of the flow were measured and used, along with local velocities, to compute the increase in thermal energy of the gas due to the spark discharge. As shown in Figure 19, the thermal energy flux was determined by integrating the local product of velocity and ΔT across the exit area of the duct, see Eq.2.8. The air was assumed to be calorically perfect because of the small temperature range. The measurements carried out to determine the energy transfer into the flow include the temperature of the thermistor, the flow velocity, the calculated density and the electrical current and voltage. Each of these has its own uncertainty. These are cited in Table 1. These quantities were used to determine the electrical and deposited power using Eq.2.8 and Eq.2.9. Eq.2.10 was used to calculate the energy deposition efficiency η_{dep}. Measurement errors in these calculations propagate throughout the analysis. The resultant errors in the power and the efficiency were determined using techniques outlined in Ref [101]. The results are also cited in Table 1.

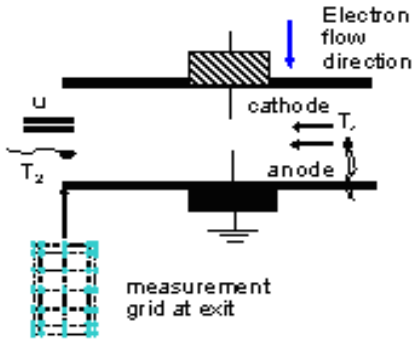

Figure 19. Calorimeter approach for energy deposition estimation.

$$\Delta P_{thermal} = c_p \int_{exit} \rho u (T_2 - T_1) dA \tag{2.8}$$

$$\Delta P_{electric} = \frac{1}{f} \int_{pulse} VIdt \quad \text{where f is spark frequency} \tag{2.9}$$

$$\eta_{dep} = \frac{\Delta P_{thermal}}{\Delta P_{electric}} \tag{2.10}$$

Table 1. Uncertainties for calculation of energy deposition efficiency. 33m/s flow speed. 300Hz spark frequency.

Measurements	Uncertainty[%]
Temperature	3.2
Density	0.07
Flow velocity	0.5
Area of measurement grid	0.2
Voltage(high voltage probe)	3
Current(current probe)	1
Propagated uncertainty in thermal power estimation of gas	3.2
Propagated uncertainty in electric power estimation of spark	3.2
Propagated uncertainty in efficiency of energy deposition estimation	4.5

2.6 Optical measurement (chemiluminescence)

For a closed system, the ignition delay is often measured using temperature or pressure time traces [102]. The temperature also rapidly increases with exothermic reactions. However, sufficient time is required to measure the temperature of the gas, because normal temperature sensors have a relatively long response time due to the thermal inertia of sensor. This time required to transfer heat from the gas to the sensor cannot be expected in the flowing gas.

For ignition of a flowing gas in an open channel, temperature or pressure measurements to detect ignition are not practical because the channel does not contain the pressure and the ignited flame moves with the flowing mixture. Therefore, $OH^*(A^2\Sigma^+ – X^2\Pi)$ chemiluminescence is used to detect the combustion process because OH* is an important combustion intermediate and produces strong emission intensity. This radiation from the reaction zone is due to changes in electronic states of the molecules. According to research into the combustion of hydrocarbon and hydrogen fuels [103, 104], the excited state OH* is formed and disappears through the following reactions (R1-R4).

$$O+H+M \rightarrow OH^*+M \quad \text{(R1)}$$

$$CH+O_2 \rightarrow CO+OH^* \quad \text{(R2)}$$

$$OH^*+M \rightarrow OH+M \quad \text{(R3)}$$

$$OH^* \rightarrow OH+ h\nu \quad \text{(R4)}$$

where hν is the energy of a photon.

Two chemiluminescence techniques for ignition detection were applied in this study. First, emission from OH* radical was allowed to pass a band pass filter (center wavelength is 308nm) and then detected with a Photomultiplier Tube (Hamamatsu

R928). According to the user manual of the PMT, the tube has a 2.2nsec response time. This is the time needed for the signal to rise from 10% to 90% of the peak amplitude, when the entire photocathode is illuminated by a "delta function" light pulse. The spectral response is high from 185nm to 900nm and the maximum quantum efficiency ranges from 200nm to 400nm. The length of the channel from the spark electrode to the exit is 50.8cm and the spark is discharged with a frequency from 20Hz to 300Hz. Therefore, if the detected region by PMT is not adjusted properly, it can detect multiple flames or the kernel can leave the region before ignition has been completed. The PMT must 'see' the region shown on the left side (Figure 20) because we are interested in ignition times up to about 2msec after the discharge and the kernel convects with a flow speed that is typically 22m/sec.

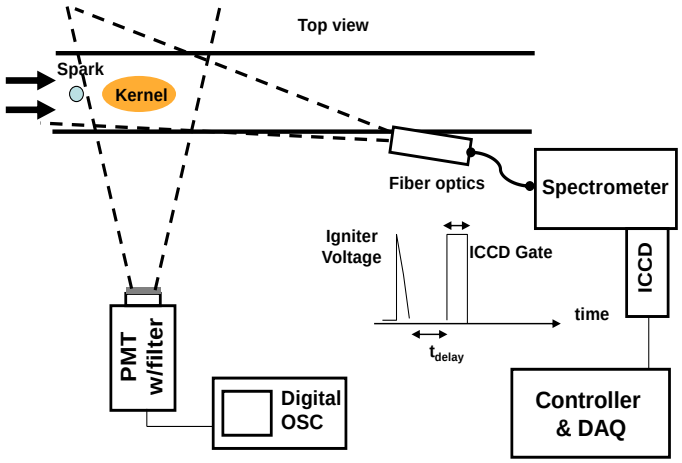

Figure 20. Detected region by PMT and spectrometer.

This PMT with filter can only detect small wavelength range. In addition it has difficulty measuring the absolute level of the OH signal because it detects that signal as well as emission features that have overlapping wavelengths. Right after the discharge,

the species produced by electron impact emit high intensity light. Therefore, we used a spectrometer to identify the species produced by the high-energy spark. The radiation was collected by an optical fiber with a numerical aperture of 0.22 that was connected to a spectrometer (Acton Spectra-Pro 300i, with 300grooves/mm grating), fitted with a 16 bit, 1024×256 intensified CCD camera(PI-MAX, 25mm intensifier). The fiber optics 'views' the electrodes at an angle and from a distance because the detection area must be long enough to contain the expanding and moving ignition kernel. The spark power supply delivers a very stable energy per spark pulse, but there may be some randomness during the ionization by electron impact inside a very high order electrical field. These ionization characteristics were investigated by monitoring the intensity of the copper signal for each discharge. This copper signal originated from the electrode material and shows randomness as shown in Figure 21. However, the spectra used for the ignition delay analysis were averaged over 100 independent spectra to eliminate the randomness.

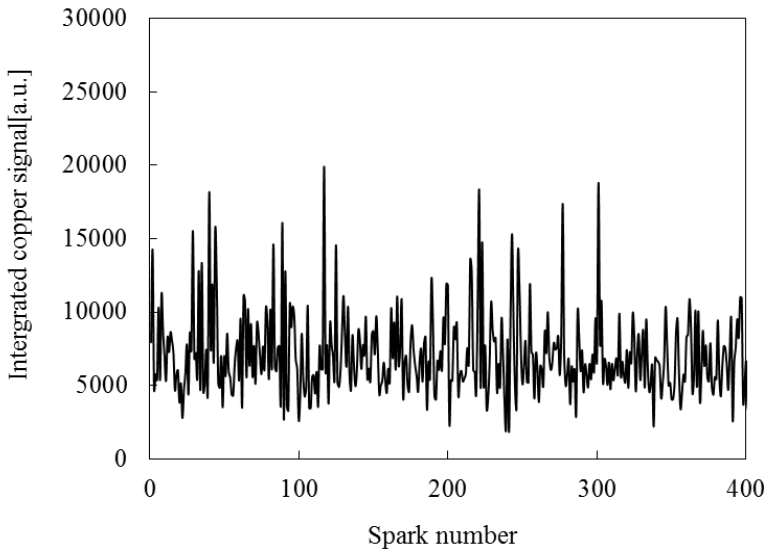

Figure 21. Integrated copper signal intensity (arbitrary unit) change at 20usec after the spark. It is integrated over the copper emission range (313-329nm).

The light intensity is very high right after the spark and then rapidly decreases with time. Therefore, variable exposure times were used to improve the signal-to-noise ratio and the signal scales were adjusted depending on the intensity level of the OH* signal during the time trace.

2.7 Electrical interference from the capacitive spark

An accurate measurement of voltage and current is essential for estimating the amount of energy delivered to the discharge. Most research reports do not mention the methodology and accuracy of the electrical energy measurement. In circuits with ordinary voltage levels, high accuracy in measurement can be attained with common data acquisition boards. However, most spark systems, except for arc discharges, generate high voltage and high current if the system can supply enough current. Industry standard high voltage probes can measure the high voltage with a high degree of accuracy but the current must be measured with care. The current is typically measured by determining the voltage across a shunt resistor in the wire. For high voltage applications, this method, without isolation, is not feasible due to ground potential change during the discharge. It is possible that a surge is generated by the high-power device i.e. spark power supply. Another possibility is that some portion of discharged electric energy penetrates into the grounded parts such as the test bed etc. This noise in the ground cable could affect the measurements that share the ground with the power supply. Therefore, for the capacitive spark, the noise was minimized by isolating the current monitor from it. There are several types of current monitoring systems with isolation such as a transformer meter, Rogowski coil, and Hall Effect sensor [40]. We selected the transformer type current monitor that is

manufactured by Pearson Electronics, Inc. model 6600. It has a response rising time of 5nsec, which is enough for spark current rising characteristics.

The phase between voltage and current can affect the calculation of the electric energy. The current monitor is installed close to the electrode but the signal cable is about 3m long. This results in a nano-second transmission delay. In addition the voltage probe generates its own delay. Therefore, a correction for those transmission delays was applied after they were determined with an impulse signal generator and digital oscilloscope. The delay between the voltage and current signal was 5nsec. This time lag was applied for all VI energy estimates. This relative delay is not very dependent on the rise time of the voltage or the current. However, for the current monitor, the placement of the wire connected to the electrodes had an effect on the measurement for very fast rising currents (faster than 120nsec). If the wire is placed near the edge of hole of the sensor, it shows 4nsec lag or lead-time (see Figure 22).

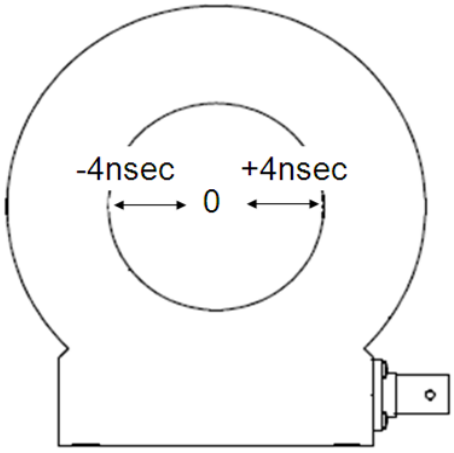

Figure 22. Transformer type current monitor (time lag and lead for fast rising current).

Direct electrical noise from the spark as well as the ground change by the discharge were expected because the DAQ measures relatively low signal voltages generated in the connection wire or circuit board by the electromagnetic interference from the high voltage spark (up to ~25kV). There are always wire connections from sensors to the DAQ. These connections pick up the impulse noise with same frequency as the spark discharge as shown in Figure 23.

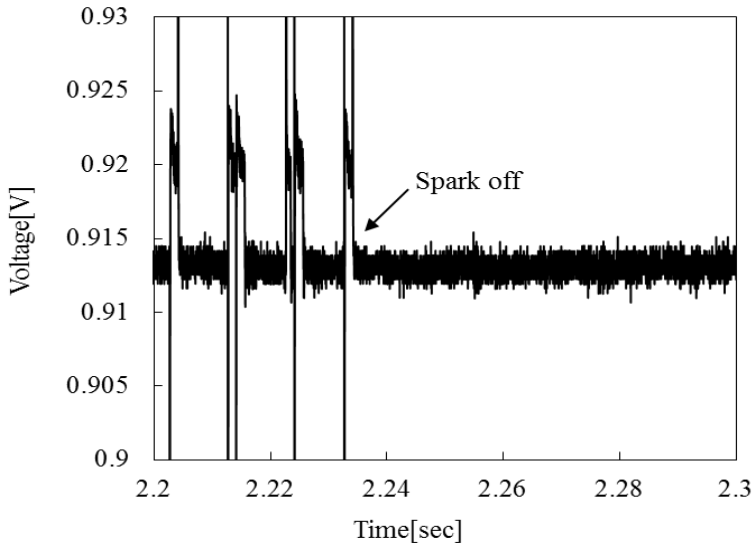

Figure 23. Noise from the electromagnetic interference within the connection wire and thermistor probe (sparking at 100Hz).

The experiment was conducted with a thermistor heated up to a similar temperature as that of the actual temperature in the energy deposition measurements. Fortunately, the signal level between the impulses was not affected by the sparking, see **Error! Reference source not found.**. Due to this characteristic, the temperature signal between the pulses could be used after some post processing.

CHAPTER 3: ELECTRICAL CHARACTERIZATION OF SPARKS (CAPACITIVE AND INDUCTIVE SPARK)

3.1 Inductive spark

This spark is generated by the circuit shown in Figure 4 of Chapter 2. An AC signal input causes the voltage at the secondary side of the transformer to alternate between positive and negative. During each cycle, the electric high potential causes a breakdown of the gas which results in the formation of a highly conductive channel (see Figure 24). The voltage drops rapidly at the end of each discharge because the power supply applies a reversely polarized voltage at the end of each cycle. A new discharge then immediately follows. The breakdown voltage for this type of spark train is less than that of a single capacitive spark with a similar inter-electrode gap.

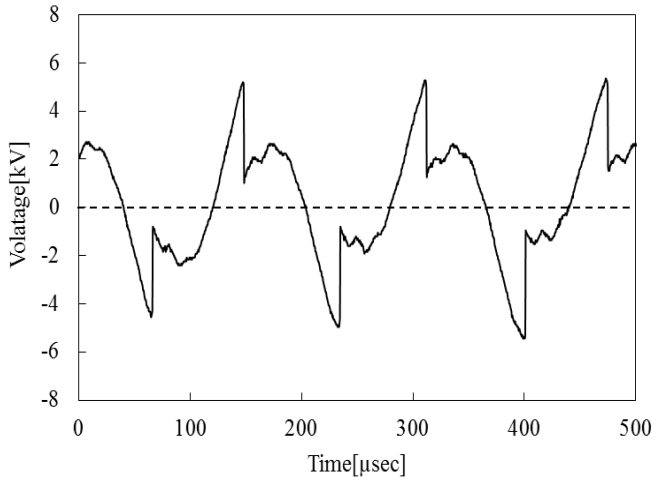

Figure 24. Typical voltage characteristics of the inductive spark (flow velocity: 5m/s).

3.1.1 Flow effect

For long duration sparks, where the time scale of the spark duration is comparable to that of the flow, each channel is convected downstream by the motion of the flow, see

Figure 25. As Swett (1956) observed, that variation of the spark channel affects the discharge voltage [105]. The rapid firing of consecutive discharges resulted in remnants of the previous discharge remaining between the electrodes. Because the breakdown voltage is highly dependent on the properties of the gas between the electrodes, the next spark then followed the partially ionized path of least resistance. The voltage increases as the length of channel is stretched. Eventually the ionized channel becomes too long to be maintained by the available voltage and breaks. The cycle then repeats and a new short channel is created between the electrodes. Because of the sinusoidal inputs that generate these long-duration sparks, a spark channel exists most of the time.

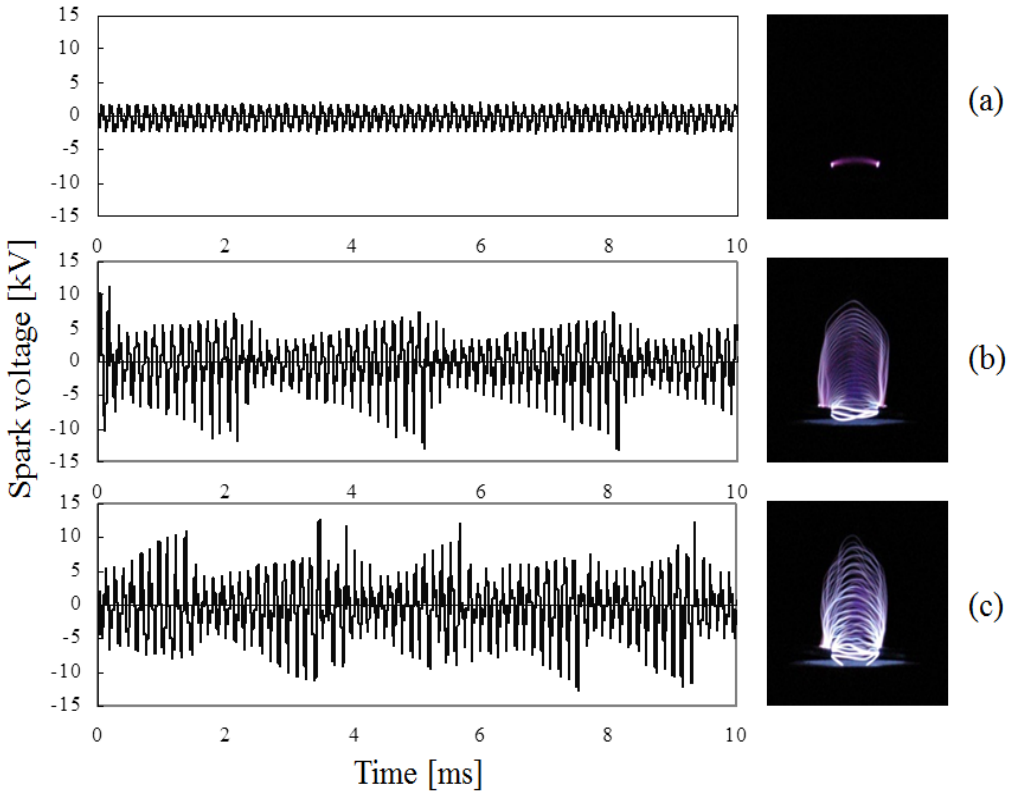

Figure 25. Effect of flow on a long-duration spark. Quiescent or low velocity flow: stationary discharge channel (a); higher velocity flow: spark channel convects before short channel is recreated (b) and (c). There are similar voltage variations in both the flammable mixture and pure air. Flow velocities [m/sec] :(a) 0 (b) 4.57, (c) 9.48.

3.1.2 Flame effect

In addition to the flow velocity effect, the equivalence ratio of the flowing gas can influence the electrical energy in the spark. In other words, if the equivalence ratio is within the range where ignition can occurs and a flame is stabilized near the electrodes, the energy delivered to the electrodes increases, as shown in Figure 26. Adding fuel has no effect on electrical energy delivery as long as the flow is leaner or richer than the limits at given condition. According to prior research concerning ionization in combustion [106], ions exist in the flame due to several different chemi-ionization processes. If the ionization potential is low enough for a reaction with the intermediates to occur, and the products or the neutral species have a very high kinetic energy (R5), ionization can occur thermally. However, the ion concentration observed in the flame in the prior research [106] is much lower than that calculated for thermal ionization assuming equilibrium. Other ionization processes are ionization by impurities and carbon particles in the soot region of the flame. An alkali metal can be involved in ionization, such as in reaction (R6). Conversely, carbon particles are involved in the ionization process in the soot region. For example, the heavy polycyclic aromatic participant in reaction (R7) is formed via ionization in the soot region of the flame. This increase in electrical energy delivery is observed when the spark discharge is continuous because ionized species from an earlier flame are convected or diffuse back into the spark discharge region. Therefore, the energy consumption in the flame zone should be considered in the design of an ignition system using a long duration spark or a continuous discharge.

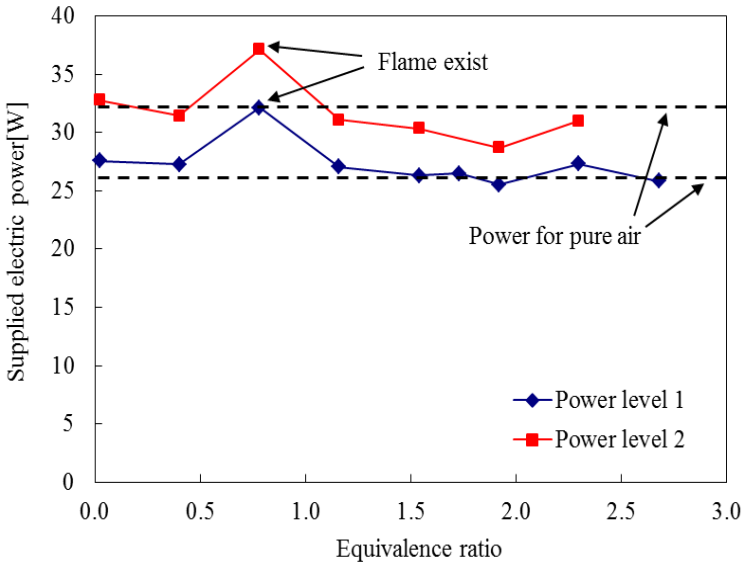

Figure 26. The power used by the spark (measured in the primary side of the coil) vs. ER (flow rate is 72cfh). The power for air-only flow is 26.4 and 32.8 Watts for power level 1 and 2, respectively.

$$CH+O \rightarrow CHO^{+} + e^{-} \quad \text{(R5)}$$

$$Pb+OH^{*} \rightarrow PbOH^{+} + e^{-} \quad \text{(R6)}$$

$$C_{16}H_{10}+C_{6}H \rightarrow C_{22}H_{11}^{+} + e^{-} \quad \text{(R7)}$$

3.2 Capacitive spark

The short-duration spark was selected to investigate the spark characteristics, because the electrical characteristics of the long duration spark were shown to be affected by the flow field. The voltage and current time traces for the short duration spark were measured and used to determine the spark duration and energy. Typical voltage and current waveforms are shown in Figure 27. The electrical breakdown of the flowing gas occurs within 100ns after applying the high voltage between the electrodes. Paschen's law, shown as Eq.3.1, provides an estimate of the breakdown voltage (V_{bd}), which agreed well with the measured value. After this phase, a period of high current was observed,

accompanied by a relatively intense emission of radiation. This emission increases with increasing the current. Most of the energy was deposited into the flow at this time. Essentially all 250mJ of electric energy was discharged within 0.5usec. The energy supplied to the electrode has a 5% RMS variation for a given setting (Figure 28).

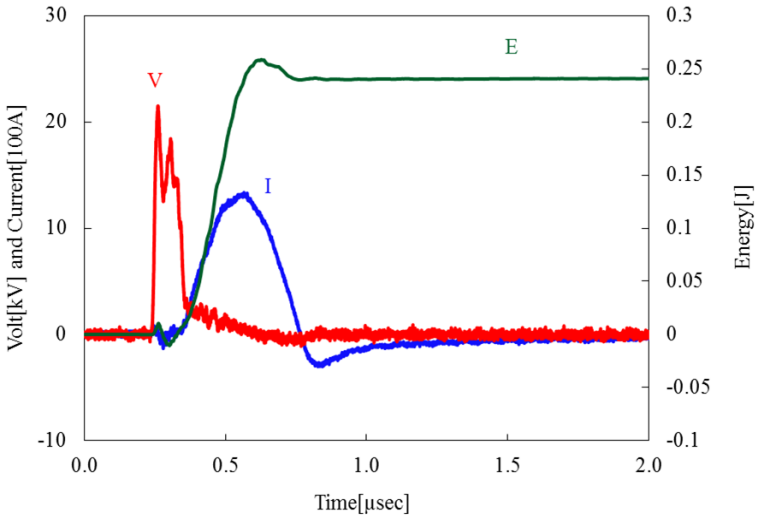

Figure 27. Voltage, current and energy trace of the spark.

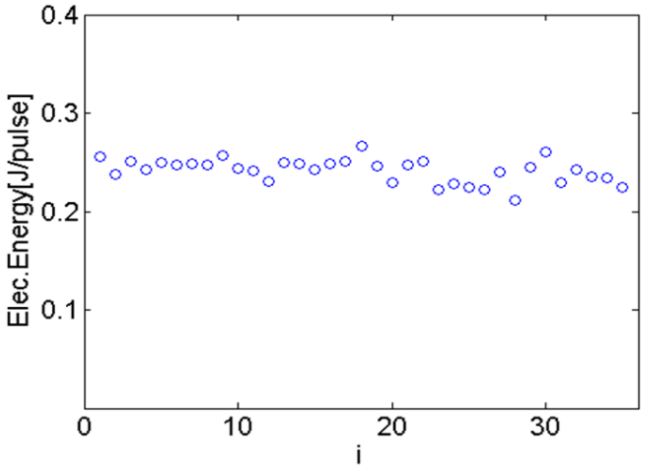

Figure 28. The energy variation of shot to shot sparks.

$$V_{bd} = 30d + 1.35[kV] \sim 21kV \text{ where d=0.64cm} \quad (3.1)$$

The behavior of the discharge as witnessed through the V-I characteristics depends on the type of discharge. It can take the form of a breakdown, an arc or a glow discharge. Initially, the air or fuel-air mixture has a very high electrical resistance. An electric field produced by an applied high voltage between the electrodes, accelerates the electrons. These electrons collide with the gas molecules, producing ions and additional electrons leading to breakdown.

As shown in **Error! Reference source not found.**, the current increases very slightly when the voltage is initially applied. Then the current remains constant as the voltage increases to around 20kV. During this stage, if the voltage is not maintained, the discharge cannot go to next stages. This saturation lasts until the electrons supplied by the cathode cause a sufficient number of collisions to ionize the gas. After this phase, the inter-electrode resistance calculated from measured voltage and current is radically decreased, as shown in Figure 29. The spark then transitions into the arc discharge mode, which is characterized by a falling of potential ~100-400V, intensive light emission, and a high current density [108]. The duration of this mode is much longer than that of the breakdown mode. Therefore, the heat loss by conduction to the electrode must be considered here. This loss is also affected by the shape and material of the electrodes. During the breakdown of the gas, the properties of the gas determine the VI characteristics. However, once the gas is ionized, the VI characteristics depend on the power supply circuit components. Therefore, an RLC circuit analysis can provide an estimate for the duration of the high-current mode that occupies most of the spark duration.

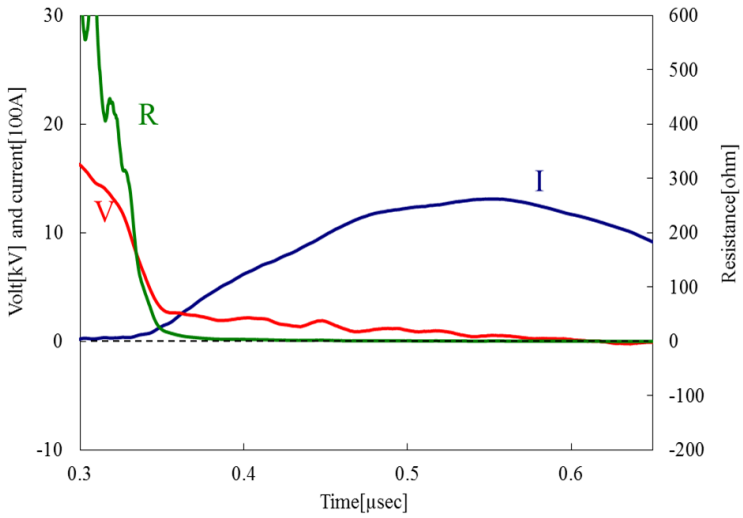

Figure 29. Temporal change of the resistance of the gas between the electrodes after breakdown voltage is applied.

As explained in the experimental setup section, the power supply amplifies the voltage applied between the electrodes via an electrical resonance circuit that includes an inductor and capacitors. Once the Thyratron is triggered by an external pulse generator, the inductor inside the power supply is no longer involved in the discharge process, and the circuit consists of transmission wires and capacitors only. Therefore, the power supply can be modeled as a capacitor and an inductor representing the inductance of the transmission wire, as shown in Figure 30. Based on the circuit analysis ($E_c = \frac{1}{2}CV^2$), the stored energy in the capacitor C_{system} is 3.4 Joules. However, the measured discharged energy is much lower (0.25 Joules). If the electrical discharge energy is estimated from the energy stored in the capacitor as has been suggested by some previous investigations [29, 109, 110], this will result in a huge error.

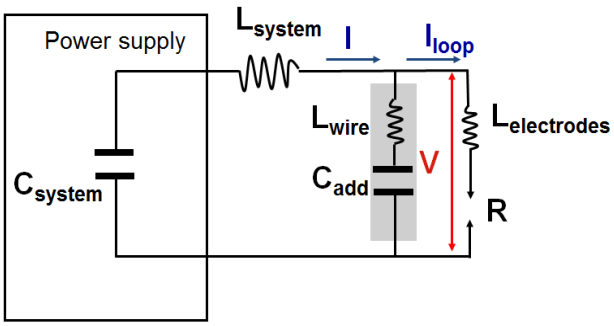

Figure 30. Connection for increasing spark energy.

Spark duration depends on the inductance and capacitance in the circuit. The calculated inductances of the transmission wire and the electrodes are about 1700nH and 110nH respectively as determined using Eq.3.2 and Eq.3.3 [111]. Based on the known capacitance and inductance, the duration of the spark is estimated to be about 1 µsec, which is similar to the measured current duration (**Error! Reference source not found.**).

$$x = \sqrt{1 + \left(\frac{d}{2l}\right)^2} \tag{3.2}$$

$$L = 2l\left[\ln\left(\frac{2l}{d}(1+x)\right) - x + \frac{\mu}{4} + \frac{d}{2l}\right] \tag{3.3}$$

Where d, ⌊ and µ are wire diameter, length and permeability.

3.2.1 Increase of spark energy

To increase the electrical energy delivered to the gas, a capacitor (C_{add}) is added in parallel near the electrode gap (as shown in **Error! Reference source not found.**). Alternatively, the capacitor (C_{system}) inside the power supply can be replaced with one with a larger one. Adding this capacitor assists us in understanding the microsecond discharge circuit, and allows us to investigate the energy deposition characteristics of the

higher electrical energy. If a second capacitor is added, the total capacitance increases, and the spark duration is changed.

First of all, we added a 1nF capacitor in a parallel near the electrodes as shown in Figure 31. The theoretical energy increase resulting from this configuration was estimated to be about 0.2 joules. However, the measured spark energy increased by only 0.08 joules. In addition, the voltage slope prior to breakdown was less steep than that without the additional capacitor. This occurred because the power supply needed to charge the added capacitor. The measured slope of the voltage was well matched to that estimated using the IV relationship ($i = C\frac{dV}{dt}$) and the measured current. It was expected that there would be a high-frequency oscillation of current in the loop created by addition of the capacitor. The estimated frequency oscillation ($f = \frac{1}{2\pi\sqrt{LC}}$) based on the calculated inductance of wire and electrodes inside the loop was about 9MHz. The measured frequency was about 9.5MHz.

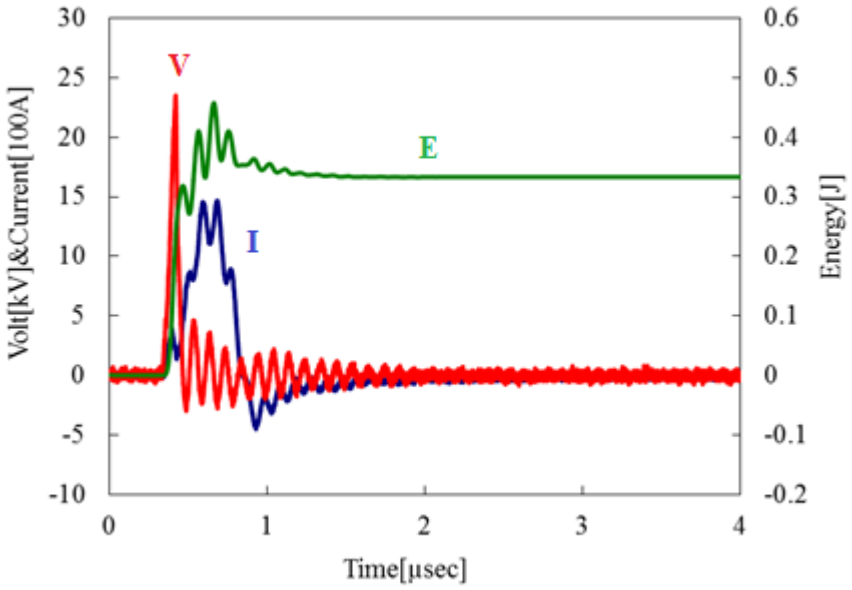

Figure 31. VI time trace after adding 1nF capacitor in parallel with electrode gap.

Practically, the voltage probe cannot measure the voltage across the spark only because it is not possible to install it directly across the spark channel. However, if the gap between the electrodes is modeled as a pure resistor and the inter-electrode gap has no capacitance, we can calculate that voltage if we know where the voltage probe is installed. The spark voltage based on the inter-electrode resistance (R), the inductance of the electrodes ($L_{electrode}$) and the measured current to the electrode (l_{loop}), is very similar to that measured during the later phase of the spark. However, there is a huge error during the breakdown stage (Figure 32). Based on this result, we can surmise that the inductance of electrodes is a time-dependent property and/or a gap capacitance exists early in the discharge.

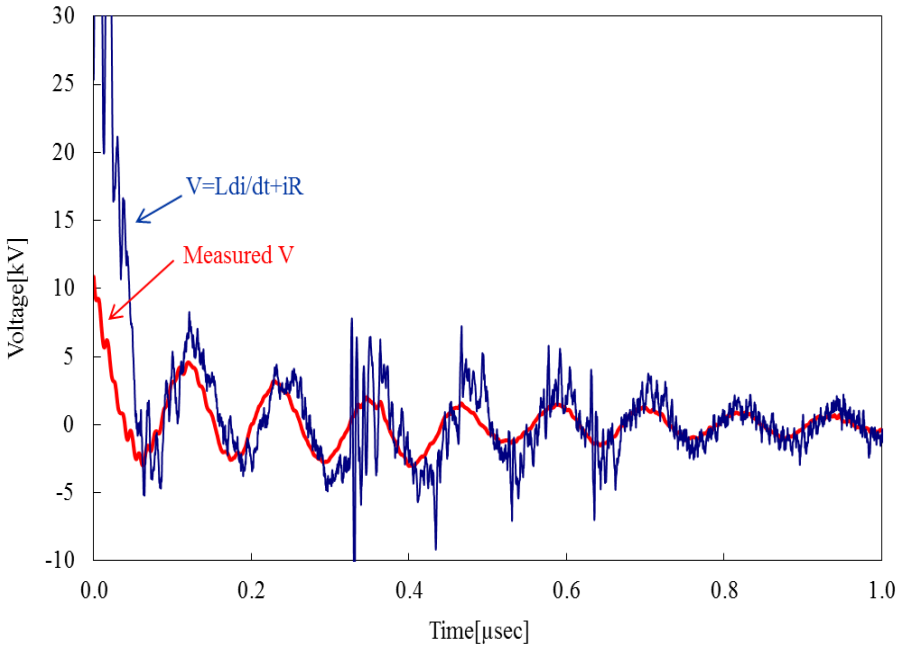

Figure 32. Comparison between the calculated voltage and the measured voltage.

$$V_{electrode} = L_{electrode}\frac{di_{loop}}{dt}, V_{gap} = i_{loop}R \quad (3.4)$$

$$V = V_{electrode} + V_{gap} = L_{electrode}\frac{di_{loop}}{dt} + i_{loop}R \quad (3.5)$$

To increase the spark energy without the high-frequency oscillation, the capacitors inside the power supply were replaced with a higher capacitance (30nF). There is no high-frequency component because the loop near the electrodes which was formed when additional capacitors were added is not present. The current after breakdown increases and more energy (0.57J/pulse) can be delivered due to the increased current. However, the duration of the current is increased by about 40% (Figure 33).

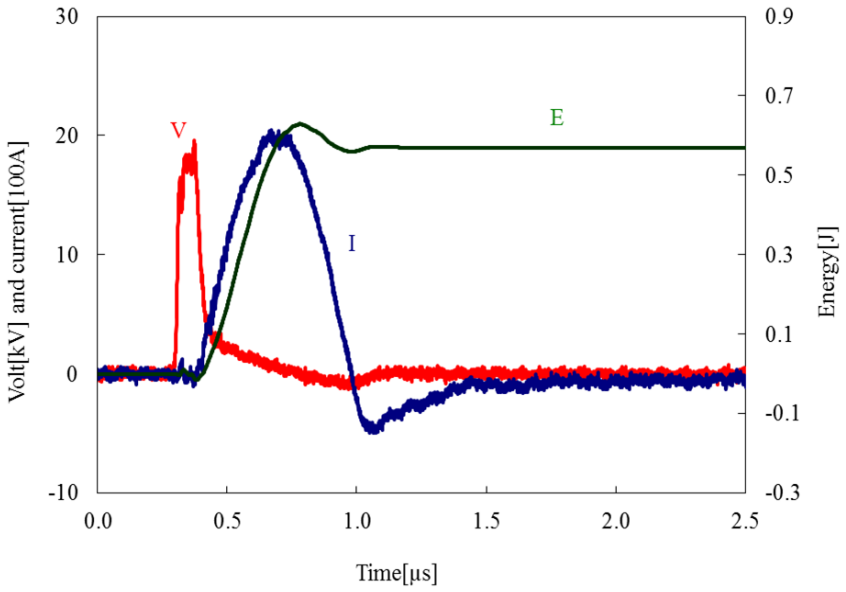

Figure 33. VI characteristics with installation of 30nF capacitor inside power supply.

3.2.2 Flow effect

Due to the characteristics of short-duration spark, the discharge is little affected by flow conditions, which stands in contrast to the inductive spark. As mentioned earlier, the inductive and continuous sparks are affected by the flammability of the mixture. This flammability effect was also investigated for the capacitive and non-continuous sparks (Figure 34). The breakdown voltage of the discharge for an equivalence ratio 1.3 mixture (flammable mixture) was slightly higher than that of the discharge in air only. However,

the voltage difference was within the shot-to-shot breakdown voltage variation. Despite the limited effect of fuel on the electrical characteristics, the probability of achieving a successful electrical discharge in the fuel-air mixture is much lower than in air only. The permittivity of air in the gas phase is not very different from methane [112]. If we compare the ionization energy of CH_4 to that of air, the order of ionization energy is N_2:15.58 > CO_2:13.78 > CH_4:12.6 > O_2:12.07eV [113]. Therefore, ionization and permittivity cannot explain the reduced discharge probability in the fuel-air mixture.

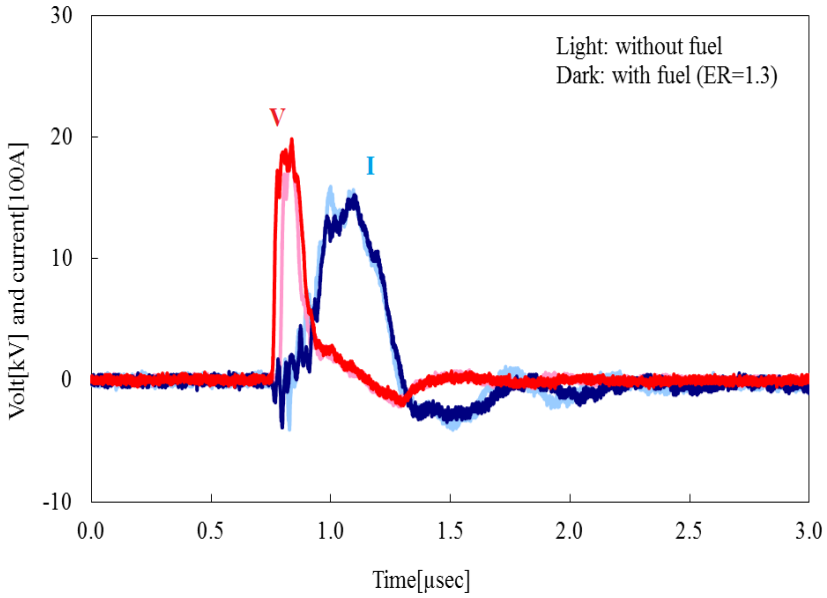

Figure 34. Voltage and current of spark in pure air and fuel-air mixture.

CHAPTER 4: ENERGY DEPOSITION FROM SPARK INTO GAS

Many researchers have investigated the minimum energy required for ignition [114, 115]. However, this ignition energy has generally not been estimated based on the true energy deposited into the gas, but rather on the electrical energy supplied by the power supply. In addition, the accurate amount of energy deposited into the gas flow must be known in order to determine the initial conditions of the spark. Using this initial condition, kernel evolution behavior can be analyzed using numerical approaches (e.g. by Large Eddy Simulation shown in Appendix B, which was conducted by Alexander Lambert) or by estimating the energy density of the spark kernel (see Appendix A showing Brandon Sfozo's results). In addition, the ignition probability is very closely related to the thermal and chemical energy density inside the spark kernel. In this study, the deposited energy was estimated by firing a set of sparks and allowing the resultant kernel to move downstream in the channel until ions and radicals have relaxed into thermal energy and sharp gradients of temperature have smoothed out. The resulting increase in enthalpy flow was then determined. Both inductive and capacitive sparks were used in this study, but the energy of the capacitive spark could be estimated far more precisely than that of inductive spark.

4.1 Inductive spark

When the inductive circuit amplifies the voltage at the electrodes, it causes the electrical breakdown of the gas between the electrodes. The duration of this inductive spark is much longer than that of a capacitive spark with a similar level of electrical energy, because the transformer usually has very high inductance (see Chapter 2). Due to this long duration, bright light emission is observed at the tip of the electrodes. This

means that the tip temperature is very high and there is a substantial heat transfer through the electrodes. Therefore, it is expected that the energy deposition efficiency is low. A preliminary measurement of the energy deposition of the inductive spark was conducted using the energy measurement facility described in the experimental section. The amount of energy supplied determined the temperature of the spark channel, and that temperature, in turn, affected the transfer of heat through the electrode and into the gas. In order to determine the degree to which the amount of deposited energy depends on the amount of initial energy, the amount of input energy for the primary coil was varied and the energy deposited in the gas was measured for each energy level. The results are shown in Figure 35. This exercise showed that only less than 30% of the electrically supplied energy was delivered to the gas, regardless of the amount of energy supplied. This efficiency value matched the one measured by other researchers who used a similar spark generation system.

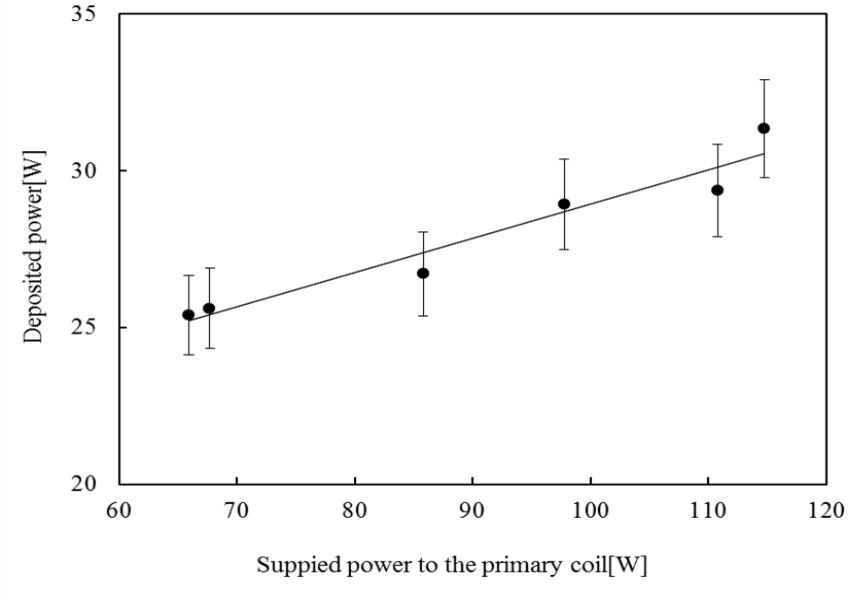

Figure 35. Delivered power into the flow by the inductive spark (flow velocity =7.2m/sec, 5% error bar).

This efficiency value indicates that most of the energy supplied by the power source is not transferred across the inter-electrode gap. One possible cause for this loss is the heat transfer through the electrodes. Further energy losses are electrical. Losses always occur in a transformer due to the relatively high resistance that results from the length of the coil and the transmission wire connecting power supply and electrodes. Resistance-based electrical losses are proportional to the voltage applied, which is adjusted to change the power of the spark. If the temperature of the spark channel near the electrode during the heat transfer is much higher than the boiling temperature of the material, the amount of heat loss through the electrodes is less affected by the spark channel temperature because the conductive heat transfer through the electrodes is dependent on the tip temperature (which, at its maximum is the boiling temperature of the metal; the remaining energy from spark channel is then used for the vaporization of the material). Usually, the spark channel temperature is well above a metal boiling temperature, However, the channel temperature of the inductive spark changes with time (due to its long duration and current changes during the discharge) and may fall below the boiling temperature of the material. The time history and amount of energy supplied can affect on the variation of the channel temperature and thus eventually the energy deposited into the gas.

Finally, the measurement of the level of the energy inside the kernel in the flowing gas using the inductive spark experiment was not accurate as that for the capacitive spark. That setup had not enough grid points for measuring the flow temperature and velocity. The energy inside the kernel should be estimated accurately because this energy level

affects the generation and evolution of the kernel. Therefore, a revised energy deposition test was developed and used for the capacitive spark.

4.2 Capacitive spark

The short duration spark delivers 0.25 J of energy to the inter-electrode gap within 1 µs, some of energy is then deposited into the gas. This high energy level causes the kernel to expand rapidly. Therefore, the flow channel had to be large enough to avoid its walls from disturbing the evolution of the kernel and absorbing its heat. Using the facility designed for the capacitive spark system (see Chapter 2), the efficiency of deposition was investigated for various flow velocities and turbulence levels.

A typical temperature distribution in the exit plane normal to the flow in the channel is shown in Figure 36. As expected, the hot region was located in the middle of the plane downstream of the electrodes. However, the interaction of the flow with electrodes generated large vortical structures with a strong momentum in the horizontal direction. This helped to spread the heat in that direction. The velocity profile for the 8m/s flow was uniform except very near the wall. The velocity and temperature profile for the 33m/s was measured with a longer channel (11 inches) to ensure that the flow had fully developed inside the tube. Due to this longer channel, the profiles for the high velocity case looked a little different from the low velocity flow case.

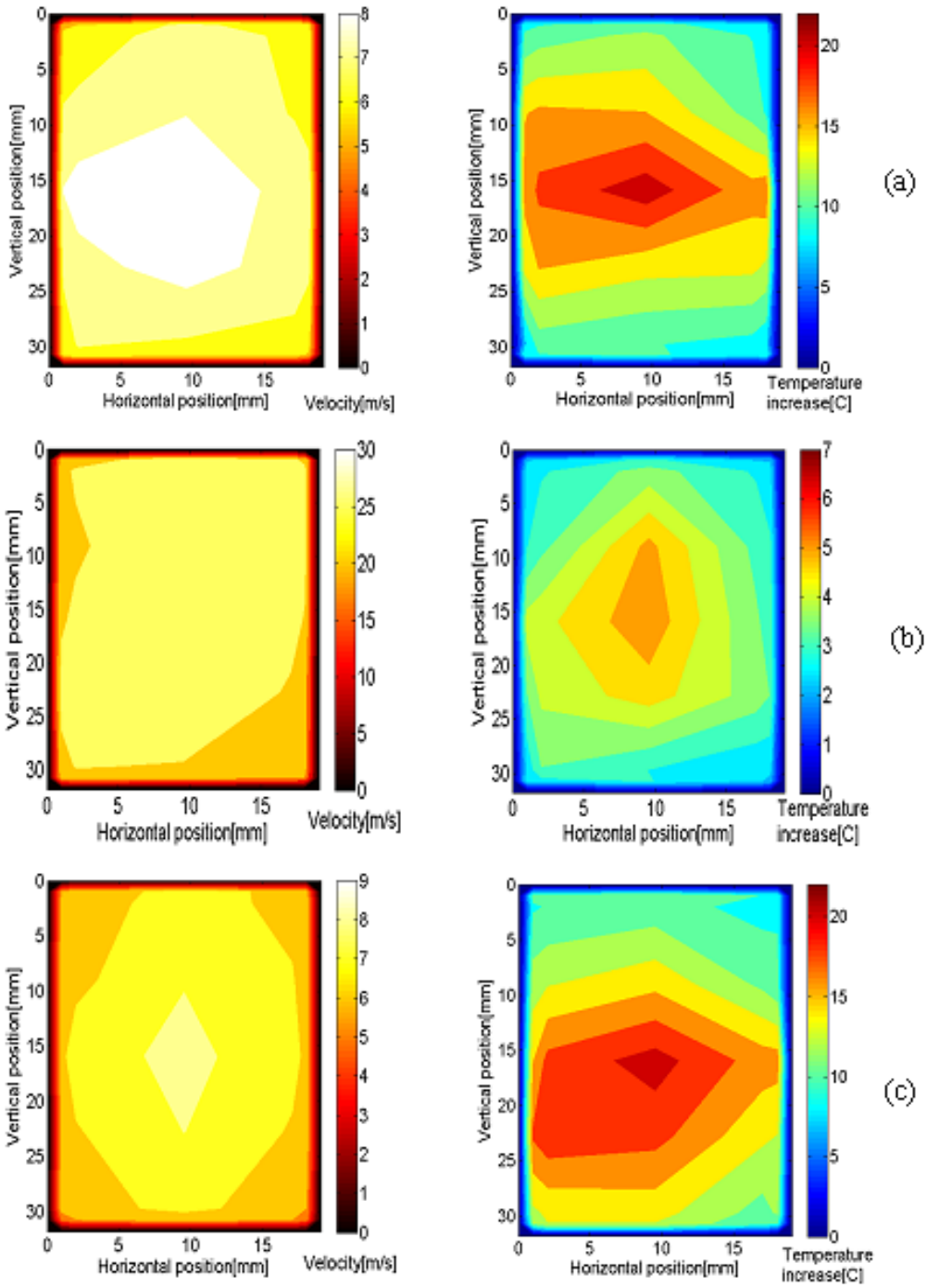

Figure 36. Velocity and temperature map at the exit plane of the channel. [Time averaged flow velocity at electrodes: (a) 8 m/s, (b) 33 m/s, (c) 8 m/s, turbulent level: (a) 5%, (b) 5%, (c) 26.4%, electric power transfer to electrodes: (a) 69.6W, (b) 69.6W, (c) 73.8W, efficiency: (a) 97%, (b) 96%, (c) 93%].

According to the energy deposition test with the improved facility and measurement system, the total energy deposited into the gas for these short sparks was above 90% of the electrical energy supplied for all cases. This did not significantly change when the flow velocity (8-40m/s) and turbulence level (5-26%) were varied. It is likely that the flow dynamics cannot affect the electric energy deposition because the time scale of this spark is much shorter than the characteristic time of the flow field. In addition, the electric energy was increased by adding a 1nF capacitor, and the energy deposition test was repeated to test the dependence of the energy deposition efficiency on the amount on electrical energy provided. This test demonstrated that the temperature in most regions of the exit plane was slightly higher than the lower energy case. The shape of temperature profile did not vary dramatically from that for the lower energy case, as shown in Figure 37. Even though there is high frequency component in the current and voltage in time trace. The measured deposition efficiency (above 90%) indicated that most of the energy was deposited into the gas.

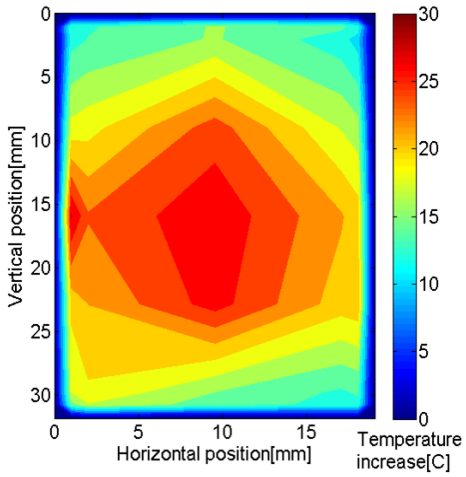

Figure 37. Temperature map at the exit plane of the channel for increased electric spark energy [flow velocity: 8m/sec, turbulent level: 5%, electrical energy: 0.33 J/pulse].

The energy deposition efficiency for this type of spark is high for several reasons. The very short duration of the spark does not provide enough time to conduct heat along the entire electrodes. What little heat is transferred to the electrodes is re-introduced into the flow by the passing gas. We were able to accurately measure the heat energy in the flow because the flow facility was designed to prevent the hot kernel from contacting the wall and the insulation around the evolution section reduced heat loss to the outside. In addition, the V-I measurement were carried out very close to the electrode gap avoiding lead losses before the current reached the spark. Finally, the measurements were conducted with very high accuracy.

4.3 Verification of energy deposition test for capacitive spark

To explain the measurements of the energy deposition tests, let us consider the thermal heat transfers during the electrical transmission from the spark power supply to the spark kernel. The possible heat generation and transfers inside flow channel are listed below (see Figure 38):

1. Heat transfers directly from the spark channel; Conduction to the electrodes, thermal radiation and shock loss to the flow
2. Convective heat transfer from the electrodes to the flow

The possible heat transfers to the outside of the flow channel are listed below (see Figure 39):

1. Conductive and convective heat losses from the electrical connection assembly
2. Convective heat transfer from the external wall of flow channel

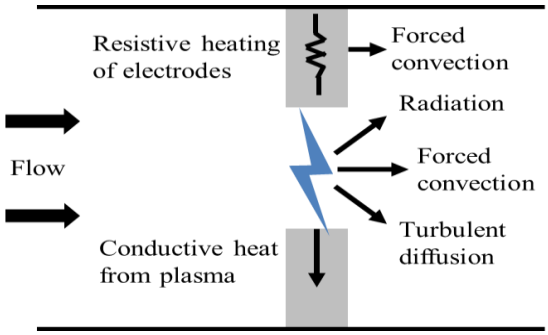

Figure 38. Heat transfer from the electrode and spark channel.

4.3.1 Heat transfers inside flow channel

Ballal [29] suggested that some of the spark energy could be dissipated from the spark channel immediately after the spark channel is formed. In other word, there could be heat transfer from the spark channel surface to the surrounding air or air/fuel mixture because the spark duration is not infinitely short. Possible dissipation mechanisms for the energy transfer from the spark channel are conduction to the electrodes, thermal radiation, forced convection and shock loss [29]. However, the electrode tip temperature cannot be higher than the electrode boiling temperature. This limits conduction heat losses from the electrodes to the wall where the electrodes are installed because the metal vapor carries energy that can eventually be used for ignition. The metal vapor can oxidize or combine with other species in the gas. Therefore, the energy of the metal vapor can be stored in chemical form or as thermal energy. The latter can contribute to the ignition energy. In addition the shock and some amount of radiation energy generated by spark deposits a substantial amount of energy into the flow which should be ignited. However, the radiation energy from the spark is absorbed by the facility wall and then transferred to the gas. Direct absorption by the gas phase is very inefficient. The heat transfer such as turbulent diffusion and convection from the cylindrical spark channel during the

electrical discharge is expected to reach only negligible levels for a short duration spark, and those heat transfers from the surface of the spark channel would be used eventually to ignite the surrounding gas.

The spark discharges most of the electric energy within a very short time (~0.5usec) during which time the kernel expands very rapidly. The effect of cross flow is, therefore, very small. In other words, the kernel inflates in all directions at a similar rate, while cold gas entrains into the center of the kernel. Due to this cold gas, the center of the kernel reaches a low temperature while the high temperature region is distributed at the perimeter in a toroidal shape. The high temperature region is convected by the cross flow and the upstream section of the toroid passes the electrodes. It is, therefore, expected that this region eventually transfers some amount of heat to the electrodes. Furthermore, the spark channel in the plasma state heats up the electrodes for a very short time while the electric potential builds up and discharges at a very high current. To estimate the convective heat transfer from the electrodes to the flow, the temperature just behind the electrodes was measured to be about 5C higher than the temperature upstream. The thermistor probe for this measurement was located near the bottom of the channel because the expanding spark kernel would not disturb the flow field in that region. In addition, to confirm the existence of heat transfer from the electrode to the gas, we installed insulation around the electrodes to prevent heat transfer between the electrodes and the flow. This resulted in a slight decrease (less than 10%) in the energy deposited in the gas. However, some of the heat from the electrodes would eventually be available for downstream ignition.

In addition, it was expected that the resistance of the electrodes would cause some self-heating because the current is very high (~1500A) even if only for a short time. However, based on the estimated resistance of the electrodes, the heating was calculated to be only 60μJ, which is 0.024% of the total supplied energy. Therefore, we can neglect it.

4.3.2 Heat transfers outside flow channel

There was also concern that a substantial amount of heat could be transferred from the plasma to the electrodes and then be lost through the external connector that is hooked up to the power supply (Figure 39). In other words, not all of the heat from the electrodes is transferred to the gas via the "fin effect" as mentioned above. Some portion of the heat loss occurs via the connector to the power supply. This heat is dissipated to the atmosphere via convection after it is conducted to an external part of the electrode assembly. The heat loss from the external part of the electrode and the external channel wall near the electrode were analyzed with limited assumptions.

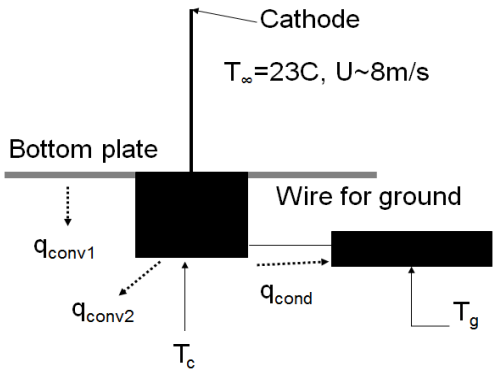

Figure 39. Heat loss from near the cathode assembly.

This analysis was conducted only for the grounded electrode, which is less affected by electric noise. It was assumed that the loss from the grounded electrode is relatively significant because it is not insulated and has a much larger surface area than does the anode. The temperature was averaged over the surface of the connecter (T_c =36.9C for a 67 Watt spark) and the ground wire (T_g =27.7C for a 67 Watt spark) after measuring it at multiple points when the temperatures are constant. The connector has a complex shape. Therefore, for the purposes of this calculation, it was modeled as a sphere with an equivalent surface area. Natural convection was assumed to exist from the connector and bottom plate to the atmosphere. Conduction was allowed for the ground wire, see Figure 39. The wire connection to ground had a relatively small cross section area, so the heat losses along it were very small. The naturally-convected heat losses were also very small because the heat transfer coefficient was small and the surface areas of the assembled connector and the bottom plate are also relatively small (see Table 2).

Additionally, there could be losses to the outer wall of the facility channel while the kernel evolves. The channel has a rectangular shape (19.1mm X 31.8mm) and is insulated with glass fiber and aluminum foil. The high temperature spark kernel does not come in contact with the internal surface of the facility at early on. After it expands, the kernel contacts the internal surface as it convects downstream and cools. The measured temperature difference between the outer wall of the insulator and room temperature is below 2C. Therefore, the loss from the wall of the evolution channel is negligible.

Table 2. Heat losses through the cathode, which affect the energy deposition in the flow.

	K[W/m-k] or h[W/m^2-k]	Heat loss for 70Watt spark[W]
Conduction to the ground wire (q_{cond})	401	0.073[0.1%]
Natural convection from the connector (q_{conv2})	13.44	0.206[0.3%]
Natural convection from the bottom plate (q_{conv1})	6.89	0.089[0.13%]

CHAPTER 5: CHEMISTRY BETWEEN FIRING ONSET OF SPARK AND COMBUSTION (IGNITION DELAY)

There is a delay between the spark energy deposition into the combustible mixture and the formation of a self-sustaining flame. This delay is an important factor in the design of combustors, especially for determining the required length of the combustor. Another major topic in ignition research is determining the MIE (minimum ignition energy) [116, 117]. As discussed previously, these studies considered only the energy provided to the spark plug and did not determine the amount of energy actually deposited in to the flow. However, it is the energy deposited that contributes to the production of radicals which facilitate the ignition and combustion processes. Thus, it is the deposited ignition energy and spark characteristics that are related to the species production at the initial stage of the combustion process. For instance, the species produced are parameters that determine variations in ignition delay [69].

Most engines can be divided into two different types: e.g. reciprocating piston internal combustion engines or gas turbine engines. The ignition problem in an internal combustion engine can be simulated in a constant volume experiment. Such tested were conducted by many researchers. Less information is available for ignition of flowing gas in gas turbine or industrial and domestic burners. For these applications, the efficiency of energy transfer from an external source to the flammable gas is affected by the flow characteristics. Therefore, the generation of radicals by the spark and their evolution in the flow of combustible gas are investigated in this chapter.

5.1 Chemiluminescence from fuel chemistry

The ignition delay is defined as the time elapsed between the spark and the instant where the essential reaction rates become large. Those reactions involve many kinds of radicals. . Emission from the electronically excited OH (OH*) is an important feature of hydrocarbon flame spectra. Therefore, we used the OH* time trace to define the ignition delay. An OH* signal can be detected after several hundred microseconds if the initial temperature is high. However, if a spark is used as an ignition source, chemistry exists right after the discharge because of electrons impacting the oxygen, nitrogen and fuel molecules as well as the generated heat. No OH* signal is found if pure air is used and the intensity of the OH* signal (308nm) increases with the increase of amount of fuel. Interestingly, fuel addition suppresses the copper peaks (324,327,510,515,521nm). However, the fuel as shown in Figure 38 increases the other peaks at 355nm, 383nm, and 415nm wavelengths for a given electrical condition. Further investigation is required to explain this effect of fuel addition on copper signal. The fuel does not affect the voltage and electric current history, during the discharge if the electric breakdown of gas occurs.

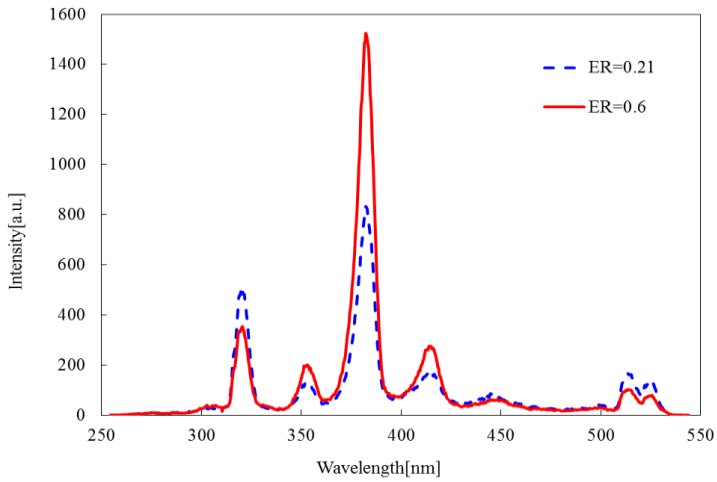

Figure 38. Spectrum for the ER=0.6 and 0.21 at 40usec after discharging.

5.2 Choosing OH* chemiluminescence as a marker

The light intensity is very high right after the spark fires and rapidly decreases with time. Therefore, a variable exposure times was used to improve the signal-to-noise ratio. The signal scales were then adjusted depending on the intensity level of the OH* signal. During the first 80usec, a 2.5usec exposure time was used. After that the exposure time was increased to 50usec. The gain was kept constant because the sampling duration for the spectrum was longer. Spectra acquired without the spark were used to subtract the dark current of camera and background room light from each exposure. An example spectrum is shown in Figure 39. The effect of the signal of nearby species emissions was removed. For example, a high intensity line around 324nm was found near the OH* signal, which was identified as a Cu signal [119]. This copper emission lasts for about 80µsec. In addition, a broadband signal exists over most of the range of the detectable wavelength. It was compensated for when obtaining the OH* signal level. The broadband emission level was identified by adding a polynomial trend line that connects the bottoms of peaks and then subtracted from the overall signal.

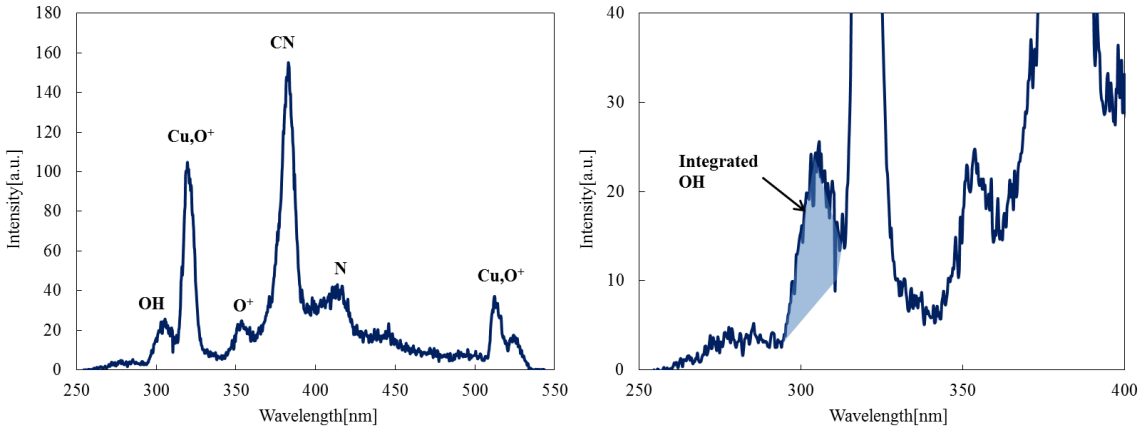

Figure 39. Spectrum at 60µsec after the spark, ER=0.6 (RHS: zoomed in around 308nm).

5.3 Ignition delay measurement using OH* chemiluminescence

Traditional thermal ignition theory suggests that few radicals are initially produced by heat then their number increases with time. In other word, no OH* chemiluminescence signal is initially expected during the ignition process. This is different if a spark is used. In these experiments the OH* signal history was acquired to estimate the ignition delay from the instant of discharge. As shown in Figure 40, the OH* signal for a flammable mixture early on is very high. It is, however, also possible that the high amplitude at 308nm prior to 200 μs is generated by reactions that are unrelated to OH* emission from flame chemistry, because the electric energy is concentrated in a small region. This kind of high energy density can generate huge numbers of species in multiple energy levels. For the flammable mixture, the spectral signal rapidly decreases until it reaches a steady, low level after about 200 μs. However, for non-flammable mixtures, the signal drops to zero in with 200 μs. If we remove the fuel completely, the OH* is not detected by this spectral approach.

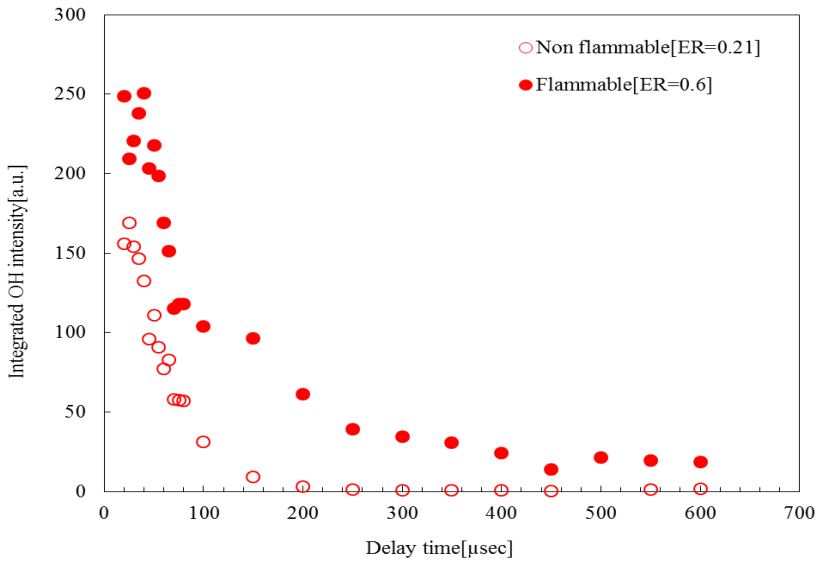

Figure 40. Time trace of OH* signal for ER=0.6 and ER=0.21 by spectrometer.

For a longer observation than the spectrometer allowed, a PMT only was used. The PMT chemiluminescence approach is reliable after 300 μs because no other emissions, such as the copper signals, were detected near the OH* emission wavelength.

As shown in Figure 41, the signal near 308nm does not drop to zero for the flammable mixture as also seen in **Error! Reference source not found.**. In other words, there is continuous chemistry prior to the flame propagation that starts later than the spark chemistry caused by the discharge. This means there is, strictly speaking, no ignition delay but a continuous reaction because the radicals and atoms produced by the high-energy spark react with the surrounding gas before the flame propagates. The PMT signal in **Error! Reference source not found.** shows an approximate 1msec delay before the signal begins to increase. However, this delay is not same with the ignition delay in auto ignition without initial extra radicals or atoms.

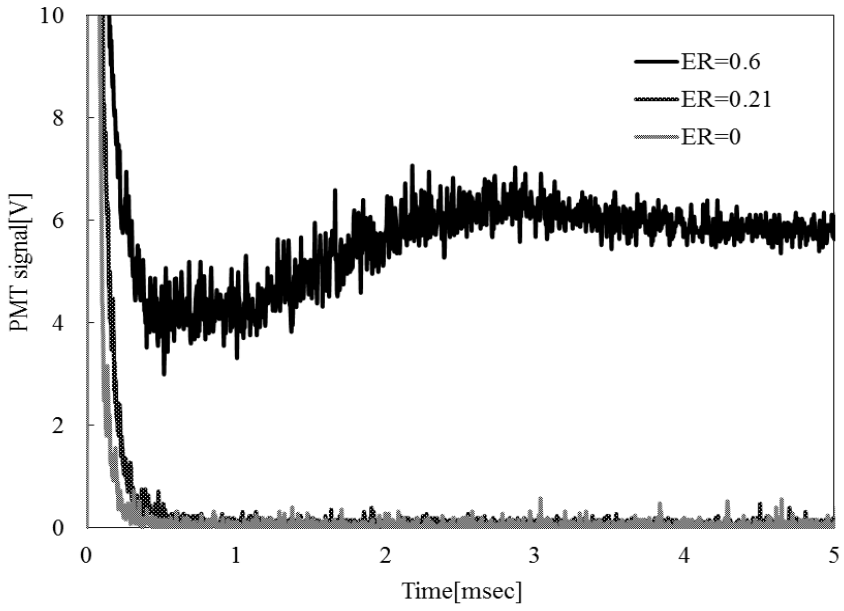

Figure 41. The longer time trace of OH* signal by PMT with OH filter.

The continuous chemistry was confirmed by visible observation with an ordinary digital camera. Figure 42 shows long exposure time pictures that were averaged over several spark discharges and their flames. The light at visible wavelengths was detected very near the discharged region. The reaction zone reaches about 20mm downstream of the discharge for a 20m/sec flow velocity, even if the equivalence ratio of mixture is not high enough so that the flame is self-sustained. The visually detected zone is a trace of the spark kernel movement. The kernel may be a reacting mass because the reacting gas emits visible light. For low equivalence ratio mixture, the kernel or flame decays within 20mm downstream. However, if fuel is added, the reaction survives and grows into a self-sustaining flame as shown in **Error! Reference source not found.**(b). High speed schlieren imaging carried out by Brandon Sforzo are shown in Figure 43 (see Appendix A). The spark kernel expands rapidly for the first 100 µs. Then, the kernel moves with the convection velocity of the flow. During this period of expansion and convection, the growth of the kernel in air-fuel mixture is different from that of the kernel in air only. This suggests that the fuel chemistry starts before 100 µs.

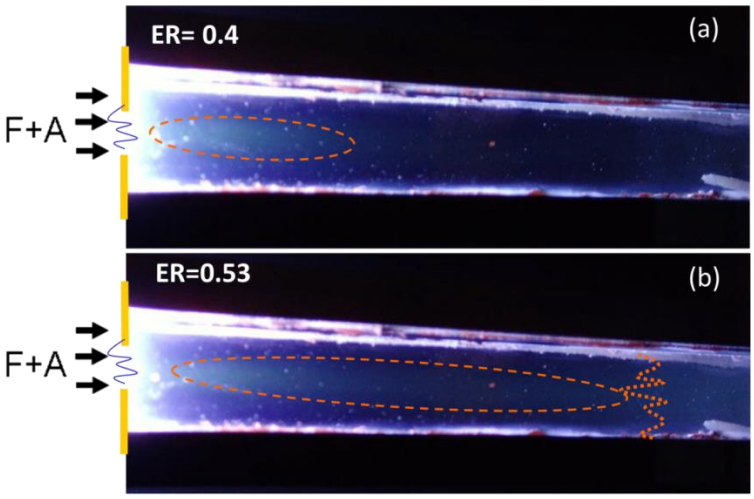

Figure 42. Reaction zone near flammability limit. (a) flame that is not self-sustained flame (b) self-sustaining flame.

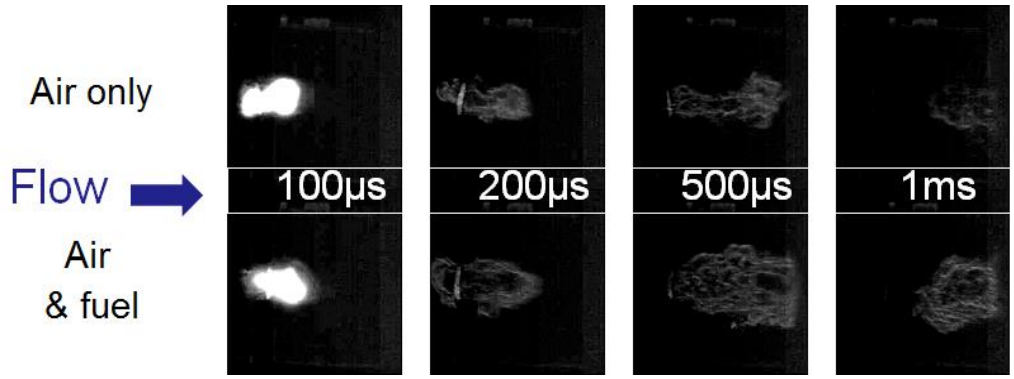

Figure 43. Kernel evolution images for air only and fuel-air mixture(ER=0.6).

5.4 Analysis of early reactions

As shown by the experimental results, there exists a continuous chemical reaction. The high-energy spark decomposes the mixture, and the resulting spark kernel, which now contains the decomposed species and ions, convects in the mixture until it develops into a flame. Unlike thermal ignition inside a closed reactor, the kernel in the flowing gas mixes with the surrounding cold reactants as it convects. Simultaneously, the inside of the kernel is reacting (undergoing recombination as long as it has not reached chemical equilibrium) and the kernel size keeps changing. This complicates observing the kernel ignition process using experimental methods. Therefore, this kernel ignition process must be investigated using a numerical method. These numerical measurements were conducted via the San Diego Mechanism using CHEMKIN.

To theoretically investigate the effect of radicals on the ignition process, an estimated amount of radicals was added to the reactants based on LES results (detail in Appendix B). Early in the reaction the radical concentration is very high. In practice, there are various radicals and ions present in the spark channel. However, when using the numerical approach to investigate the effect of the radicals on the ignition process, only

the O radical was added, because it is more effective for decreasing ignition delay than, for example the same amount of OH (Figure 44). In addition, if the igniter is located in pure air or in a very lean region, the O radical is predominant.

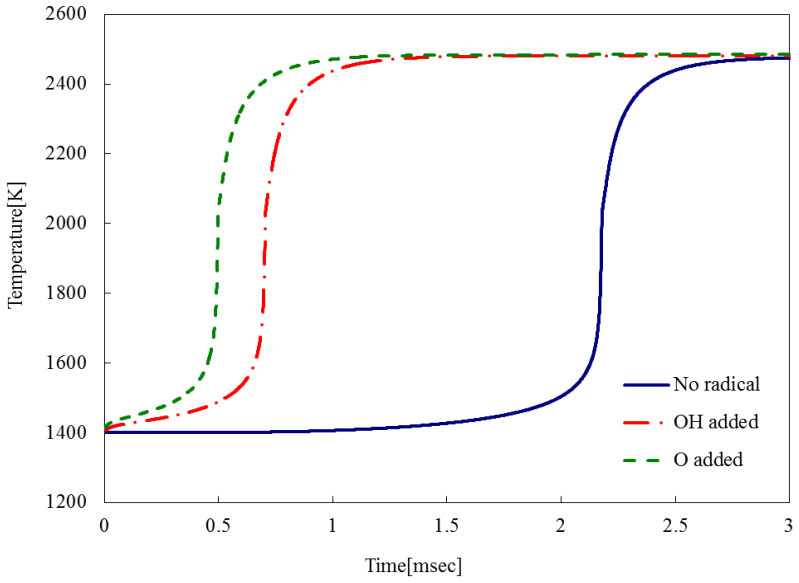

Figure 44. Comparison between effect of O and OH for ignition with same concentration (2000ppm).

The initial O concentration for CHEMKIN model was selected based on the LES results (see Appendix B). Lambert's modeling used the same conditions as the experiment using the capacitive spark. According to his results, the temperature distribution in the spark kernel (Figure 45) is a result of the chemistry inside the kernel and of the mixing with the surrounding cold reactants. Figure 46 shows the radical concentration along the line shown in **Error! Reference source not found.**. According to the OH* time trace (Figure 40), the signal from the chemistry in a non-flammable mixture ends within around 250 µs, while in the flammable condition there is continuous chemistry between the onset of the spark and flame propagation. The 'combustion' chemistry of the flammable mixture is detected from 250 µs, and the O concentration

should decrease due to mixing after 267 µs because radicals are recombined. Therefore, a lower O concentration should be selected than that of the LES data in the high temperature region at 267 µs. Furthermore, the initial temperature should be substantially lower than the maximum temperature (3320K) in the kernel at 267 µsec.

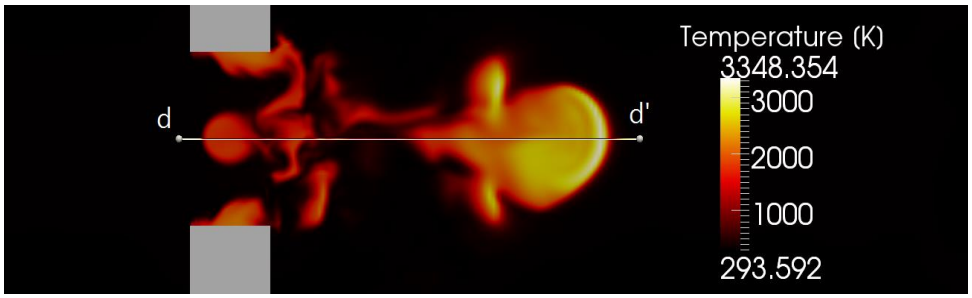

Figure 45. Temperature profile of spark kernel at 267 µs after spark generation.

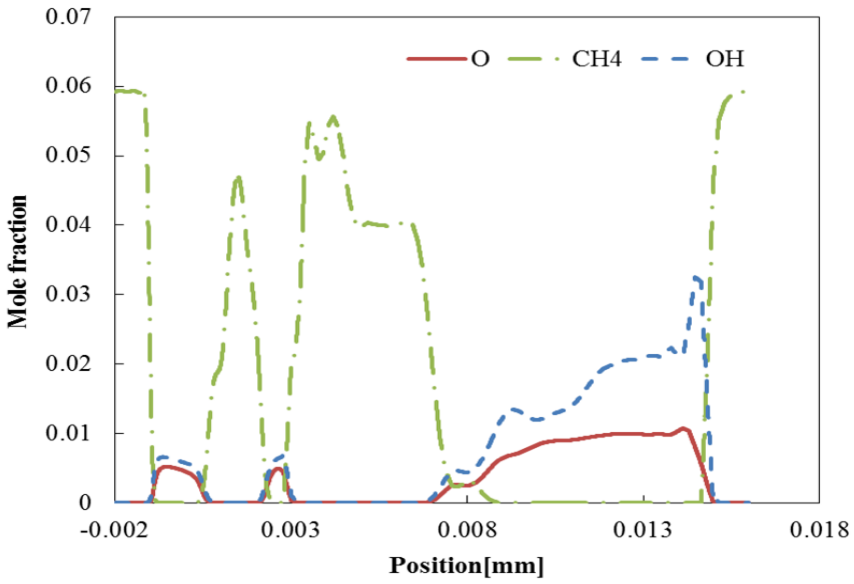

Figure 46. Concentrations of O, CH_4 and OH along the line (dd') inside spark kernel at 267 µs after spark generation shown in Figure 45.

The initial kernel temperature has been calculated by Brandon Sforzo (Appendix A) based on a schlieren image. He distributed the initial energy that is transferred from the

electrical spark uniformly on the toroidal shape of the kernel, after careful observation of its evolution and comparison with Alexander C Lambert's LES data. The average temperature of the kernel decreases rapidly due to its rapid expansion during the first 100 µs. The rate of heat loss slows until at around 250 µsec, when the average temperature has fallen to about 2000K.

According to the reaction pathway analysis for combustion of CH_4 with air in the well-stirred reactor in [118], CH_4 is destroyed by radicals such as O, H, and OH at the initial stage of methane-air combustion. Then, intermediate species such as CH_3 and CH_2O are produced, as shown in Figure 47. The methyl (CH_3) radicals then react with the O radicals, producing formaldehyde (CH_2O). The formaldehydes are thus transformed to formyl radicals (HCO) as they react with the O radicals. This pathway analysis is mainly for overall flame chemistry. However, there is a difference between flame chemistry and auto ignition chemistry. Nevertheless, the analysis of the early steps in the pathway can help understand the auto ignition process.

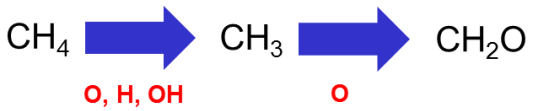

Figure 47. Combustion process of methane-air.

If O radicals (5600ppm) are added to the mixture at an initial temperature of 1400K, the reactions in the above chemistry are enhanced. The reaction rate of this enhanced chemistry is much higher than that expected for ordinary flame chemistry which does not contain initial radicals, even though it reacts at a temperature of 1700K as shown in Figure 48. This initial temperature 1700K was selected to compare the reaction mechanisms of no radical ignition and radical-added ignition with similar ignition delays.

The production rate of the CH_3 is very high, due to the fact that O efficiently abstracts H atoms from the methane molecules ($CH_4+O \rightarrow CH_3+OH$) as shown in Figure 48. The production rate of CH_3 early in the reaction should be higher than that during the ordinary ignition process, which has no initial O atoms. In addition, the CH_4 destruction rate should be very high, due to the extensive presence of O radical attacks. The O concentration decreases rapidly, falling to very low levels (14 ppm) within about 10 μs, and its production rate is very low (about 7.5×10^{-6} mole/cm^3-sec) until ignition occurs. Therefore, the effect of the O atom is not significant in the later part of the reaction process. Furthermore, the evolution of the CH_3 and CH_2O concentrations (Figure 49) with initial O radicals are very different from that without O radicals for similar ignition delay. In addition, the intermediate species such as CH_3 and CH_2O survive in relatively constant concentrations until the combustion chemistry begins. Therefore, the separate chemistries (initial chemistry with extra radical and combustion chemistry) can be compared to each other if the delay for the combustion chemistry is sufficiently short or the initial species due to the radical supplement can last until the combustion chemistry occurs. In addition, the intermediates survive longer than radicals such as O, and those, therefore, have more opportunity to convectively mix with the cold surrounding reactants. However, mixing of intermediates by molecular diffusion and turbulent mixing would be less effective than mixing with radicals because the molecular weight of the former is much greater than that of the radicals. As shown in Figure 50, an intermediate species such as CH_2O does not significantly decrease the ignition delay when the same concentrations of O radical as CH_2O are added to the reactants. Compared with auto ignition without initial radicals,

there is a decrease in the ignition delay Even the enthalpy increase by addition of CH_2O is not significant. .

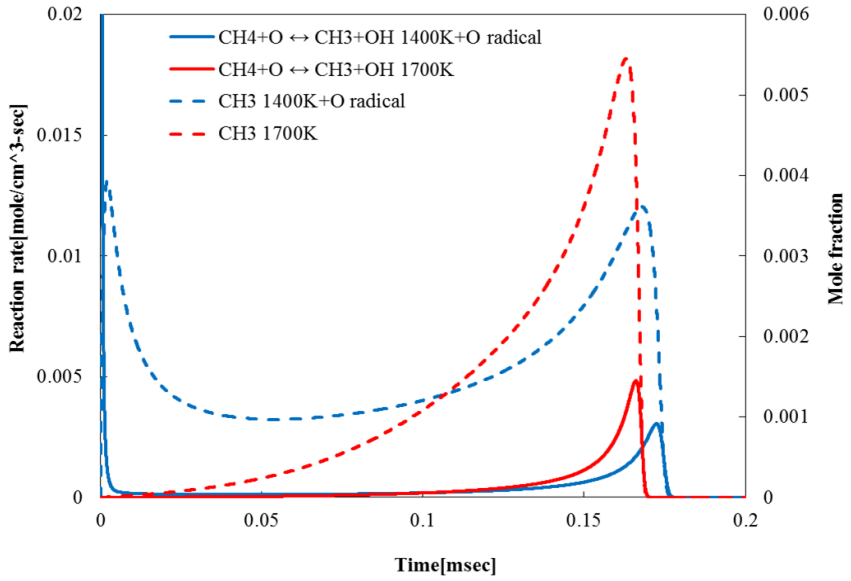

Figure 48. Production rate and mole fraction history of CH_3 [initial temperature 1400K and 1700K cases, 5600ppm of O radicals are added at 1400K case].

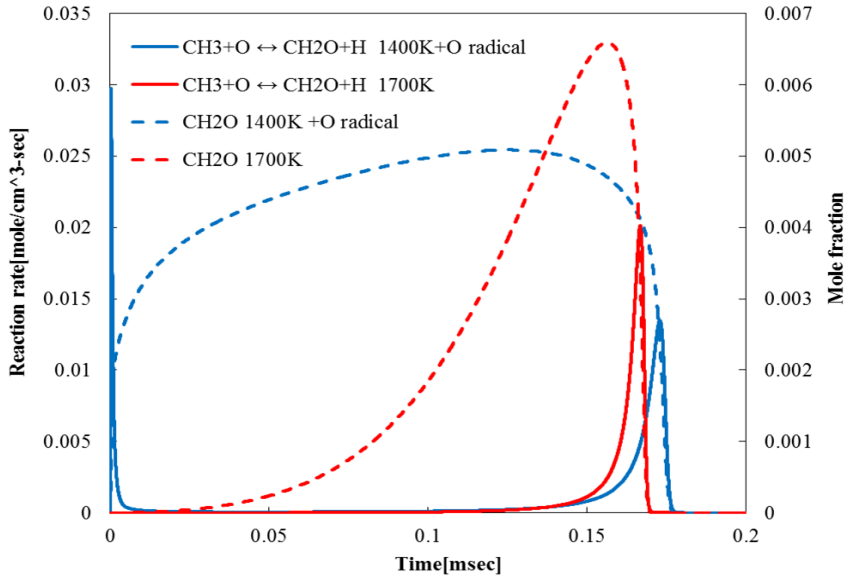

Figure 49. Production rate and mole fraction history of CH_2O [initial temperature 1400K and 1700K cases, 5600ppm of O radicals are added at 1400K case].

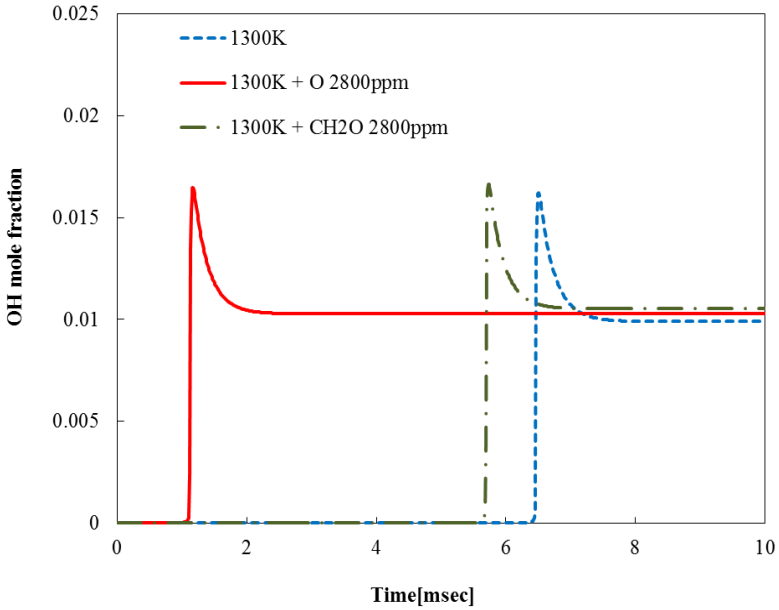

Figure 50. CH_2O effect on the ignition comparing between ignition without initial extra radicals and O added ignition.

In this chapter, it was shown that the traditional ignition delay does not exist but there are continuous reactions between the electrical discharge and the combustion because the spark initiates the reactions and those maintain until the flame is self-sustained. According to the numerical approach, the continuous reactions can be maintained not only by the radicals but also by the intermediates.

Only O radicals were added using this numerical investigation. However, the spark kernel contains many more different species. In addition, those initial species mix with the surrounding cold reactants, which lower the temperature and concentration of radicals in the kernel with time. It is expected that the radicals or intermediate species formed during the early period of chemical non-equilibrium affect, on the whole, reactions that are related to those species. Therefore, the physics and composition early on should be more complex than this numerical approach suggests. The next chapter shows the effect

of mixing between the kernel contents and the surrounding cold reactants using a more realistic and complex initial condition containing a greater variety of radicals. In addition, the discussion of the RJG will be discussed in the next chapter. The RJG's performance will then be explained using the radical effect on the flow in the main combustor.

CHAPTER 6: EFFECT OF RADICALS ON COMBUSTION

In the previous chapter, it was shown that the decomposed species including radicals and intermediate species generated by the spark differentiate the spark ignition process from ordinary auto ignition without initial radicals. This chapter discusses two ignition methods. First, it describes the direct ignition by the spark kernel with an explanation of the effect of the active radical generated by the spark. Second, the RJG developed to help stabilize the flame will be analyzed with special attention paid to the assistance of radicals under various conditions in main combustor flow.

6.1 Kernel ignition with capacitive spark

A capacitive spark system generates spark kernels with a very low duty cycle and whose energy is concentrated into a small region. The individual kernel initially expands very rapidly. Then the kernel convects downstream and mixes with the surrounding gas until it evolves into a flame if the fuel-air mixture is flammable. For this kernel based ignition, there is no flame holder to stabilize the flame and the focus of this study is on the process from the onset of the spark to the start of the combustion process. Therefore, the characteristic time for the chemical reaction between the gas inside the kernel and the surrounding cold reactants is of interest.

6.1.1 Mixing of reactive kernel with surrounding gas

The high density energy in the spark channel breaks the molecular bonds of the reactant and generates huge amounts of radicals. Figure 51 shows the spectra for the flammable condition shortly after the onset of the spark. During the first 10 μs, a very intense, broadband light emission is detected. This is caused by very large numbers of

species excited by the electric spark. The narrow bands, such as those at 320nm, 350nm, etc., remain stronger than the broadband component. However, the broadband signal rapidly decays after about 20 µs. As mentioned in the previous section, the narrow band signals are enhanced by nearby broadband signals and should thus be carefully quantified. Figure 52 shows the spectra for the flame that is not successfully self-sustained. The two spectra are virtually the same. This means that the chemistry that occurs during the initial stages after the spark is similar whether a self-sustained flame is generated or not. In other words, the chemistry immediately after sparking is not flame chemistry. Instead the spark generates radicals and heat without 'burning'.

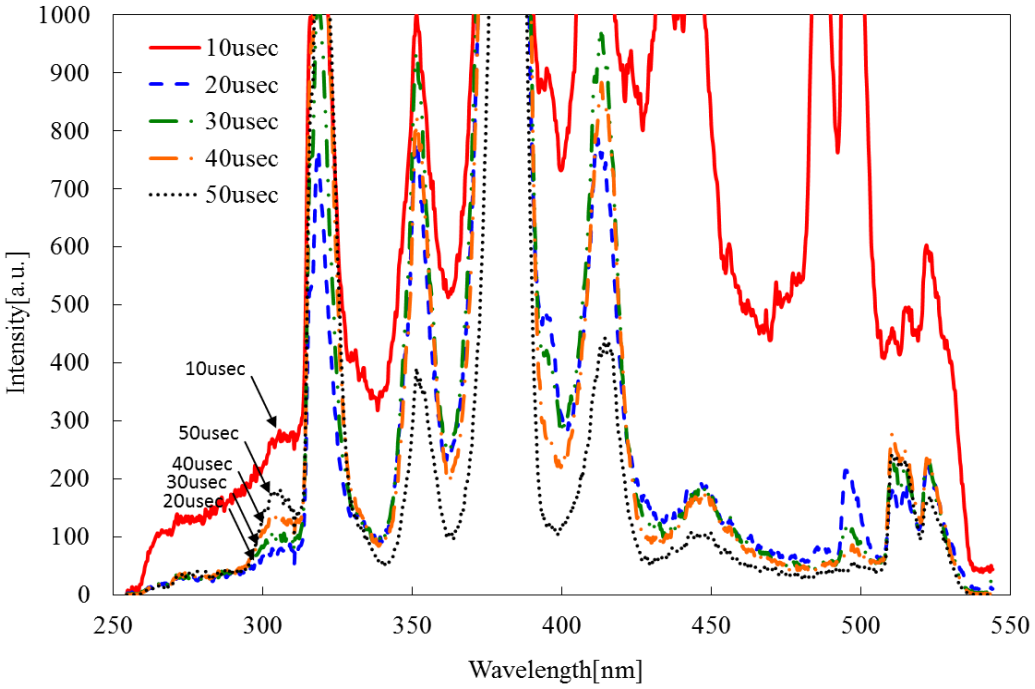

Figure 51. Emission spectra after spark from 10 to 50 µs at ER=0.6.

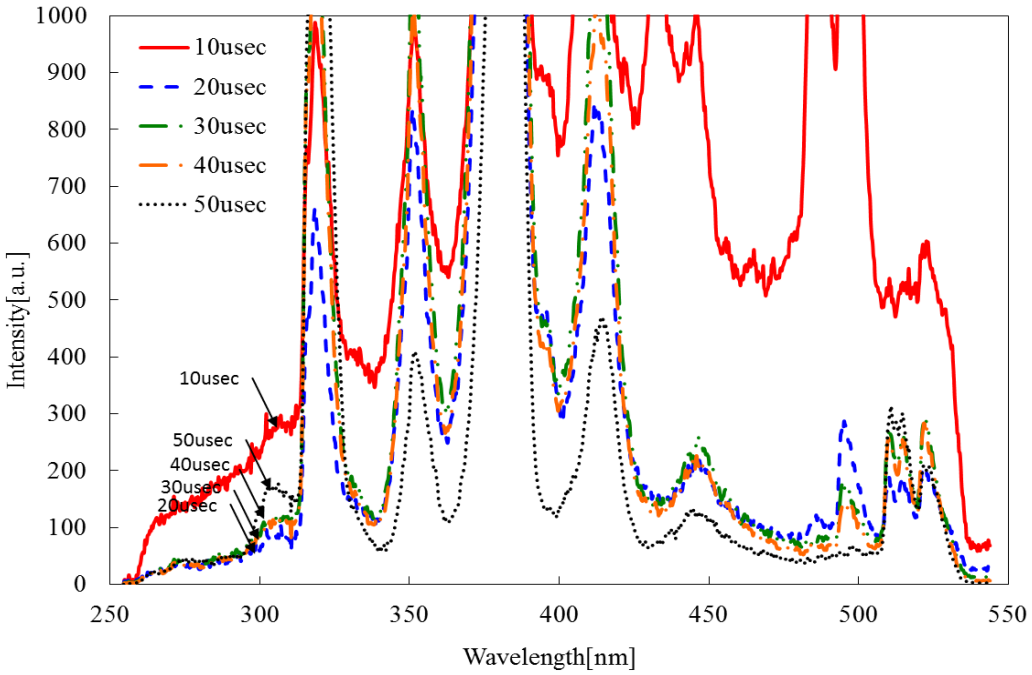

Figure 52. Emission spectra after spark from 10 to 50 µs at ER=0.49.

The radicals and heat generated by the spark form a kernel at the electrodes. As it is convected downstream it continuously changes its shape due to mixing with the bulk flow. The channel starts as a vertical cylinder. It then rapidly evolves into a toroidal structure because its gas dynamic expansion is constrained by the electrodes. Much later, the toroidal shape transforms to a disk-like kernel. Due to the expansion and shape change of the kernel, the mixing level calculation is not simple. The mixing process is very random. In addition, the content inside the kernel is reacting during the mixing.

The LES prediction of mixing of the kernel is shown in Figure 53 (see Appendix B). It shows the concentration of the species that originated in the initial spark channel. In this section, the effect of mixing on the ignition process is investigated using the CHEMKIN code and SDMech.

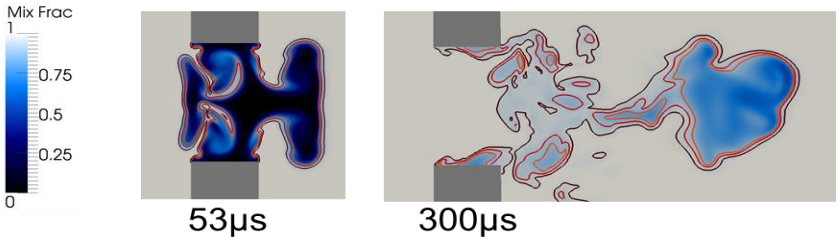

Figure 53. Mixing of kernel in the LES model of spark kernel.

The kernel can contain a reacting gas mixture that originated in the uniform flow with constant fuel fractions. Otherwise certain species can be added into the initial gas in the kernel as it convects because the electrodes can be located in an atmosphere that has a different gas composition from where the flame is ultimately ignited. For instance, the flow near the gas turbine combustor wall is mostly air because cooling air is applied to protect the combustor wall from overheating. For the afterburner system of a fighter jet, the spark plug is located in the recirculation zone behind the bluff body flame holder. Commonly, the fuel spray bars for the pilot flame are arranged inside the flame holder. Therefore, the species composition near the spark plug would be very different from where the main flame exists.

A calculated gas composition from the LES is used as the initial condition of the kernel. The mixture is allowed to react in a closed reactor model. These products are then it is mixed with additional cold reactants instantly in another closed reactor. We can choose a certain level of mixing (percent mass of the cold reactant in the total mixture) and then this mixture reacts in another closed reactor. Figure 54 shows temperature profiles for multiple mixtures with 10 to 70% by mass of the surrounding gas in the mixture. These temperatures were calculated for two regions in the kernel. **Error! Reference source not found.** shows that the level of mixing near the electrode is much

higher than that at the front of the kernel. Due to the initial mixing near the electrodes, the gas has cooled down and more time is needed for it to be ignited. In other words, the ignition delay time of the mixture is dependent on the location of the kernel. In both cases, the demarcation between slow and rapid auto ignition occurs suddenly over a small variation in level of mixing. For highly mixed regions (LHS graph), the practical ignition occurs below 40% of cold reactant and mixtures of more than 50% of cold reactant cannot be ignited within the 5msec time range of interest.

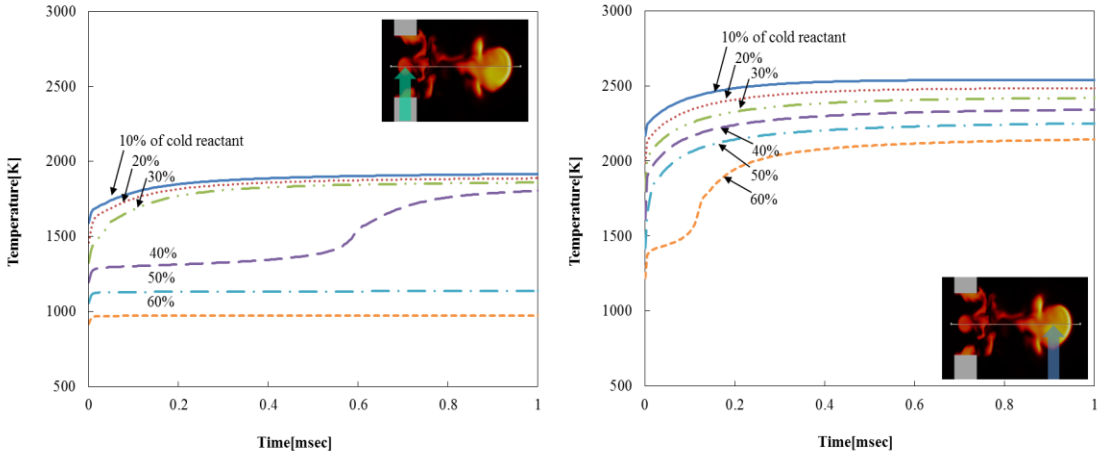

Figure 54. Temperature histories of mixture between the kernel contents and surrounding gas using two regions in the kernel.

6.1.2 Effect of composition in the kernel

If the kernel is generated in air only or under very lean conditions as in the dilution flow of a gas turbine combustor, it would contain more species that originate from nitrogen and oxygen. To investigate how species produced by air affect combustion, two initial conditions of the kernel are assumed. First, the kernel is assumed to consist of air in chemical equilibrium at 2343K. Second, the kernel composition is taken from the equilibrium result calculated at an equivalence ratio of 0.6. Both equilibrium

compositions at that temperature were calculated using the GASEQ equilibrium solver. In other words, the temperature for the two cases is the same but the composition is different. The O and NO concentrations are around 50% higher in the dissociated air. However, the latter does not contain the highly reactive species such as H, OH and CO. The presence of any fuel has a dramatic effect on the eventual ignition of the mixture of the kernel as shown in Figure 55. If the kernel is mixed with large quantities of cold reactants (above 50%), the presence of fuel in the kernel decreases the ignition delay in the flow. This means that if significant amount of fuel can be added to the dilution flow in the combustor of a gas turbine, the ignition characteristics of a spark can be greatly improved. However, if the cold reactant entrainment is less than about 40%, the ignition delay is short enough even for the pure air diluent. Thus, the fuel effect is not significant and improvement of the ignition delay is not needed for practical delay duration.

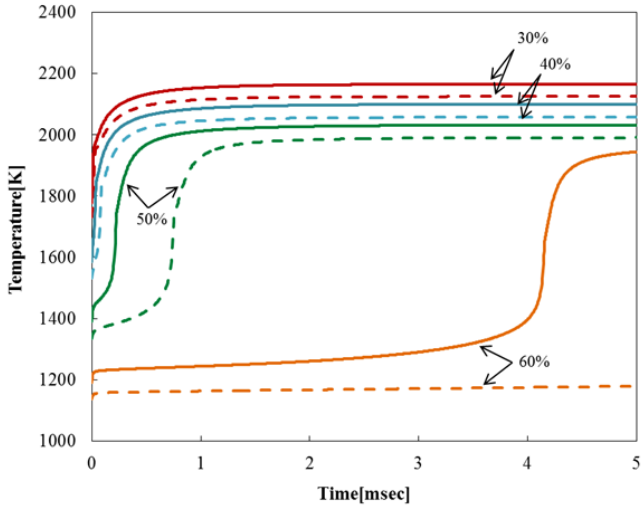

Figure 55. Fuel effect on the combustion in multiple mixing levels of kernel (dashed and solid line are for pure air and ER=0.6 mixture respectively).

In addition, the composition of the gas in the kernel can be changed to out of chemically equilibrium. The trailing edge of the kernel exhibits high mixing levels due to

the entrainment of flow near the electrodes. These entrained fresh reactants have not had sufficient time to reach chemically equilibrium. Therefore, in the current mixing analysis which allows for variations of composition due to chemical non-equilibrium, the calculations were conducted based on the results obtained by LES near the electrodes. The reacting species approach chemically equilibrium when they mix with the surrounding gas. Thus the kernel ignition process can be affected by the proximity to chemical equilibrium as well as by the mixing level.

In the closed reactor model, the chemical time is increased and the kernels with various chemical times are mixed with the surrounding gas instantly. If selected radicals like O, OH and H in the kernel are tracked (see Figure 56), O and H are seen to increase during the first 20μsec and then decrease, resulting in a peak value at around 20μsec. The OH radical on the other hand has a peak value at around 50μsec elapsed time in the kernel.

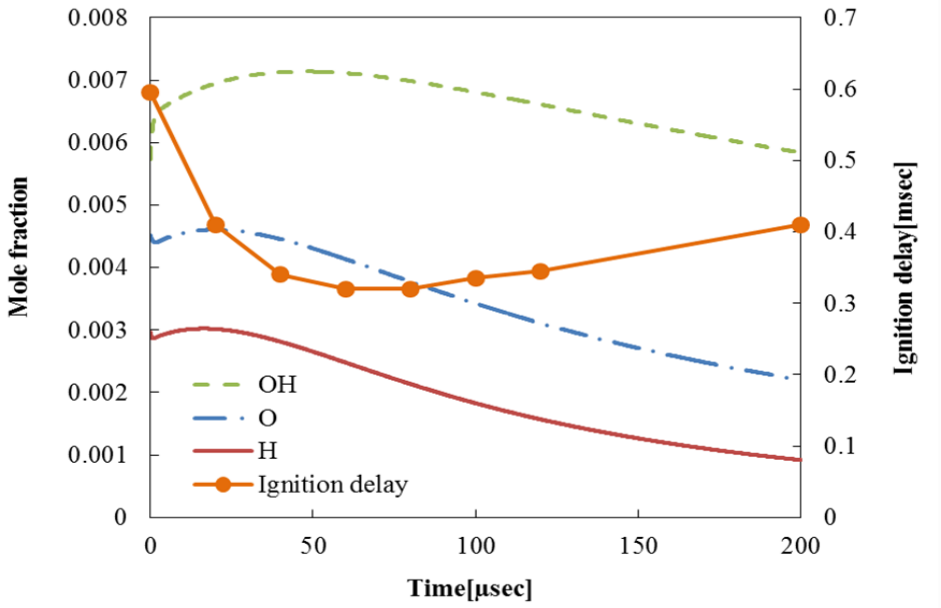

Figure 56. Change of radicals in the kernel with time and ignition delay in mixture that contains 40% cold reactant.

The OH radicals are produced by the reactions below (R8-R10). As shown in these elemental reactions, the O and H radicals are needed to produce the OH radicals. Therefore, the OH peak occurs at a later time than the peaks of the O and H radicals.

$$H+O_2 \leftrightarrow OH+O \quad \text{(R8)}$$

$$H_2O+O \leftrightarrow 2OH \quad \text{(R9)}$$

$$CO+OH \leftrightarrow CO_2+H \quad \text{(R10)}$$

Over the time range covered in **Error! Reference source not found.**, the temperature of the kernel gas (not shown in the plot) keeps increasing. If the mixture containing 40% cold reactant and 60% kernel gas is considered, the ignition delay found from the temperature history of the mixture is shortest, closer to the peak time of the OH radical than that of the O or H radicals. This suggests that OH radical is a key radical that leads to ignition [81]. Of course there is an initial reaction due to the radicals supplied by the kernel gas. However, the ignition delay is not based on this initial reaction which occurs within a few microseconds but on the development of an ordinary flame at a later time.

6.2 RJG for ignition and flame stabilization

Active species like radicals can also be produced by RJGs. The previous study dealing with long duration sparks in a moving flow suggests that the RJG has a profound stabilizing effect upon an otherwise unstable combustion flow. A flame can be stabilized with the assistance of spark or RJG generated active species because these can modify reaction rates and, eventually, affect reaction rates and flames speed as long as those species can reach the flammable region. The radicals generated during the incomplete combustion process in the RJG provide for significant combustion support in the

mainstream while consuming little electrical energy. A related concept has been suggested by Weinberg [120]. However, he used an inert gas such as argon or nitrogen to transport the radicals. In contrast, the RJG can partially burn the air-fuel mixture so that less electrical energy is needed to form radicals. In addition, this device has the ability to adjust the ratio of heat to radical levels. This flexibility in the heat to radical ratio can be used to compare the effect of radicals with that of heat effect. This section explores relative effect of radicals generated with and inductive spark in a fuel-air mixture with that of heat addition. Both experimental and numerical considerations are presented.

6.2.1 Inductive spark system in RJG

In a typical dump combustor, the re-circulating radical and heat from the flame take on the role as radical and heat supplier to increase reaction rates. A sufficient amount of energy from the recirculation region is needed to maintain a flame. This region is highly dependent on the flow condition. If the flow velocity is too high, the supplied energy from the region is insufficient to allow new reactants to react. However, if a long-duration spark is used as an additional source of heat/radicals, the limits for producing substantial radicals and heat can be expanded. By using a long duration and high duty cycle spark, the partially burned mixture for the RJG and the generated heat can be injected continuously into mixture to stabilize combustion there. In addition, a partial or complete combustion can occur successfully at higher velocities and over a wider range of equivalence ratios (Figure 57). As expected, an increase in the power of the spark expands the self-sustaining flame limits of the mixture as shown in Figure 59. This wider range of operation helps maintain reactions to produce radicals and heat in the RJG even at high velocities or outside the flammability limits in main combustor. Reactions near or

outside the flammability limit leads to incomplete combustion, which is particularly appropriate for flame stabilization in the main mixture flow because of the higher level of radicals due to incomplete combustion.

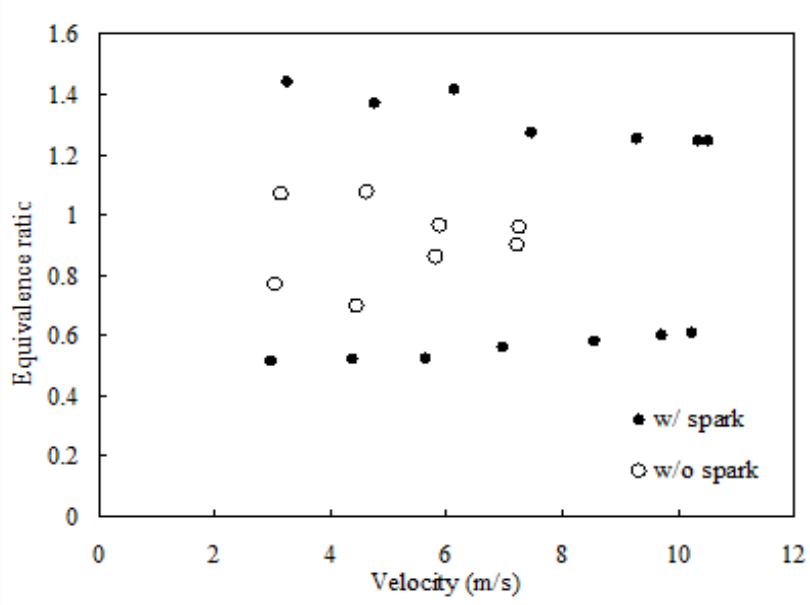

Figure 57. Expanded limit of self-sustaining flame existence inside RJG.

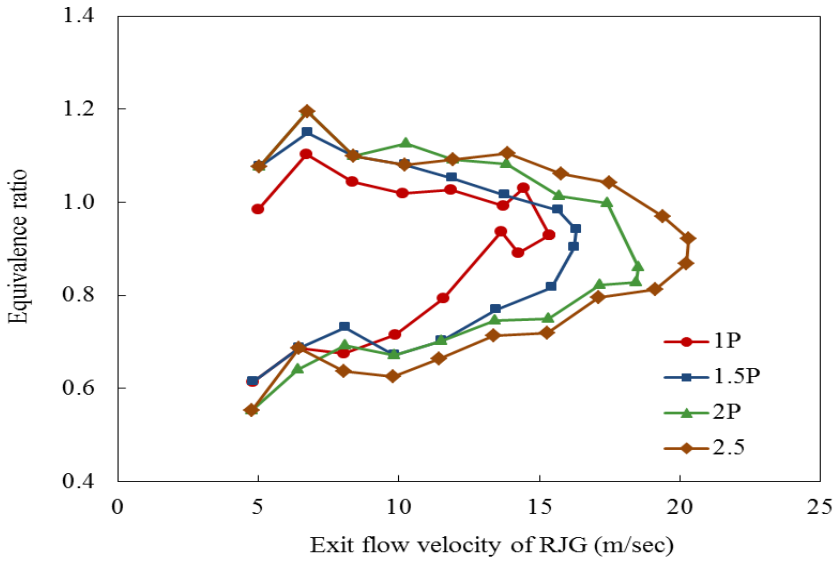

Figure 58. Limit of self-sustaining flame existence in RJG for various power settings at the power supply (the power shown in the plot does not represent the power at

the electrodes but instead at the power supply side. P is the minimum power from the amplifier and 2P means twice the minimum power P).

As was discussed earlier, the long duration spark channel is moved by the air flow (See Figure 25 in Chapter 3). When the air in the tests in Figure 25 was replaced by a flammable mixture the process in the RJG remained essentially similar. However, the spark also ignited the mixture and, in the progress, generated unburned mixture region inside the RJG chamber as seen in the high-speed camera image shown in Figure 59. For relatively low flow velocities each flame channel formed a flame kernel that was convected downstream. In between these kernels, while a new, straight ionized channel was formed, pockets of unburned reactants passed through the RJG. However, if the flow velocities were sufficiently low, most of the reactants were at least partially consumed before reaching the exit nozzle of the RJG. Thus, the injection process of RJG was essentially steady. This partial reaction can help to deliver more radicals into the main combustor. This is particularly important if the RJG chamber length is too long to otherwise supply enough of the rapidly decaying radicals.

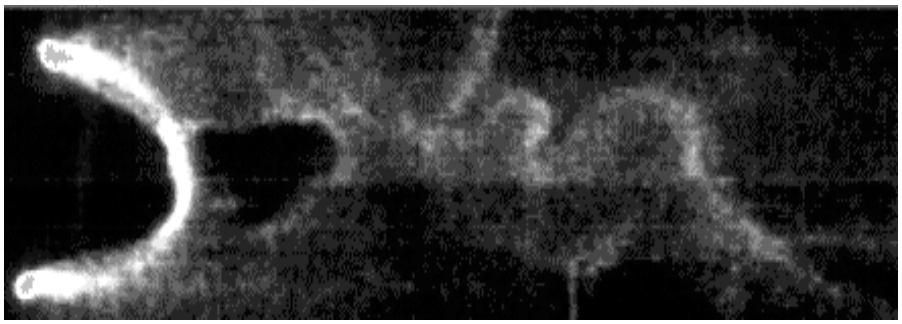

Figure 59. The reaction zone of a long duration spark discharge in the methane and air mixture in the cavity of an RJG. The unburned region locates right after spark channel [flow is coming from left to right].

6.2.2 Operation of RJG in main combustor

A RJG fitted with a long-duration, high-duty cycle spark maintains a combustion process, which generates radicals and heat. These can be used for increase of reaction rates and stabilization of flame in the main combustor. The partially burnt RJG products include an abundance of radicals, and their heat can be supplied quasi-continuously to the main mixture flow. This results in a cascade process that can increase the flame speed of main flow. Figure 60 compares the performance of an RJG with that of a disk shaped flame holder in the main flow. Cleary the RJG supports a flame at a much higher flow velocity and over a wider range of equivalence ratios. In addition, more spark power can stabilize a faster mixture flow in the main combustor (Figure 61).

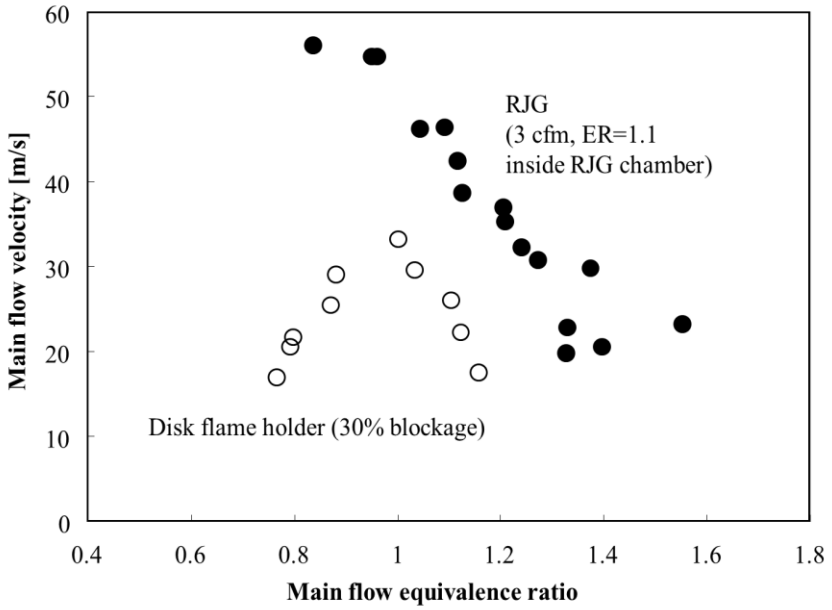

Figure 60. The performance of the RJG in the main combustor compared with that of a traditional bluff body flame stabilizer. Flames can be stabilized for all conditions under the curves.

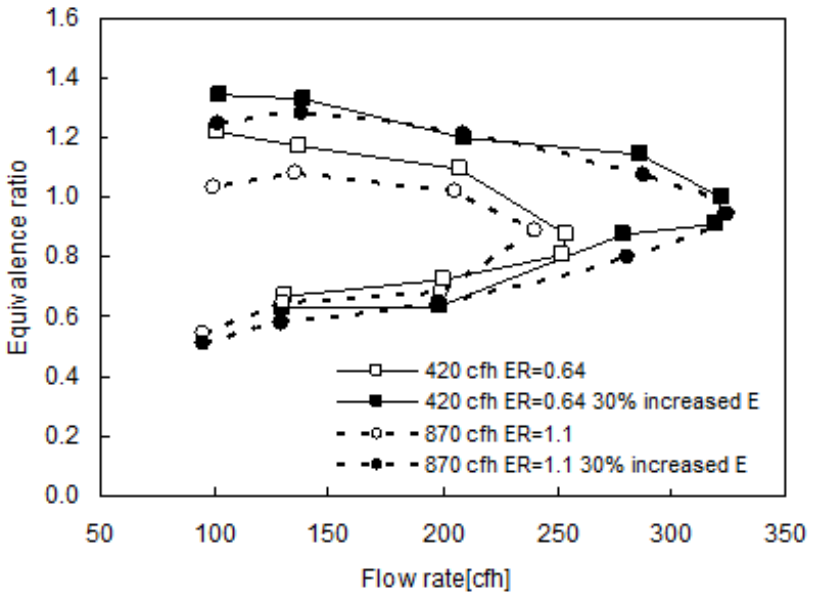

Figure 61. RJG performance various spark powers for flame stabilization of main flow.

The chamber configuration of an elbow type RJG (see Figure 10(b) in Chapter 2) is similar to a dump combustor except for the electrical discharge downstream of the step. Using this configuration, it is possible to control the amount of radicals relative to the thermal energy by using different operating conditions. If the combustion is completed in the chamber of the RJG, the exhaust gas contains fewer radicals than if that gas is still burning. In other words, if the flow speed is low through the RJG and the flame speed is not too slow; the flame inside the RJG can be stabilized inside its chamber. The flame can be attached behind the step inside the chamber, or behind the blunt structure that holds the electrodes. For slightly higher velocities, the flame attaches at the electrodes themselves because they are at a slightly higher temperature than the surrounding gas. However, if the flow velocity is high enough and the flame speed is slow (e.g. under rich or lean conditions) the flame is not stabilized inside the chamber. Instead the mixture would continue to react as it convects downstream outside of the RJG nozzle.

To investigate the RJG's performance for ignition and flame stabilization, we used the elbow type RJG shown in Figure 10(b) in Chapter 2 and it also reported in [121]. Picture (b) in Figure 62 shows the RJG with a flame (ER=0.83) attached at the step end without a spark. For this operational condition, the spark ignited the flame and the fuel flow was then adjusted to attach the flame at the step. Once the flame was stabilized the spark was turned off. The flame can then be maintained continuously. The experiment was carried out after the RJG was significantly pre-heated. Therefore, the heat loss from the casing of the RJG was minimal. The reactants undergo almost complete combustion inside the RJG and, therefore, inject stable products with mostly thermal energy into the main flow. This 'thermal jet' could not ignite the slightly rich main flow that was perpendicular to the flow of RJG. In contrast under lean (a) and rich (c) conditions the flame does not anchor inside the RJG. Instead there is a partially external burning process as shown in **Error! Reference source not found.**. This type of reacting flow can deliver more radicals outside of the RJG as shown in **Error! Reference source not found.**, where they assist in stabilizing the flame. However, this does not imply that radicals generated near stoichiometric condition are less helpful in stabilizing the main flame. The temperatures at the exit of RJG for both (b) and (c) are almost same based on thermocouple readings. This means the heat loss is significant if the combustion is completed inside the RJG. Instead, if a significant part of the reacting region of the RJG flame could be located outside the RJG, a flame could probably also be stabilized in the main flow because the heat loss can be avoided. The difference between the lean (Figure 62(a)) and rich (Figure 62(c)) condition is that the rich jet ignites and stabilizes the flame closer to the exit of RJG than lean jet.

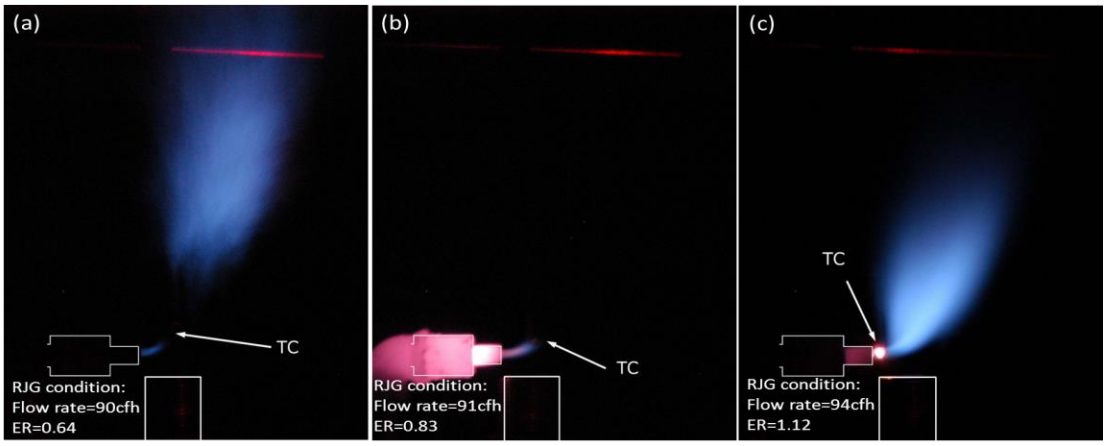

Figure 62. Interaction of RJG with mainstream combustible mixture. (a) RJG sustained by the spark in fuel lean flow, (b) RJG operating without the spark but with self-sustaining flame (c) RJG sustained by the spark in fuel rich flow. For all cases, main flow rate of slightly rich mixture is 22.65 m3/h or 13 m/s. RJG operating conditions are noted in figures.

In the above experiments the RJG was set up in a jet in cross flow configuration. This results in a complex flow pattern behind the radical jet, a vortical structure, consisting of the horseshoe vortices, the jet shear layer, the wake structures and the counter-rotating vortex pair [122]. Therefore, the fluid dynamics can also affect the ignition by the jet in the cross-flow not just the chemistry from the radical jet.

In addition, the flame inside the RJG could attach at the step when the flame speed is sufficiently high. Therefore, the jet contains mostly burned gas. To minimize the effect of the flow field on the flame stabilization process, the co-axial flow RJG described in the experimental setup chapter is used to investigate the RJG's performance. This configuration has no step in the internal structure and the reaction region is, therefore, located outside of the RJG chamber. Figure 63 shows the maximum flow velocity for which a flame can be ignited as a function of the equivalence ratio as reported in [123]. Three radical jets with equivalence ratios, 0.89, 1.0 and 1.22 were used to ignite the flame in the main flow. For all RJG equivalence ratios, the maximum flame holding velocity is

dependent on the equivalence ratio of the main mixture flow and the peak velocity exists near stoichiometric in main flow. In addition, the maximum flame holding velocity is increased as the RJG equivalence ratio increases from 0.89 to 1.22 for lean mixtures in the main combustor.

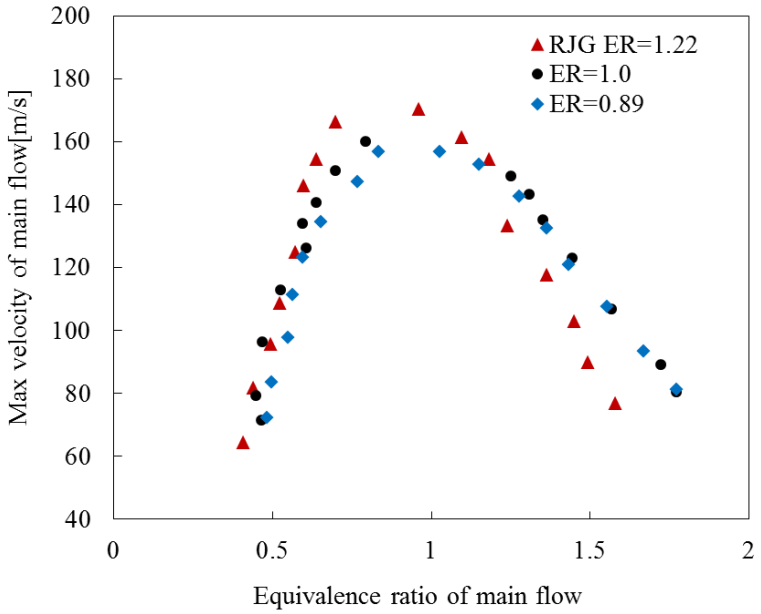

Figure 63. Flame holding velocity in main combustion by RJG with various equivalence ratios.

6.2.3 Analysis of RJG performance

The RJG supplies mostly thermal energy when the reaction is completed inside the RJG chamber. However, at higher flow rates when the reaction zone of the RJG moves into the main flow, the gas from the RJG convects downstream in parallel with the main flow. Here the main flow can mix the gas issued from the RJG which carries thermal energy as well as active species. The resulting reaction region then depends on the equivalence ratio of RJG which affects the flame speed and ignition delay. Those two combustion characteristics were investigated using a numerical approach.

A Plug Flow Reactor model combined with SDmech were used to model the effect of chemical energy on the flame speed and ignition delay when the RJG jet mixes with the flow in the main combustor. This PFR can provide representative RJG jets and those include various equivalence ratios, burning and bunt gases. Equivalence ratios of 0.8-1.22 in the RJG were used. The initial sensible enthalpy of reactor was calculated and used as the initial condition of the RJG. In this process the electric energy contribution from the inductive spark was estimated to be 30watts. The constant sensible enthalpy was used as the initial conditions for comparing the chemistry at different equivalence ratios in the RJG. The amount of deposited electrical energies is not very different over this range of fuel concentration and the initial temperature is only very slightly different for these equivalence ratios. In addition, the inductive spark produced by a high frequency, AC current generates many spark channels in a narrow region. Therefore, it was assumed that the electric energy is equally deposited over the volumetric flow at a given time. The calculated time traces of the sensible enthalpies for various fuel concentrations are shown in Figure 64.

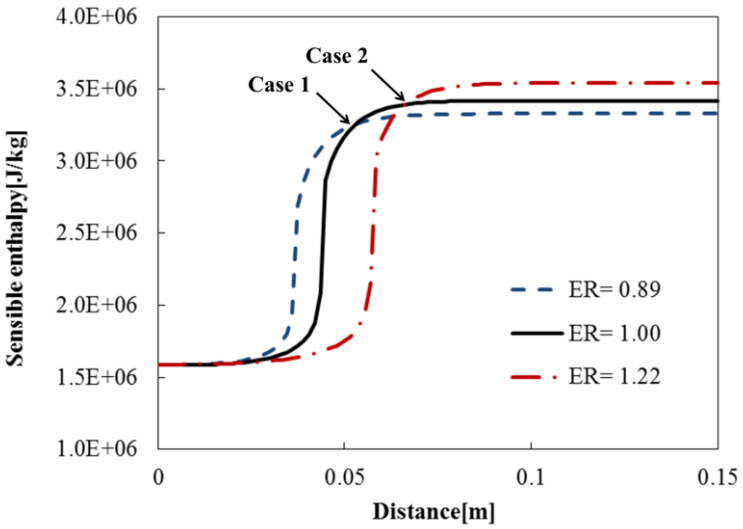

Figure 64. The time trace of sensible enthalpy for various equivalence ratio of RJG.

This figure shows that ignition delay for the lean cases are shorter than that for the richer case. An analysis of reaction rates for three cases shown in this figure suggest that early in the reaction, the production rate of O, H and OH is higher in the leaner condition. These radicals then attack the CH_4 and produce a large numbers of CH_3. Due to the faster production of radicals and intermediates, the ignition delay is shorter for the lean mixtures. For the comparison between the rich and lean conditions of the RJG, equivalence ratios of 0.89, 1.00 and 1.22 were selected since they match those of the experiments. Two cases shown in **Error! Reference source not found.** were selected to make comparisons. The sensible enthalpy was the same for both stoichiometric and lean (or stoichiometric and rich) jets but their composition was different. In addition, case 1 and case 2 on the stoichiometric curve can be used to compare partially burned and completely burned gases.

Like for the ignition by a spark kernel discussed in Chapter 5, the radical jet containing radicals and heat mixes with the main flow. This level of mixing depends on the location. For example, the mixing level along center line of a jet with co-flow is a function of centerline distance as shown in Figure 65 (based on the results of [124]) and the radial distance from the center line. The combustion characteristics such as ignition delay and flame speed are determined by the local species composition and temperature after the center jet mixes with co-flow. For sufficiently large outer diameters, the center flow mixes with co-flow very rapidly and the flame is stabilized downstream. We have limited information about the mixing level in the flow field where the flame exists and it is difficult to know how the mixing levels change as time goes on. However, there should exist a wide range of mixing levels from 0 to 100% of the main flow gas.

Therefore, the analysis of ignition was carried out over a wide range of mixing levels. Some of these mixing levels will be emphasized for comparison purposes. Using the CHEMKIN software, the burned or partially burned gases are mixed with the flammable main flow at various mixing levels. The mixture is then allowed to react in a closed reactor or a plug flow reactor to observe ignition delay and flame speed in the main mixture.

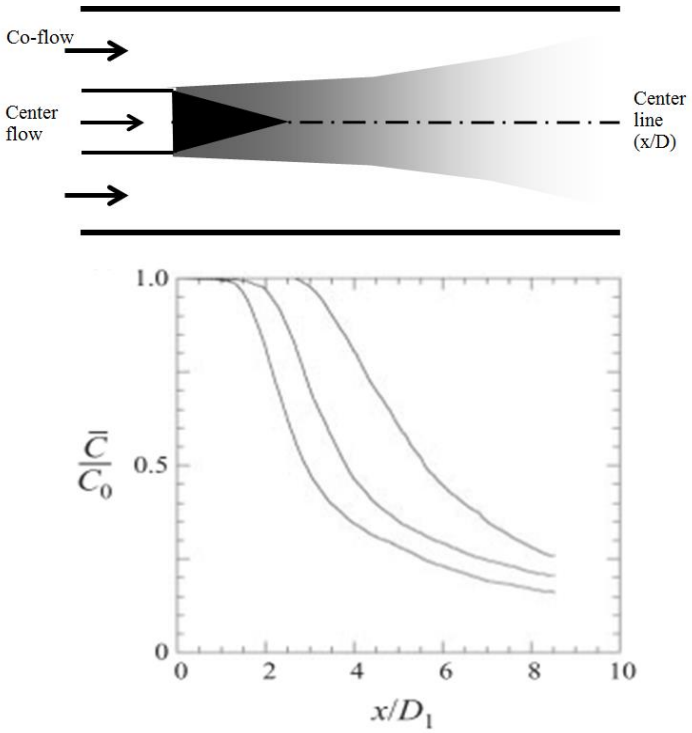

Figure 65. Concentration change of center flow along the center line for a coaxial flow [124].

Figure 66 shows ignition delays for several mixtures between RJG jet and main flow. The equivalence ratio of the main flow is 1.0 which is an easy to ignite mixture. The calculation is conducted for four conditions in the RJG. Comparisons between the lean and the stoichiometric radical jets of the RJG and between the rich and the stoichiometric were made. If the radical jet is mixed with a small amount of the main flow, the ignition

delay is too fast to be observed. In contrast, if the total mixture consists of 25% main flow it cannot be ignited within a practical time delay because the temperature and amount of radicals provided are not sufficient. For mixtures containing 20% of main gas there is a difference in ignition delay between lean and rich condition of the RJG.

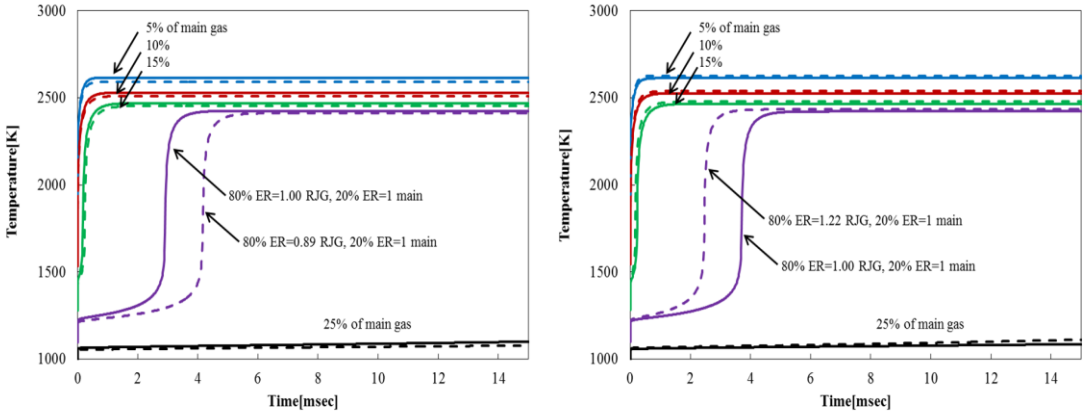

Figure 66. Comparison of mixture ignition between ER=1 and lean (or rich) radical jets for various mixing levels (LHS and RHS show the results using lean and rich RJG, respectively. Solid line: ER=1.00).

Therefore, the mixture containing 20% of the main gas was analyzed to determine how the main combustion characteristics are assisted by the RJG. For the four conditions representing the two cases shown in **Error! Reference source not found.**, the ignition delay for various equivalence ratios and states of chemical equilibrium were calculated as shown below in Table 3. The ignition delay is shorter for mixtures with richer RJG jet. This is true for all equivalence ratios (0.6-1.6) of main flow. However, the mixture of the rich RJG and the lean main gas is closer to the stoichiometric condition. Therefore, the rich RJG jet is more effective for the lean main mixture condition which is used for most modern combustors. For the stoichiometric RJG jet a jet carrying still reacting gases shortens the ignition delay more than one that is made up of combustion products only. In

addition, the laminar flame speeds for these cases were calculated in the plug flow reactor model containing a mixture of the radical jet (80%) and main gas (20%). All flame speeds are much faster than for pure main flow that does not contain added radicals. The flame speed is not very different (less than 5% difference) for the entire range of main flow equivalence ratios except for the very rich main flow. For an equivalence ratio of 1.6 in the main flow mixed with a rich (ER=1.22) jet the flame speed is 15% lower than if both the main flow and the jet are stoichiometric. This explains why the rich (ER=1.22) jet causes slower ignition for very rich (ER~1.5) main flow in the experiment result as shown in **Error! Reference source not found.**.

Table 3. Cases and calculated ignition delay for the comparisons about equivalence ratio and states of chemical equilibriums.

Main flow ER	RJG ER	Region in RJG	Calculated ignition delay[msec]	Case
0.6	lean[0.89]		1.52	1
0.6	1.00	Burning	0.95	1
0.6	1.00	Burned	1.25	2
0.6	rich[1.22]		0.68	2
0.8	lean[0.89]		2.66	1
0.8	1.00	Burning	1.79	1
0.8	1.00	Burned	2.31	2
0.8	rich[1.22]		1.41	2
1.00	lean[0.89]		4.16	1
1.00	1.00	Burning	2.91	1
1.00	1.00	Burned	3.71	2
1.00	rich[1.22]		2.46	2
1.2	lean[0.89]		6.05	1
1.2	1.00	Burning	4.32	1
1.2	1.00	Burned	5.44	2
1.2	rich[1.22]		3.75	2
1.6	lean[0.89]		10.98	1
1.6	1.00	Burning	8.19	1
1.6	1.00	Burned	10.11	2
1.6	rich[1.22]		7.38	2

To analyze the above results, the composition of the radical jet before mixing with the main flow was noted. The combustion of the stoichiometric mixture for case 1 is not complete. Therefore, the concentration of radicals or intermediates in this partially burned mixture is larger than for the mostly burned gas (case 2) for the same energy, see Figure 67. Thus the total energy is kept constant while it is portioned differently between thermal and chemical (radical) energy. This allows us to separate the radical effect from that of temperature on the ignition process.

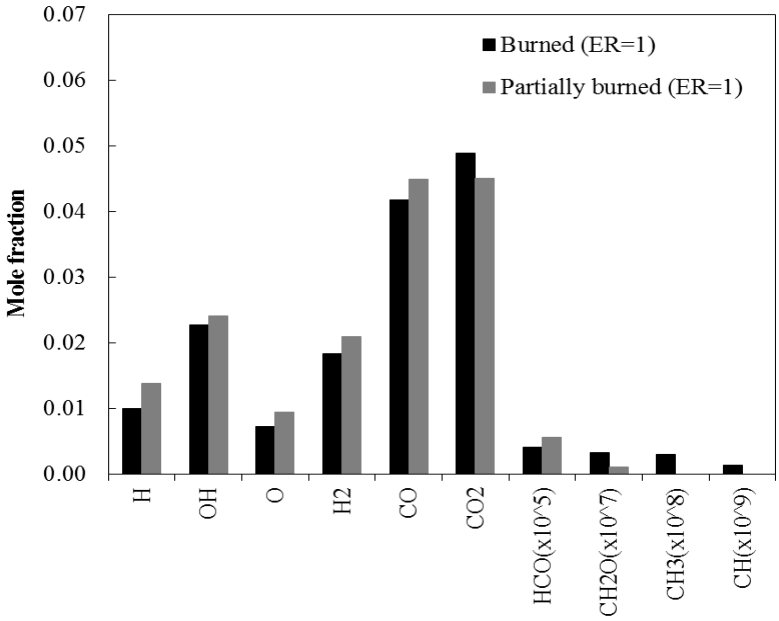

Figure 67. Comparison of compositions for partially burned and burned gas in the RJG jet.

The concentrations of selected species in RJG jets for case 1 and case 2 in **Error! Reference source not found.** are shown in Figure 68. Those provide comparisons between stoichiometric and lean or stoichiometric and rich jets. The major difference between the lean radical jet and stoichiometric one is that the latter jet has a larger amount of H, H_2 and some intermediates such as CO, HCO compared to the lean radical

jet. Those higher levels of intermediates and radicals have a dominant effect on the combustion characteristics such as ignition delay. However, the lean jet contains more intermediates such as CH_2O and CH_3. If the rich radical jet is compared with the stoichiometric jet, the radicals and intermediates such as H, H2, CO, HCO, CH_2O and CH_3 are present at the significantly higher level in the rich jet. Therefore, the ignition delay is shorter for the mixture between rich jet and main flow.

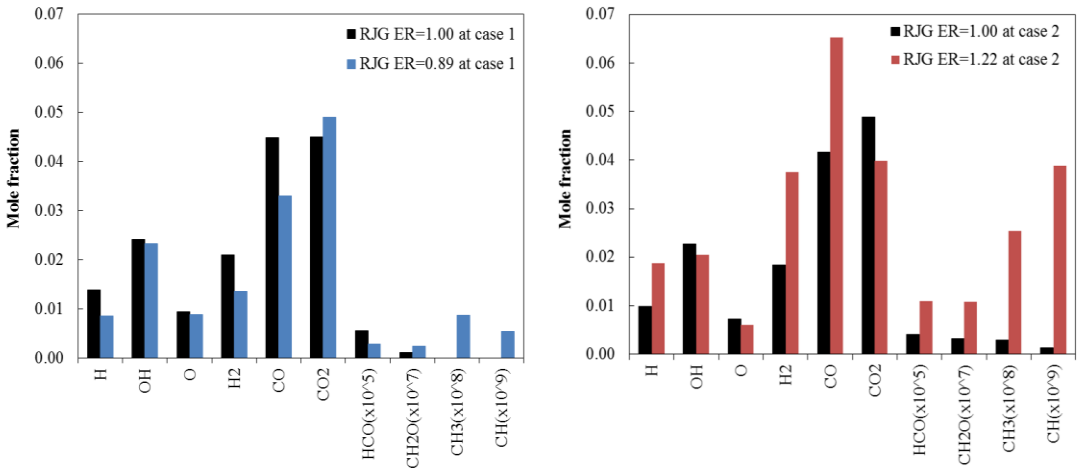

Figure 68. Comparison of compositions for various equivalence ratios in the RJG jet.

The initial sensible enthalpies were kept constant and, therefore, the initial temperatures for all cases were not very different (max variation 3%). However, the difference in ignition delays was significant, which suggests that the initial composition of the mixture of radical jet and main gas for each case affects the performance of the combustor.

CHAPTER 7: CHARACTERISTICS OF RJG OPERATION

As reported in the previous chapter, a relatively simple RJG was developed that is able to stabilize a flame in a high-speed flow. This was accomplished largely with the help of radicals that are produced in an incomplete combustion process, initiated by a spark. The radicals injected into the main combustor change the combustion field and affect the dynamics of the combustion. The goals of the work reported here, are to determine both the mechanism that causes the observed instability inside the RJG and the effect of a radical jet on the combustion characteristics in the main combustor. Special attention was also focused on the effects of the motion of the spark channel.

7.1 Pulsation of radical jet due to unsteady combustion in the RJG

At low flow rates the RJG injects a steady stream of radicals into the main combustor. However, for high throughputs of main flow these radicals will not penetrate that flow. As the flow rate of the RJG is increased, it injects radicals with periodical pulsation into the main flow. This affects radical level supplied. To investigate this operating condition, special attention was focused on four possible factors related to the unsteadiness. These factors are listed below:

1. Unburned reactant pockets by spark channel motion
2. Spark frequency
3. Flame propagation speed
4. Ignition delay

An inductive spark is used to initiate combustion in the chamber of the RJG. As mentioned in the Chapter 3, when a high frequency spark is first discharged in pure

quiescent air, a straight spark channel is formed between the two electrodes. Consecutive sparks discharge through the same channel, choosing the path of least resistance. When the discharge occurs in a slow moving flow, the spark channel becomes slightly bowed, see Figure 25 in Chapter 3. As the flow speed is increased, the flow convects the center of the ionized channel downstream. When the channel lengthens, the breakdown voltage required increases until it becomes so high that less energy is required for the discharge to generate a new, short spark, at which point the process repeats itself. As the flow velocity is increased, the process becomes more and more random and no clear downstream motion of the spark channel can be discerned. When the air in the above tests was replaced by a flammable mixture the process remained essentially similar. However, the spark also ignited the mixture. For relatively low velocities (below 5m/s), each spark channel formed a flame kernel as it was convected downstream, see Figure 69. In between these kernels, while a new, straight ionized channel was formed, pockets of unburned reactants passed through the RJG. However, if the flow velocities were sufficiently low, most of the reactants were at least partially consumed before reaching the exit nozzle of the RJG and the overall combustion process was essentially steady.

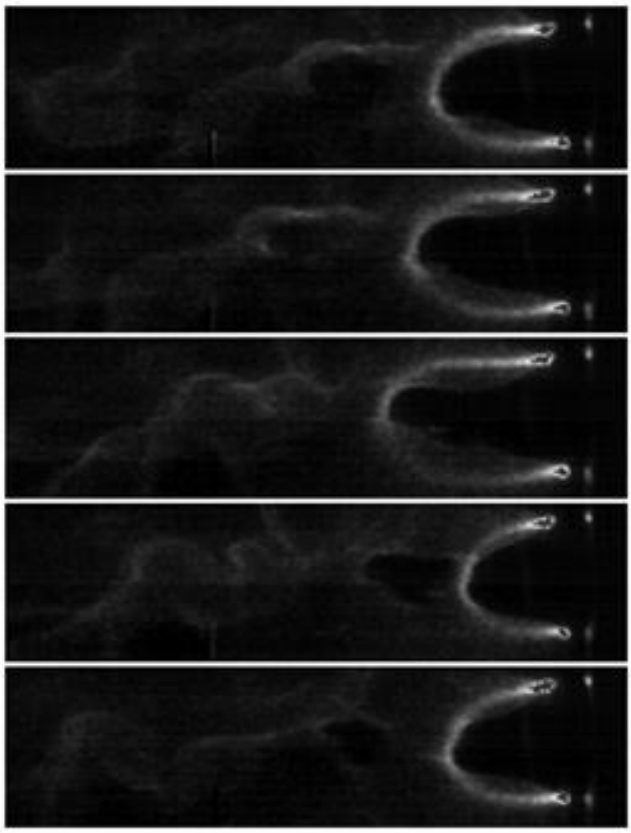

Figure 69. High-speed camera images near the electrodes in the cavity at relatively low flow velocity (incoming reactant velocity = 2.5m/s) showing the spark channels and the pockets of reacting gases that they have ignited.

When the flow velocity in the RJG was increased, the combustion process became audibly much more unsteady, which suggests that weak, periodic detonations may have been produced in the device. Images obtained under these conditions are shown in Figure 70. This shows more intensely burning structures being convected downstream. The resulting expansion of the combustion products causes propagation of these products towards the downstream and upstream ends of the RJG. The upstream flow can interfere with the spark and thus with the ignition process, as seen in the middle frame of **Error! Reference source not found.**. Using the RJG fitted with a quartz window (see Chapter 2), a set of experiments was conducted to investigate the mechanism of the unsteady

combustion. Firstly, the pressure and light emission were monitored. Whenever the reacting pocket was pushed towards the RJG exit it provided a signal from the photomultiplier, see Figure 71. Each peak of the pressure signal in this figure corresponds to the generation of a flame kernel. The associated expansion, which generates the pressure peak also seen in **Error! Reference source not found.**, pushes the combusting gases upstream as well as downstream.

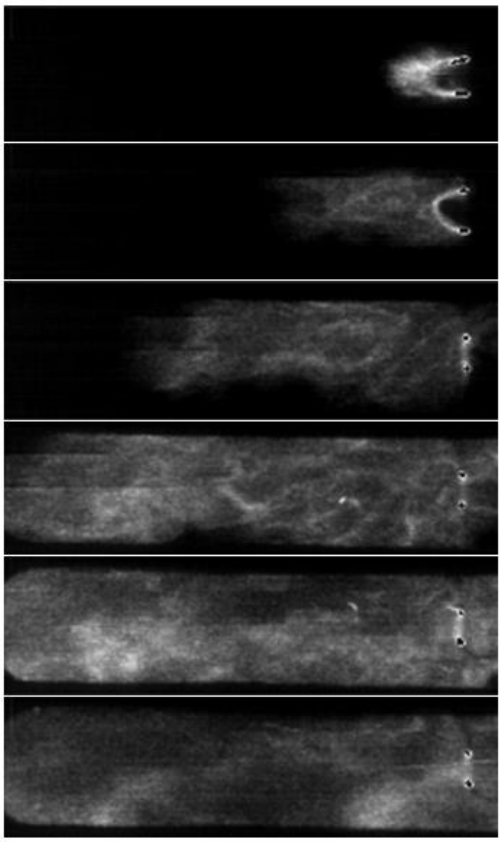

Figure 70. High speed camera images near the electrodes in the cavity at higher flow velocity (incoming reactant velocity = 9m/s, E.R. = 1.27, the time interval between frames = 1/500 sec, the exposure time = 1/1000sec) showing unsteady combustion behavior and its effect on the HF spark.

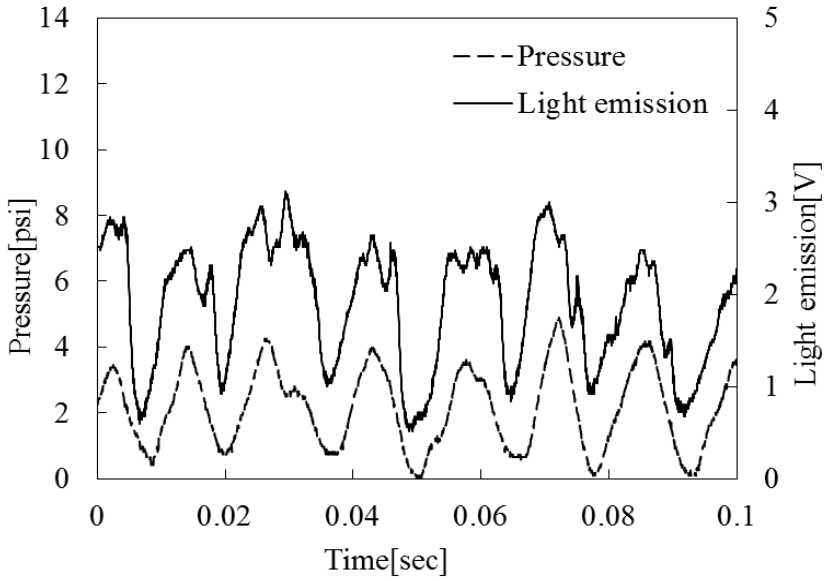

Figure 71. Pressure and spontaneous radiation signals obtained by photomultiplier tube near the exit of the RJG showing the effect of periodic combustion product expansion while also causes intermittent ignition of newly incoming reactants (incoming reactant velocity = 9m/s, E.R. = 1.27).

Secondly, the pressure and the spark voltage were measured periodically to determine the effect of the spark on the combustion process. Figure 72 shows simultaneous traces obtained from the pressure transducer and from a circuit that monitors the voltage across the spark gap. An inductive spark utilizes a harmonic signal to amplify the primary voltage by a transformer. This is the cause of the high frequency of spark discharge (6 kHz of sinusoidal input to the primary coil). The electrode voltage curve was low-pass filtered to remove the high frequency (6 KHz) component of the spark in the RJG. In addition to the high frequency component, there exists a low-frequency component in the spark voltage due to the convecting channel. It is likely that the periodic characteristic of the inductive spark in the flowing gas affects the periodic combustion process in the RJG. The discharge voltage peak does not exactly overlap with

the pressure peak due to the intensive combustion, as shown in (**Error! Reference source not found.**). The change in electrode voltage represents the previously discussed variation in spark channel length. When the flame expands towards the electrodes, the discharge voltage is sharply reduced. In addition, the lowest voltage exists near the pressure peak. It is possible that the expansions of the products and of the reacting gases also occasionally disturb any new ignition of incoming reactant. This is also seen in some of the high speed camera images. However, there is no definite proof from the high speed images or the pressure vs. spark voltage graphs that the expansion and/or flame propagation causes the observed unsteadiness. This is because the voltage variation can also induce the change of ignition. In other words, it needs to be clear that the voltage oscillation is not driving the periodic combustion inside the RJG chamber.

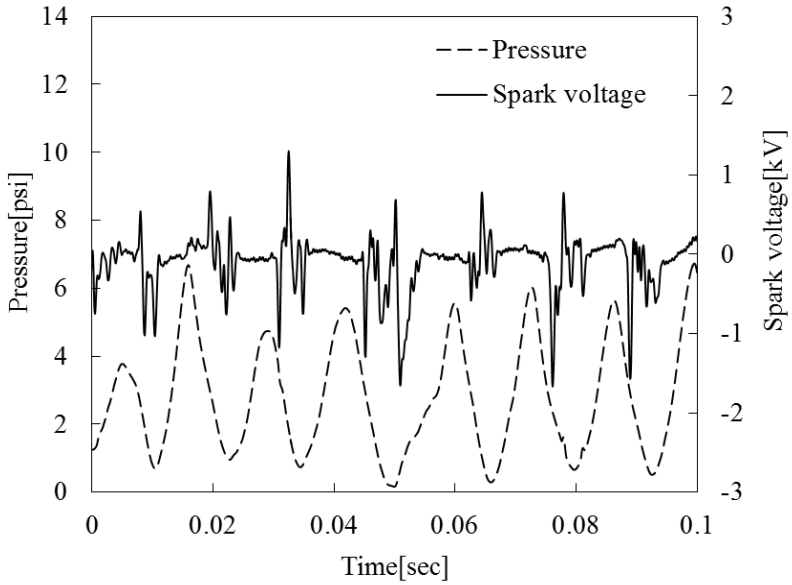

Figure 73. Comparison between electrode voltage and pressure signals. The electrode voltage is absolute value and the 6 KHz of spark is filtered out to indicate flame kernel formation. (Incoming reactant velocity = 9m/sec/s, E.R. = 1.27).

To investigate the spark's effect on the periodic combustion in the RJG, the duty cycle of the spark was varied by pulsating the input voltage signal to the primary side of the transformer. To adjust the intermittency of the spark with variable frequency, a pulse generator limits the input sinusoidal signal to a certain time period. This produces a series of high frequency intermittent spark with a controlled period of intermittency (Figure 73). The frequency ranges from 30Hz to 340Hz. For low frequency (below 100Hz) intermittency, each series of sparks initiates combustion and the intermittent frequency matches well with the frequency of combustion unsteadiness. However, when the frequency of intermittency is above 120 Hz (Figure 74), the peak frequency of the PMT signal remains near 110Hz. If an additional spark is applied during the process of intensive combustion, the additional discharge has no significant effect on the instability of combustion. In other words a given amount of time is required to complete an intensive combustion cycle.

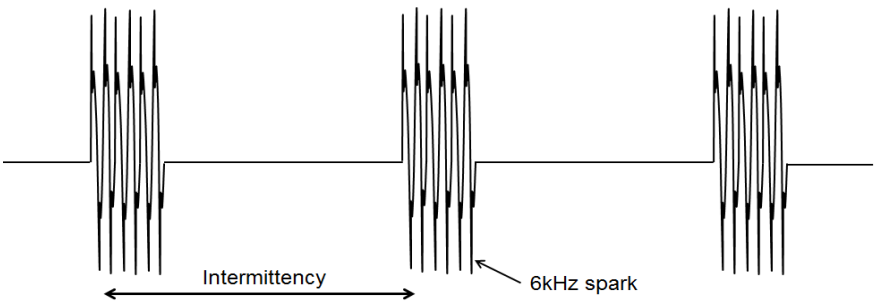

Figure 73. Spark intermittency.

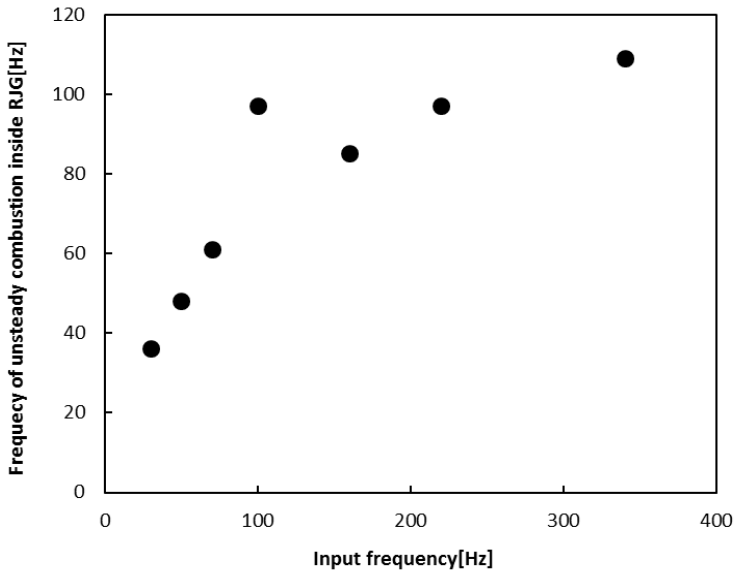

Figure 74. Frequency of the unsteady combustion in the RJG with various intermittency of spark (flow velocity = 3.2 m/sec, ER=1.77).

As shown in the above analysis, if the periodic violent combustion does not originate from interference with the spark, the required time to complete a combustion cycle inside the RJG is a function of: flame speed, ignition delay, bulk convection of product and device dimensions. As the flow velocity is increased, the small exit nozzle causes the chamber pressure to increase. This results in changes in ignition delay time[81, 125-127] and flame speed[92]. For the range of cavity pressures considered here (up to 2PSI under cold flow conditions), the effect of pressure on the ignition delay can be neglected. However, the effect on burning velocity was further investigated. The increase in laminar burning speed was determined using a plug flow model in CHEMKIN. The increases in turbulence intensity and the resulting, higher turbulent flame speed were also calculated using Eq.7.1 and Eq.7.2 taken from Ref. [89]:

$$\mathrm{Re}_T = 13.45\times10^{-3}(\mathrm{Re})^{0.902} \tag{7.1}$$

Where Re_T is turbulent Reynolds number and

$$\frac{S_T}{S_L} = \left\{1.34\mathrm{Re}_T^{0.47}\frac{u'}{S_L}\left[1-\exp(-3.178\mathrm{Re}_T^{-0.5}\frac{u'}{S_L})\right] + 10.9\mathrm{Re}_T^{0.22}\frac{u'}{S_L}\left[1-\exp(-0.391\mathrm{Re}_T^{-.025}\frac{u'}{S_L})\right]\right\}^{0.5} \quad (7.2)$$

Where S_L, S_T and u' are laminar burning speed, turbulent flame speed and turbulent intensity respectively. The mean velocity, U was estimated from the monitored flow rate while the turbulent intensity, u' was measured using hot-wire anemometry in the middle of the cross section of the chamber.

The range of reactant flow velocities for which the combustion process in the RJG was unstable and that were investigated here ranged from about 4 to 9m/s. This corresponds to a Reynolds number of about 10,000 and turbulent flame speeds ranging from 1.87 m/s to 4 m/s at an ER=1.27; i.e., an increase by a factor of more than two. Both the ignition delay time as well as the flame speed, both laminar and turbulent, vary with equivalence ratio. While the ignition delay time for a methane-air mixture is shortest at about E.R. =1.1 [35], the flame speed is largest near that value. A decrease in ignition delay and an increase in flame speed should both lead to an increase in the frequency of the observed combustion instability. Furthermore, the final product temperature should be highest when the methane-air mixture burns close to stoichiometric. This would lead to a most rapid expansion process and further increase the frequency of the instability. This was, in fact, observed in a series of experiments whose results are reported in Figure 75. The frequency of the unsteadiness in the combustion process increased from about 65Hz at the rich or lean extremes to over 80 Hz at an E.R. close to 1.1.

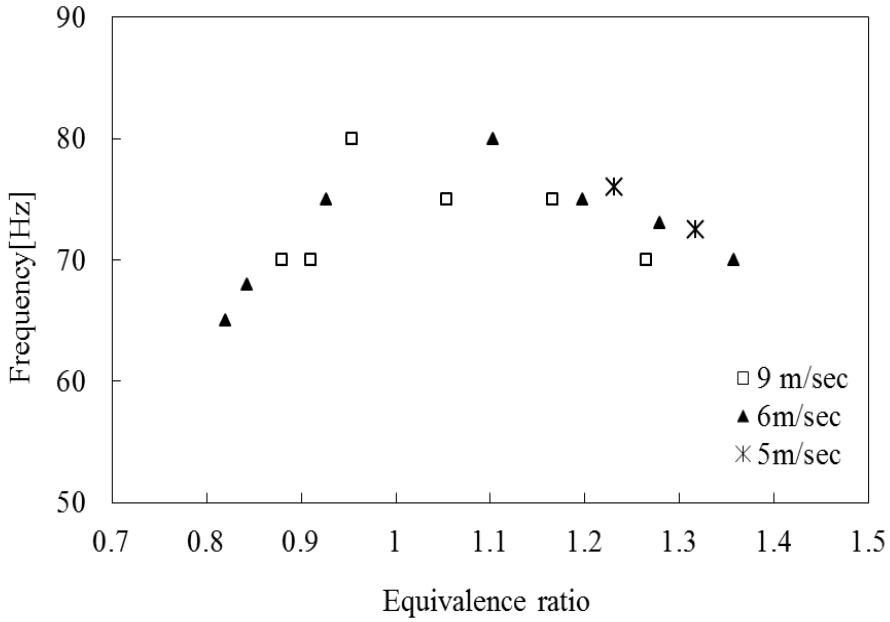

Figure 75. Effect of equivalence ratio on the pulsation frequency of the unsteady pressure (with various incoming reactant flow velocities).

7.2 Influence of Injected radical on the combustion dynamics

In order to determine the effect of the RJG on flame dynamics in a main combustor we investigated the behavior of a flame in a long duct with and without RJG support. The main combustor was comprised of a feed tube through which premixed reactants enter into a long quartz tube. A PMT was situated near the base of the quartz tube. A piezzo-electric pressure sensor measures pressure fluctuation in the supply cavity of the main combustor as shown in Figure 11 of Chapter 2. The flow conditions in the RJG were set at a high enough velocity so that combustion could not be sustained without the plasma. Instead, the partially burned air/fuel mixture from the RJG joined the mixture in the main combustor. This way we could observe changes in the flame behavior with and without the spark while changing the air/fuel flow conditions. The spark was produced by supplying a train of short pulses at a frequency of 1.1 KHz to the electrode.

Figure 76 shows the behavior of the pressure and the flame radiation with and without the RJG operation. **Error! Reference source not found.** indicates that activation of the spark (and, therefore, the RJG) eliminated the peaks while increasing the random noise i.e., the pressure spectrum between and around the peaks. Visual observations indicated that the activation of the spark modified the otherwise long combustion zone into a very compact and intense heat release zone around the radical jet discharge. Finally and most importantly, it was determined that the stabilizing effect of the plasma does not depend upon the frequency of the excitation. Particularly interesting is the result obtained when the spark was excited at the frequency of the instability, around 250 Hz, see Figure 77. The spectrum of the unexcited combustion shows a strong pressure and PMT response at the natural frequency of the instability. When the spark is turned on, the pressure peak near 250 Hz becomes very small. Even for the PMT spectrum, the peak at the excitation frequency is much smaller than that in the unexcited case. Had the system behaved linearly, the actuation at this frequency would have increased the heat released fluctuation and, therefore, the pressure oscillations. Since this did not occur, it appears that the plasma actuation entirely modifies the combustion process. Under this modified process the acoustic feedback no longer creates heat release oscillations. Instead, the plasma produces lower heat release fluctuations which, in turn, generate lower pressure oscillations.

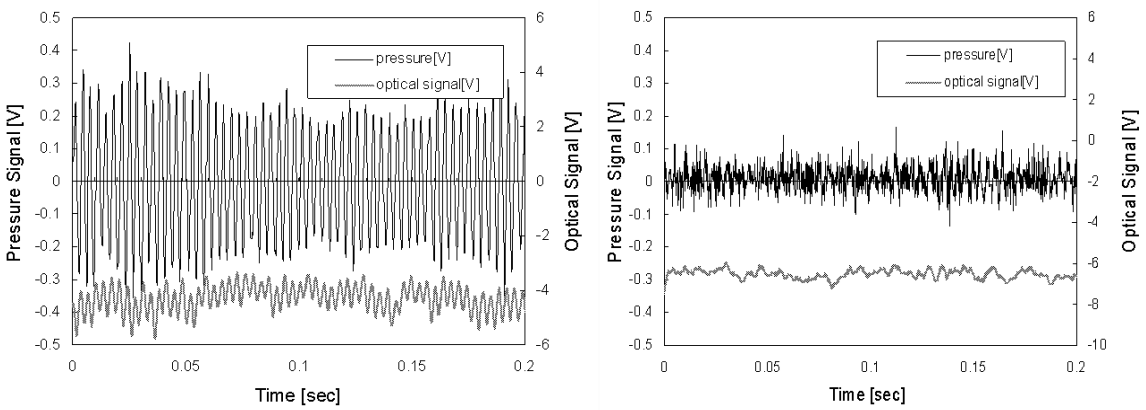

Figure 76. Time history of pressure and flame radiation without (left) and with (right) spark excitation at 1.1 kHz.

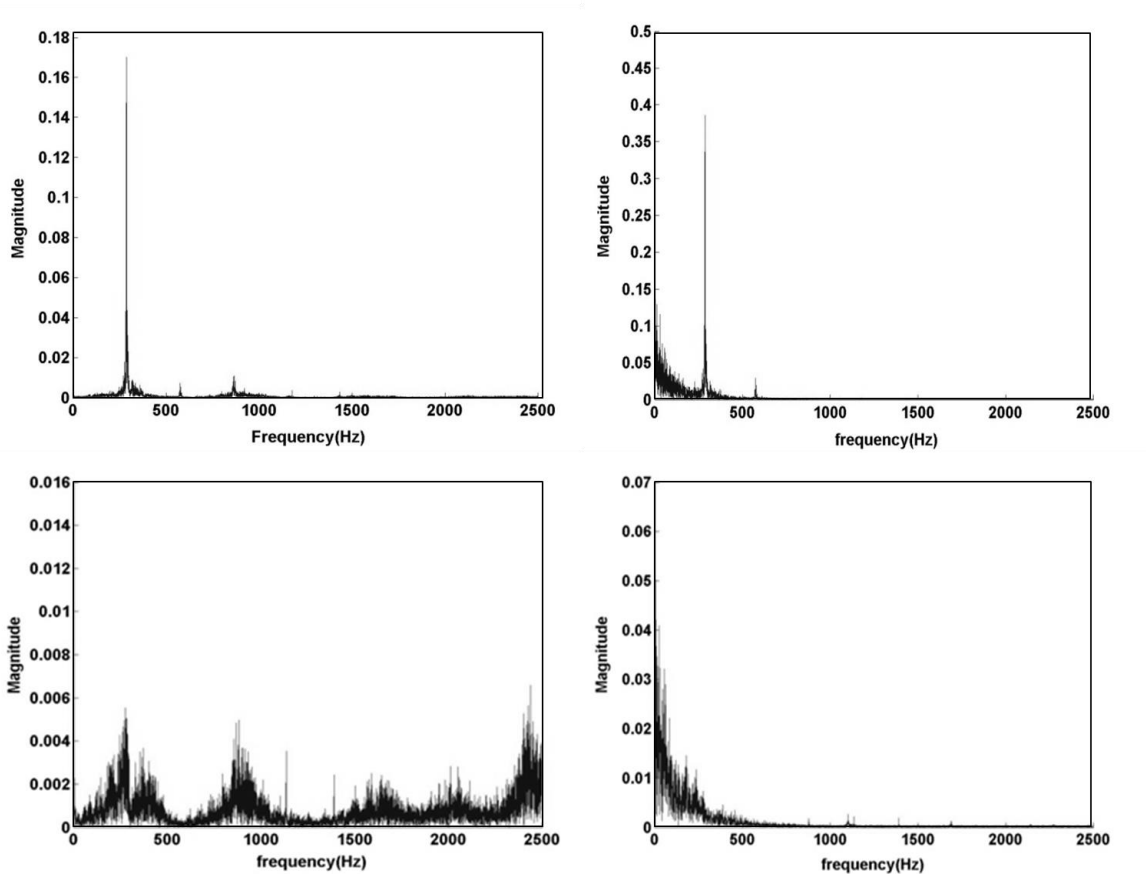

Figure 77. Frequency spectra of pressure (left) and flame radiation (right) without (top) and with (bottom) spark excitation at 1.1 KHz.

CHAPTER 8: CONCLUSION AND RECOMMENDATIONS

This thesis deals with some of the issues that arise when a spark ignites a flammable mixture. In addition, the electrical characteristics of sparks as an ignition sources were investigated.

We used two systems to supply energy directly and indirectly into a combustible flow. First, the spark energy was directly deposited into the flow. The spark was characterized to define the initial conditions that are more likely to lead to ignition. Based on voltage-current (VI) measurements and Schlieren images, the channel of the long-duration (inductive circuit) spark is convected by the flow. The voltage of the spark increases with the length of the channel. Due to this voltage increase, more energy is transferred into faster moving flows. The amount of transferred electrical energy is also slightly increased if a flame exists near the spark. However, the overall energy transfer efficiency from the long-duration spark into pure air is relatively low (~30%) because there is time for energy to be lost to the electrodes. In addition, it was observed that the convected spark channel forms reactant pockets that contain mostly unburned gas.

Another spark of very short-duration was generated using a capacitive circuit. An extremely accurate measurement system for the determination of the VI characteristics was developed as part of this research. As a results it was demonstrated that the energy deposition efficiency of these sparks into the gas is very high (above 90%) with minimal heat loss. Furthermore, the flow conditions (velocity and turbulence intensity) do not affect the energy deposition efficiency or the VI characteristics for this case.

The kernel generated by the short-duration spark was characterized using optical techniques. Until 30μs after the discharge, the species present in the kernel were found to

be similar, whether the mixture can develop into a self-sustaining flame or not, at least within a limited range of equivalence ratios. Time resolved observations showed that there is continuous reaction from the onset of the spark to the transition to a self-sustaining flame. This means that there is no delay like was observed for auto ignition, instead the ignition delay should be carefully defined and measured for the forced ignition. In addition, the effect of mixing of the kernel with surrounding gas on the kernel composition and, therefore, the ignition process was investigated using a numerical method. It was shown that kernels with high mixing levels (high levels of surrounding gas) could not ignite the reactants within a practical time period. However, the presence of additional radicals shortens this delay. In addition, the presence of fuel inside the kernel can supply additional chemical energy, which improves the eventual ignition of the flammable mixture by the kernel. Therefore, if there is an oscillation of fuel concentration in the flow near the electrodes, this can cause the power fluctuation, for example in an IC engine. This implies that the location of spark should be carefully chosen in the flow to assure successful ignition.

In the second ignition system, the electrical energy was supplied indirectly. A relatively simple Radical Jet Generator (RJG) was developed that is able to stabilize a flame in a high-speed flow largely with the help of radicals that are produced in an incomplete combustion process, initiated by an electrical spark, in a small chamber. The partially-burned products carrying large amounts of radicals and heat are then injected into a main stream, where they are able to initiate combustion and hold a flame in a rapidly moving, flammable flow. The RJG requires small amounts of electrical power since most of the radical species are produced in the incomplete combustion process. The

importance of radicals in the reaction was analyzed using data obtained during experiments. We then used a numerical method, to investigate the relative importance of the radicals in the reaction in the main combustor. This analysis showed that radical jet operating rich performed better as an igniter of the main combustor operating lean than it did when operating lean. It was also shown that this result is due to the presence of more chemical energy in the rich radical jet. This was determined through a numerical analysis of reactions at various equivalence ratios but for constant sensible enthalpy.

The RJG can stabilize a flame in the main flow exceeding 100m/s. In that configuration, a methane-air mixture is partially burned with a high frequency spark in the cavity of an RJG. In order to maintain combustion in rapidly moving main flows, radicals and heated gas from the RJG must penetrate well into the main flow. This can be achieved by increasing the flow rate through the RJG and by allowing the partially-burned gas to exit through a small orifice. Unfortunately, this often leads to unsteady combustion in the RJG. That unsteadiness reduces the number of radicals provided to the main flow. Possible explanations for the "pulse combustion" in the RJG include periodic combustion of reactant pocket due to movement of the spark channel, oscillations of the spark, ignition delay and limited flame speed. It was determined that the frequency of the unsteady combustion in the RJG chamber is highly dependent on the equivalence ratio. Therefore, the ignition delay and flame speed appear to be major reasons for the pulsations. This finding can produce guidance for design or sizing of the pilot type igniter. In addition, it is worth noting that there is coupling between the RJG operation and combustion dynamics in the main combustor. The high pressure oscillations due the acoustic coupling in the main combustor are lowered by the RJG because it moves the

flame zone in the main combustor. The RJG can, therefore, be used to stabilize a flame and to prevent the destructive combustion instability in combustors.

Some interesting questions were raised in this study. First, various equivalence ratios were used in the ignition experiments with capacitive spark. Under identical electrical conditions but for different equivalence ratios, the electrical potential did often not result in a conducting spark channel. Thus, the electric energy for ignition was not delivered to the gas, which in turn, can cause the engine combustor to miss-fire for certain conditions around the spark. The capacitance and dielectric constant of the fuel are not very different from those of pure air. Therefore, other fuel properties must be affecting the discharge. Further study therefore, is required to better understand this phenomenon.

Secondly, modern engines must be designed to satisfy stringent emission requirement such as NOx emission regulations. In this study the electric energy is deposited into a very small region. The temperature of this region is, therefore, very high. The NOx emission should be considerable when the fuel and air mixture is dissociated at such a high temperature. If the spark is used for the starting combustion in a continuous burner, its NOx production is not a problem. However, if the high energy density spark such as short-duration spark is used in an IC engine or if a spark is used to stabilize a continuous flame, the spark could be a major source of NOx.

APPENDIX A: INTRODUCTION TO IMAGING OF SPARK KERNEL

This work was conducted by a co-worker, Brandon Sforzo [128,129]. The evolution of the spark kernel was characterized using a combination of high-speed schlieren and emission imaging. The kernel was viewed through the quartz windows on the sides of the test section. The single pass collimated schlieren system (Figure A1) uses a 12 V, 50 W halogen light source. The light passes through a 1 mm diameter pin hole and is then collimated by a 0.2 m diameter, 1 m focal length off-axis parabolic mirror. The reflected collimated light is directed to a flat mirror, which redirects the light at right angles through the test section. The rays are redirected once again toward a second (identical) parabolic mirror. This mirror refocuses the light to a point. The schlieren stop was produced by a glass slide with an opaque spot, roughly the size of the focus of the light beam with the flow facility not running.

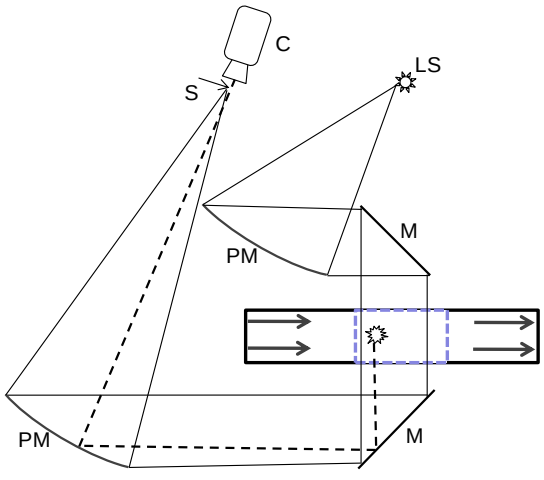

Figure A1. Schematic of the Schlieren setup. LS – light source, PM – parabolic mirror, M – mirror, S – schlieren stop, C – camera.

A high speed CMOS camera (Photron Fastcam SA3) focused on the test section is used to record the data. An 80 mm telephoto photographic lens with a 2× teleconverter was mounted on the camera, and a 200 mm diverging lens was placed in front to correct for refraction through the focusing mirrors. A digital delay/pulse generator (SRS DG535) was used to trigger the discharge and the camera, with a delay between the two triggers (Figure A2). This allows the spark to fire just before the camera exposure begins. The framing rate of the camera was set to 250Hz.

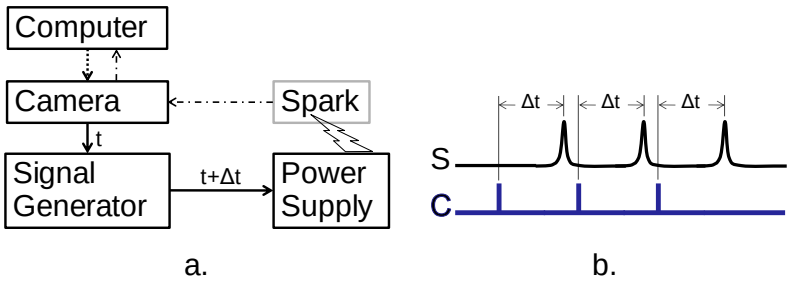

Figure A2. (a) Schematic of signal transfer between components of the image capturing system; (b) timing diagram of the camera output signal, C, and the resulting spark emission, S, with delay Δt.

APPENDIX B: INTRODUCTION TO LES MODELING OF SPARK KERNEL

B.1 Numerical setup

This work was conducted by a co-worker, Alexander Lambert. In order to appropriately capture the initial shock produced by the spark, a Hybrid differencing formulation was used for the initial 10μs, which incorporated a second-order MacCormack central-differencing scheme and a MUSCL method for resolving local discontinuities. For times greater than 10μs, only the second-order MacCormack scheme was used to solve for the relevant fluxes. A laminar flame approximation was used where the subgrid flame structure is assumed to be laminar. The unresolved turbulent terms, such as Reynolds stresses, species and energy turbulent fluxes were closed using the LDKM model. A thermally-perfect ideal gas assumption was used with mixture-averaged transport. The effect of magnetic fields and radiation were assumed to be negligible.

Most dimensions were similar to those used in the experimental setup and the inflow condition was matched with that of the experiment.

B.2 LES results for kernel evolution in flammable mixture

The calculated kernel evolution in the flammable mixture shows a similar structure as that observed experiment only at given time. According to the temperature profile of the kernel, the temperature in the leading edge is higher than in the trailing edge (Figure B). In addition, a sensitivity test for initial condition was conducted for the discharge in air. For different initial kernel compositions with the same initial energy, the species are quickly dissociated and the composition converges to a similar value within a few μs.

This means the initial energy and the mixing with surrounding reactants is influences ignition after a few µs. The detailed mixing process is also observed in the LES results. As was experimentally observed, there exists a high level of entrainment of cold air into the kernel near the electrodes, which lowers the local temperature (Figure B).

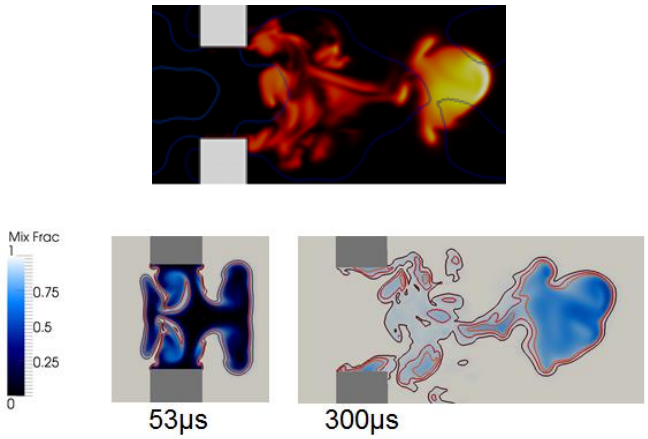

Figure B. Tracked mixing of hot kernel with cold reactants (lower) and the kernel temperature distribution at 400 µs after discharge (upper).

REFERENCES

[1] Williams, F.A., "Combustion theory". 2nd ed. 1985.

[2] Akindele, O.O., et al., "Spark ignition of turbulent gases". *Combustion and Flame*, **47**, 1982.

[3] Arpaci, V.S., et al., "Spark kernel development in constant volume combustion". *Combustion and Flame*, **135**, 2003.

[4] Ahmed, S.F. and E. Mastorakos, "Spark ignition of lifted turbulent jet flames". *Combustion and Flame*, **146**, 2006.

[5] Starikovskii, A.Y., "Plasma supported combustion". *Proceedings of the Combustion Institute*, **30**: p. 2405-2417, 2005.

[6] Bozhenkov, S.A., S.M. Starikovskaia, and A.Y. Starikovskii, "Nanosecond gas discharge ignition of h2- and ch4- containing mixtures". *Combustion and Flame*, **133**: p. 133-146, 2003.

[7] Harrison, A.J. and F.J. Weinberg, "Flame stabilization by plasma jets". *Proceedings of the Royal Society of London. Series A, Mathematical and Physical Sciences*, **321**(1544): p. 95-103, 1971.

[8] Marcum, S.D. and B.N. Ganguly, "Electric-field-induced flame speed modification.". *Combustion and Flame*, **143**: p. 27-36, 2005.

[9] Takita, K., et al., "Effect of addition of radicals on burning velocity". *AIAA Journal*, **39**(4): p. 742-744, 2001.

[10] Masuya, G., et al., "Effects of airstream mach number on h2/n2 plasma igniter". *Journal of Propulsion and Power* **18**(3): p. 678-685, 2002.

[11] Jacobsen, L., et al., "Toward plasma-assisted ignition in scramjets", in *41st AIAA Aerospace Sciences Meeting & Exhibit*: Reno, NV. 2003.

[12] Meyer, R., et al., "Ignition of premixed hydrocarbon-air flows using a non-equilibrium rf discharge", in *34th AIAA Plasmadynamics and Lasers Conference*: Orlando, FL. 2003.

[13] Wagner, T.C., et al., "Development and evaluation of a 1kw plasma torch igniter for scramjets", in *Joint Army-Navy-NASA-Air Force Interagency Propulsion Committee, Combustion Meeting, 23rd*: Hampton, VA. p. 13. 1986.

[14] Takita, K., "Ignition and flame-holding by oxygen, nitrogen and argon plasma torches in supersonic airflow". *Combustion and Flame*, **128**(3): p. 301-313, 2002.

[15] O'Brien, W.F., R.J. Roby, and S.D. Stouffer, "Improved plasma torch for ignition and flame holding in supersonic combustion", in *AIAA, ASME, SAE, ASEE, Joint Propulsion Conference, 25th*: Monterey, CA. 1989.

[16] Ben-Yakar, A. and R.K. Hanson, "Supersonic combustion of cross-flow jets and the influence of cavity flame holders", in *37th AIAA Aerospace Sciences Meeting and Exhibit*: Reno, NV. 1999.

[17] Chintala, N., R. Meyer, and I. Adamovich, "Non-thermal ignition of premixed hydrocarbon-air and co-air flows by non-equilibrium rf plasma", in *42nd AIAA Aerospace Sciences Meeting and Exhibit*: Reno, NV. 2004.

[18] Jian, T., et al., "Spectral property investigation of air plasma generated by pulsed co2 laser". *Plasma Science, IEEE Transactions on*, **39**(4): p. 1114-1119, 2011.

[19] Ronney, P.D., "Laser versus conventional ignition of flames". *Optical Engineering*, **33**(2): p. 510-521, 1994.

[20] El-Rabii, H., et al., "Laser ignition in a lean premixed prevaporized injector". *Combustion Science & Technology*, **176**(9): p. 1391-1417, 2004.

[21] Bradley, D., et al., "Fundamentals of high-energy spark ignition with lasers". *Combustion and Flame*, **138**(1-2): p. 55-77, 2004.

[22] Phuoc, T.X., "Laser-induced spark ignition fundamental and applications". *Optics and Lasers in Engineering*, **44**(5): p. 351-397, 2006.

[23] Bazelyan, E.M., "Spark discharge", ed. Y.P. Raizer. Boca Raton, Fla. :: CRC Press. 1998.

[24] Veldhuizen, E.M.v. and W.R. Rutgers, "Pulsed positive corona streamer propagation and branching". *Journal of Physics D: Applied Physics*, **35**(17): p. 2169, 2002.

[25] Dhali, S.K. and P.F. Williams, "Numerical simulation of streamer propagation in nitrogen at atmospheric pressure". *Physical Review A*, **31**(2): p. 1219-1221, 1985.

[26] Pierre, T., M. Emmanuel, and A. André, "Tracking an individual streamer branch among others in a pulsed induced discharge". *Journal of Physics D: Applied Physics*, **35**(21): p. 2823, 2002.

[27] Starikovskaia, S.M., "Plasma assisted ignition and combustion". *Journal of Physics D: Applied Physics*, **39**(16): p. R265, 2006.

[28] Beynon, J.H., "The conduction of electricity through gases". Topics in modern physics. London: Harrap. 1972.

[29] Ballal, D.R. and A.H. Lefebvre, "The influence of spark discharge characteristics on minimum ignition energy in flowing gases". *Combustion and Flame*, **24**(0): p. 99-108, 1975.

[30] Kogelschatz, U., "Dielectric-barrier discharges: Their history, discharge physics, and industrial applications". *Plasma Chemistry and Plasma Processing*, **23**(1): p. 1-46, 2003.

[31] Starikovskii, A.Y., et al., "Nanosecond-pulsed discharges for plasma-assisted combustion and aerodynamics". *Journal of Propulsion and Power*, **24**(6): p. 1182-1197, 2008.

[32] Cobine, J.D., "Gaseous conductors: Theory and engineering applications". Dover Publications: New York. 1958.

[33] Sher, E., J. Ben-Ya'Ish, and T. Kravchik, "On the birth of spark channels". *Combustion and Flame*, **89**(2): p. 186-194, 1992.

[34] Maly, R. and M. Vogel, "Initiation and propagation of flame fronts in lean ch_4-air mixtures by the three modes of the ignition spark". *Symposium (International) on Combustion*, **17**(1): p. 821-831, 1979.

[35] Fei, W., et al., "Transient plasma ignition of quiescent and flowing air/fuel mixtures". *Plasma Science, IEEE Transactions on*, **33**(2): p. 844-849, 2005.

[36] Jianbang, L., et al., "Effect of discharge energy and cavity geometry on flame ignition by transient plasma", in *42nd AIAA Aerospace Sciences Meeting and Exhibit*. American Institute of Aeronautics and Astronautics. 2004.

[37] Kono, M., S. Kumagai, and T. Sakai, "The optimum condition for ignition of gases by composite sparks". *Symposium (International) on Combustion*, **16**(1): p. 757-766, 1977.

[38] Orrin, J.E., I.M. Vince, and F.J. Weinberg, "Ignition by radiation from plasmas". *Combustion and Flame*, **37**(0): p. 91-93, 1980.

[39] Chen, F.F., "Time-varying impedance of the sheath on a probe in an rf plasma". *Plasma sources science and technology*, **15**: p. 773-782, 2006.

[40] Guha, A., S. Roy, and P.K. Mishra, "Development of an improved voltage and current measurement system for studying spark characteristics with application to electrodischarge machining". *Proceedings of the Institution of Mechanical*

Engineers, Part B: Journal of Engineering Manufacture, **218**(8): p. 935-938, 2004.

[41] Randolph, D.W. and F.B. Silsbee, "Flame speed and spark intensity": NACA. p. 14. 1925.

[42] Eichenberger, D.A. and W.L. Roberts, "Effect of unsteady stretch on spark-ignited flame kernel survival". *Combustion and Flame*, **118**(3): p. 469-478, 1999.

[43] Gettel, L.E. and K.C. Tsai, "Flame kernel development with the multiple electrode spark plug". *Combustion and Flame*, **54**(1-3): p. 225-228, 1983.

[44] Ishii, K., H. Shimomura, and T. Tsuboi. "Interaction between a flame kernel and a shock wave generated by spark discharge". 2001. Sendai, Japan: SPIE.

[45] Thiele, M., et al., "Numerical simulation of spark ignition including ionization". *Proceedings of the Combustion Institute*, **28**(1): p. 1177-1185, 2000.

[46] Lim, M.T., R.W. Anderson, and V.S. Arpaci, "Prediction of spark kernel development in constant volume combustion". *Combustion and Flame*, **69**(3): p. 303-316, 1987.

[47] Bradley, D. and F.K. Lung, "Spark ignition and the early stages of turbulent flame propagation". *Combustion and Flame*, **69**: p. 71-93, 1987.

[48] Sher, E. and J.C. Keck, "Spark ignition of combustible gas mixtures". *Combustion and Flame*, **66**(1): p. 17-25, 1986.

[49] Beduneau, J.L., et al., "Laser-induced radical generation and evolution to a self-sustaining flame". *Combustion and Flame*, **156**: p. 642-656, 2009.

[50] Mastorakos, E., "Ignition of turbulent non-premixed flames". *Progress in Energy and Combustion Science*, **35**(1): p. 57-97, 2009.

[51] Dixon-Lewis, G. and I.G. Shepherd, "Some aspects of ignition by localized sources, and of cylindrical and spherical flames". *Symposium (International) on Combustion*, **15**(1): p. 1483-1491, 1975.

[52] Wiriyawit, S. and E.K. Dabora, "Modeling the chemcial effects of plasma ignition in one-dimensional chamber". *Symposium (International) on Combustion*, **20**(1): p. 179-186, 1985.

[53] Dixon-Lewis, G., "Effect of core size on ignition energy by localized sources". *Combustion and Flame*, **33**(0): p. 319-321, 1978.

[54] Sloane, T.M. and A.Y. Schoene, "Energy requirements for spherical ignitions in atmospheric-pressure methane-air mixtures: A computational study". *Symposium (International) on Combustion*, **22**(1): p. 1669-1676, 1989.

[55] Kosarev, I.N. and et al., "Kinetic mechanism of plasma-assisted ignition of hydrocarbons". *Journal of Physics D: Applied Physics*, **41**(3): p. 032002, 2008.

[56] Adamovich, I.V., et al., "Plasma assisted ignition and high-speed flow control: Non-thermal and thermal effects". *Plasma Sources Science and Technology*, **18**(3): p. 034018, 2009.

[57] Shebeko, Y.N., et al., "Characteristics of the combustion of mixtures of combustible gases with refrigerants during downward flame propagation". *Combustion, Explosion and Shock Waves*, **18**(6): p. 634-636, 1982.

[58] Zhang, J.X., R.M. Clements, and P.R. Smy, "An experimental investigation of the effect of a plasma jet on a freely expanding methane-air flame". *Combustion and Flame*, **50**(0): p. 99-106, 1983.

[59] Eugene, M., et al., "Rapid combustion achievement by nanosecond barrier discharge", in *44th AIAA Aerospace Sciences Meeting and Exhibit*. American Institute of Aeronautics and Astronautics. 2006.

[60] Kim, W., et al., "Optimal discharge placement in plasma-assisted combustion of a methane jet in cross flow". *Combustion and Flame*, **153**(4): p. 603-615, 2008.

[61] Kim, W., M.G. Mungal, and M.A. Cappelli, "Formation and role of cool flames in plasma-assisted premixed combustion". *Applied Physics Letters*, **92**(5): p. 051503, 2008.

[62] Takita, K., et al., "Ignition and flame-holding of h2 and ch4 in high temperature airflow by a plasma torch". *Combustion and Flame*, **132**(4): p. 679-689, 2003.

[63] Aleksandrov, N.L., et al., "Mechanism of ignition by non-equilibrium plasma". *Proceedings of the Combustion Institute*, **32**(1): p. 205-212, 2009.

[64] Mintoussov, E., S. Pancheshnyi, and S. Andrei, "Propane-air flame control by non-equilibrium low-temperature pulsed nanosecond barrier discharge", in *42nd AIAA Aerospace Sciences Meeting and Exhibit*. American Institute of Aeronautics and Astronautics. 2004.

[65] Penetrante, B.M., et al., "Comparison of electrical discharge techniques for nonthermal plasma processing of NO in N_2". *Plasma Science, IEEE Transactions on*, **23**(4): p. 679-687, 1995.

[66] Kim, W., M. Godfrey Mungal, and M.A. Cappelli, "The role of in situ reforming in plasma enhanced ultra lean premixed methane/air flames". *Combustion and Flame*, **157**(2): p. 374-383, 2010.

[67] Do, H., et al., "Plasma assisted flame ignition of supersonic flows over a flat wall". *Combustion and Flame*, **157**(12): p. 2298-2305, 2010.

[68] Do, H., M.A. Cappelli, and M.G. Mungal, "Plasma assisted cavity flame ignition in supersonic flows". *Combustion and Flame*, **157**(9): p. 1783-1794, 2010.

[69] Kosarev, I.N., et al., "Kinetics of ignition of saturated hydrocarbons by nonequilibrium plasma: Ch4-containing mixtures". *Combustion and Flame*, **154**(3): p. 569-586, 2008.

[70] Hagelaar, G.J.M. and L.C. Pitchford, "Solving the boltzmann equation to obtain electron transport coefficients and rate coefficients for fluid models". *Plasma Sources Science and Technology*, **14**: p. 722-733, 2005.

[71] Zhang, H., P. Guo, and Z. Chen, "Critical condition for the ignition of reactant mixture by radical deposition". *Proceedings of the Combustion Institute*, **34**(2): p. 3267-3275, 2013.

[72] Sloane, T.M. and J.W. Ratcliffe, "Mass spectrometer sampling of a plasma jet igniter with a methane plasma feed". *Symposium (International) on Combustion*, **21**(1): p. 1877-1883, 1988.

[73] Lucas, D., et al., "Pulsed plasma jet igniters: Species measurements in methane combustion". *Symposium (International) on Combustion*, **22**(1): p. 1661-1667, 1989.

[74] Cattolica, R. and S. Vosen, "Combustion-torch ignition: Fluorescence imaging of oh concentration". *Combustion and Flame*, **68**(3): p. 267-281, 1987.

[75] Kimura, I., H. Aoki, and M. Kato, "The use of a plasma jet for flame stabilization and promotion of combustion in supersonic air flows". *Combustion and Flame*, **42**: p. 297-305, 1981.

[76] Kitagawa, T., et al., "Ignition characteristics of methane and hydrogen using a plasma torch in supersonic flow". *Journal of Propulsion and Power*, **19**(5): p. 853-858, 2003.

[77] W, O.B. and R. R, "Improved plasma torch for ignition and flame holding in supersonic combustion", in *25th Joint Propulsion Conference*. American Institute of Aeronautics and Astronautics. 1989.

[78] Warris, A.-M. and F. Weinberg, "Ignition and flame stabilization by plasma jets in fast gas streams". *Symposium (International) on Combustion*, **20**(1): p. 1825-1831, 1985.

[79] Harrison, A.J. and F.J. Weinberg, "A note on electromagnetically induced motion of spark ignition kernels". *Combustion and Flame*, **22**(2): p. 263-265, 1974.

[80] Varatharajan, B. and F.A. Williams, "Ignition times in the theory of branched-chain thermal explosions". *Combustion and Flame*, **121**(3): p. 551-554, 2000.

[81] Li, S.C. and F.A. Williams, "Reaction mechanisms for methane ignition". *Journal of Engineering for Gas Turbines and Power*, **124**(3): p. 471-480, 2002.

[82] Gussak, L., M. Turkish, and D. Siegla, "High chemical activity of incomplete combustion products and a method of prechamber torch ignition for avalanche activation of combustion in internal combustion engines". *SAE Technical Paper 750890*, 1975.

[83] Supat, K., et al., "Synthesis gas production from partial oxidation of methane with air in ac electric gas discharge". *Energy & Fuels*, **17**(2): p. 474-481, 2003.

[84] Yamaguchi, S., N. Ohiwa, and T. Hasegawa, "Structure and blow-off mechanism of rod-stabilized premixed flame". *Combustion and Flame*, **62**(1): p. 31-41, 1985.

[85] Williams, G.C., H.C. Hottel, and A.C. Scurlock, "Flame stabilization and propagation in high velocity gas streams". *Symposium on Combustion and Flame, and Explosion Phenomena*, **3**(1): p. 21-40, 1949.

[86] Fetting, F., A.P.R. Choudhury, and R.H. Wilhelm, "Turbulent flame blow-off stability, effect of auxiliary gas addition into separation zone". *Symposium (International) on Combustion*, **7**(1): p. 621-632, 1958.

[87] Longwell, J.P., et al., "Flame stabilization by baffles in a high velocity gas stream". *Symposium on Combustion and Flame, and Explosion Phenomena*, **3**(1): p. 40-44, 1949.

[88] Andrews, G.E., D. Bradley, and S.B. Lwakabamba, "Measurement of turbulent burning velocity for large turbulent reynolds numbers". *Symposium (International) on Combustion*, **15**(1): p. 655-664, 1975.

[89] Abdel-Gayed, R.G. and D. Bradley, "A two-eddy theory of premixed turbulent flame propagation". *Philosophical transactions of the royal society of London. Series A, Mathematical and physical sciences*, **301**(1457): p. 1-25, 1981.

[90] Bradley, D., A.K.C. Lau, and M. Lawes, "Flame stretch rate as a determinant of turbulent burning velocity". *Philosophical Transactions: Physical Sciences and Engineering*, **338**(1650): p. 359-387, 1992.

[91] Chen, J.H. and H.G. Im, "Correlation of flame speed with stretch in turbulent premixed methane/air flames". *Symposium (International) on Combustion*, **27**(1): p. 819-826, 1998.

[92] Hassan, M.I., K.T. Aung, and G.M. Faeth, "Measured and predicted properties of laminar premixed methane/air flames at various pressures". *Combustion and Flame*, **115**: p. 539-550, 1998.

[93] Peters, N., "The turbulent burning velocity for large-scale and small-scale turbulence". *J. Fluid Mech.*, **384**: p. 107-132, 1999.

[94] Chong, C.T. and S. Hochgreb, "Measurements of laminar flame speeds of acetone/methane/air mixtures". *Combustion and Flame*, **158**(3): p. 490-500, 2011.

[95] Nikolay, A., et al., "Nonequilibrium plasmas and its applications for combustion and hypersonic flow control", in *41st Aerospace Sciences Meeting and Exhibit*. American Institute of Aeronautics and Astronautics. 2003.

[96] E.I.Mintoussov, S.V.Pancheshnyi, and A.Yu.Starikovskii, "Propane-air flame control by non-equilibrium low-temperature pulsed nanosecond barrier discharge ", in *42nd AIAA Aerospace Sciences Meeting and Exhibit*. 2004.

[97] Cetegen, B., et al., "Performance of a plasma jet igniter". *SAE Technical Paper 800042*, 1980.

[98] Marcum, S.D. and B.N. Ganguly, "Electric-field-induced flame speed modification". *Combustion and Flame*, **143**(1–2): p. 27-36, 2005.

[99] Naidu, M.S. and S. Kamakshaiah, "Introduction to electrical engineering". New Delhi Tata McGraw-Hill c2000. 2000.

[100] Lawton, J., "Electrical aspects of combustion", ed. F.J. Weinberg. Oxford, Clarendon P. 1969.

[101] Taylor, J.R., "An introduction to error analysis : The study of uncertainties in physical measurements". 2nd ed. ed. Sausalito, Calif. :: University Science Books. 1997.

[102] Bane, S.P.M., et al., "Statistical analysis of electrostatic spark ignition of lean h2/o2/ar mixtures". *International Journal of Hydrogen Energy*, **36**(3): p. 2344-2350, 2011.

[103] Porter, R.P., et al., "A study of hydrocarbon flames". *Symposium (International) on Combustion*, **11**(1): p. 907-917, 1967.

[104] Nori, V.N., "Modeling and analysis of chemiluminescence sensing for syngas, methane and jet-a combustion", in *Aerospace Engineering*. Georgia Institute of Technology. 2008.

[105] Swett, C.C., Jr, "Spark ignition of flowing gases". NACA. 1956.

[106] Fialkov, A.B., "Investigations on ions in flames". *Progress in Energy and Combustion Science*, **23**(5–6): p. 399-528, 1997.

[107] Bradley, D., et al., "Fundamentals of high-energy spark ignition with lasers". *Combustion and Flame*, **138**: p. 55-77, 2004.

[108] Engel, A.v., "Ionized gas". second ed.: Oxford university Press. 1965.

[109] Swett, C.C., Jr, "Spark ignition of flowing gases I : Energies to ignite propane-air mixtures in pressure range of 2 to 4 inches mercury absolute". NACA. 1949.

[110] Roth, W., et al., "Heat generation by electric sparks and rate of heat loss to the spark electrodes". *The Journal of Chemical Physics*, **19**(12): p. 1530-1535, 1951.

[111] "Crc handbook of chemistry and physics". Cleveland, Ohio: CRC Press. 1977.

[112] Schmidt, J.W. and M.R. Moldover, "Dielectric permittivity of eight gases measured with cross capacitors". *International Journal of Thermophysics*, **24**(2): p. 375-403, 2003.

[113] Afeefy, H.Y., J.F. Liebman, and S.E. Stein. "Neutral thermochemical data". NIST Chemistry WebBook, NIST Standard Reference Database Number 69 2011 [cited 2012; Available from: http://webbook.nist.gov/chemistry/ie-ser.html.

[114] Oancea, D., et al., "High voltage and break spark ignition of propylene/air mixtures at various initial pressures". *Journal of loss prevention in the process industries*, **16**: p. 353-361, 2003.

[115] Ballal, D.R. and A.H. Lefebvre, "The influence of spark discharge characteristics on minimum ignition energy in flowing gases". *Combustion and Flame*, **24**: p. 99-108, 1975.

[116] Ballal, D.R. and A.H. Lefebvre, "Ignition and flame quenching in flowing gaseous mixtures". *Proceedings of the Royal Society of London. Series A, Mathematical and Physical Sciences*, **357**(1689): p. 163-181, 1977.

[117] Ballal, D.R. and A.H. Lefebvre, "Ignition and flame quenching of flowing heterogeneous fuel-air mixtures". *Combustion and Flame*, **35**(0): p. 155-168, 1979.

[118] Turns, S.R., "An introduction to combustion : Concepts and applications". Mcgraw-hill series in mechanical engineering. New York :: McGraw-Hill. 1996.

[119] Ralchenko, Y., et al. "Nist atomic spectra database". 2011 Wednesday, 28-Dec-2011 18:12:26 EST [cited 4.1.1; Nov 2011:[Available from: http://physics.nist.gov/asd.

[120] Weinberg, F.J., et al., "Ignition by plasma jet". *Nature*, **272**: p. 341-343, 1978.

[121] Choi, W.-S., et al., "Preliminary study of a low power plasma radical jet generator for combustion systems". *ASME Turbo Expo 2006: Power for Land, Sea, and Air*, **1**: p. 877-885, 2006.

[122] SMITH, S.H. and M.G. MUNGAL, "Mixing, structure and scaling of the jet in crossflow". *Journal of Fluid Mechanics*, **357**: p. 83-122, 1998.

[123] Choi, W.-S., "Flame stabilization by a plasma driven radical jet in a high speed flow", in *Mechanical Engineering*. Georgia Institute of Technology. 2009.

[124] VILLERMAUX, E. and H. REHAB, "Mixing in coaxial jets". *Journal of Fluid Mechanics*, **425**: p. 161-185, 2000.

[125] Haidara, M., A. Denat, and P. Atten, "Corona discharges in high pressure air". *Journal of Electrostatics* **40**: p. 61-66, 1997.

[126] Oancea, D., et al., "High voltage and break spark ignition of propylene/air mixtures at various initial pressures". *Journal of Loss Prevention in the Process Industries*, **16**(5): p. 353-361, 2003.

[127] Linan, A. and F.A.Williams, "Ignition in an unsteady mixing layer subject to strain and variable pressure". *Combustion and Flame*, **95**: p. 31-46, 1993.

[128] Jaecheol, K., et al., "High energy spark discharges for ignition", in *48th aiaa/asme/sae/asee joint propulsion conference & exhibit*. American Institute of Aeronautics and Astronautics. 2012.

[129] Sforzo, B., et al., "Post discharge evolution of a spark igniter kernel". *Combustion and Flame*, Accepted 24 July 2014, Available online 14 August 2014

VITA

JAECHEOL KIM

KIM was born in Beolgyo, South Korea. He received a B.A. in Aerospace engineering from Hankook Aviation University, Goyang City, South Korea in 2002 and a M.S. in Aerospace engineering from Georgia Institute of Technology, Atlanta, Georgia in 2005.